Journal of Quantitative Spectroscopy & Radiative Transfer 110 (2009) 533–572

Contents lists available at ScienceDirect

Journal of Quantitative Spectroscopy & Radiative Transfer

journal homepage: www.elsevier.com/locate/jqsrt

The *HITRAN* 2008 molecular spectroscopic database

L.S. Rothman [a,*], I.E. Gordon [a], A. Barbe [b], D.Chris Benner [c], P.F. Bernath [d], M. Birk [e], V. Boudon [f], L.R. Brown [g], A. Campargue [h], J.-P. Champion [f], K. Chance [a], L.H. Coudert [i], V. Dana [j], V.M. Devi [c], S. Fally [k,1], J.-M. Flaud [i], R.R. Gamache [l], A. Goldman [m], D. Jacquemart [n], I. Kleiner [i], N. Lacome [n], W.J. Lafferty [o], J.-Y. Mandin [j], S.T. Massie [p], S.N. Mikhailenko [q], C.E. Miller [g], N. Moazzen-Ahmadi [r], O.V. Naumenko [q], A.V. Nikitin [q], J. Orphal [i], V.I. Perevalov [q], A. Perrin [i], A. Predoi-Cross [s], C.P. Rinsland [t], M. Rotger [b,f], M. Šimečková [a,2], M.A.H. Smith [t], K. Sung [g], S.A. Tashkun [q], J. Tennyson [u], R.A. Toth [g], A.C. Vandaele [v], J. Vander Auwera [k]

[a] *Harvard-Smithsonian Center for Astrophysics, Atomic and Molecular Physics Division, Cambridge, MA 02138, USA*
[b] *Université de Reims-Champagne-Ardenne, Groupe de Spectrométrie Moléculaire et Atmosphérique, 51062 Reims, France*
[c] *The College of William and Mary, Department of Physics, Williamsburg, VA 23187, USA*
[d] *University of York, Department of Chemistry, York, UK*
[e] *DLR – Remote Sensing Technology Institute, Wessling, Germany*
[f] *CNRS-Université de Bourgogne, Institut Carnot de Bourgogne, 21078 Dijon, France*
[g] *California Institute of Technology, Jet Propulsion Laboratory, Pasadena, CA 91109, USA*
[h] *Université Joseph Fourier/CNRS, Laboratoire de Spectrometrie Physique, 38402 Saint-Martin-d'Hères, France*
[i] *CNRS et Universités Paris Est et Paris 7, Laboratoire Inter-Universitaire des Systèmes Atmosphériques, 94010 Créteil, France*
[j] *UPMC Université Paris 06, UMR 7092, Laboratoire de Physique Moléculaire et Applications, 75252 Paris, France*
[k] *Université Libre de Bruxelles, Service de Chimie Quantique et Photophysique, C.P. 160/09, B-1050 Brussels, Belgium*
[l] *University of Mass Lowell, Department of Environmental Earth & Atmospheric Sciences, Lowell, MA 01854, USA*
[m] *University of Denver, Department of Physics, Denver, CO 80208, USA*
[n] *UPMC Université Paris 06, UMR 7075, Laboratoire de Dynamique, Interactions et Réactivité, 75252 Paris, France*
[o] *National Institute of Standards and Technology, Gaithersburg, MD 20899, USA*
[p] *National Center for Atmospheric Research, Boulder, CO 80307, USA*
[q] *Institute of Atmospheric Optics, Tomsk 634055, Russia*
[r] *University of Calgary, Department of Physics and Astronomy, Calgary, AB, Canada T2N 1N4*
[s] *University of Lethbridge, Department of Physics and Astronomy, Lethbridge, AB, Canada T1K 3M4*
[t] *NASA Langley Research Center, Science Directorate, Hampton, VA 23681, USA*
[u] *University College London, Department of Physics and Astronomy, London WC1E 6BT, UK*
[v] *Institut d'Aéronomie Spatiale de Belgique, B-1180 Brussels, Belgium*

ARTICLE INFO

Article history:
Received 21 December 2008
Received in revised form
11 February 2009
Accepted 13 February 2009

Keywords:
HITRAN
Spectroscopic database
Molecular spectroscopy
Molecular absorption

ABSTRACT

This paper describes the status of the 2008 edition of the *HITRAN* molecular spectroscopic database. The new edition is the first official public release since the 2004 edition, although a number of crucial updates had been made available online since 2004. The *HITRAN* compilation consists of several components that serve as input for radiative-transfer calculation codes: individual line parameters for the microwave through visible spectra of molecules in the gas phase; absorption cross-sections for molecules having dense spectral features, i.e. spectra in which the individual lines are not resolved; individual line parameters and absorption cross-sections for bands in the ultraviolet; refractive indices of aerosols, tables and files of general properties associated with the database; and database management software. The line-by-line portion of the

* Corresponding author. Tel.: +1 617 495 7474; fax: +1 617 496 7519.
E-mail address: lrothman@cfa.harvard.edu (L.S. Rothman).
[1] Current address: Institut d'Aéronomie Spatiale de Belgique, B-1180 Brussels, Belgium.
[2] Current address: J. Heyrovsky Institute of Physical Chemistry, Prague, Czech Republic.

doi:10.1016/j.jqsrt.2009.02.013

Spectroscopic line parameters
Absorption cross-sections
Aerosols

database contains spectroscopic parameters for 42 molecules including many of their isotopologues.

1. Introduction

This article describes the data that have been added, modified, or enhanced in the *HITRAN* (*Hi*gh Resolution *Tran*smission) compilation since the previous update of 2004 [1] (hereafter called HITRAN2004 in the text). The compilation encompasses the *HITRAN* line-transition parameters, infrared cross-sections, UV (ultraviolet) line-by-line parameters and cross-sections, aerosol refractive indices, and documentation. The file structure for the compilation remains the same as the previous edition and can be seen in Fig. 1 of Ref. [1]. The compilation is available on an anonymous ftp site. Instructions for accessing the database can be found in the *HITRAN* web site (http://www.cfa.harvard.edu/HITRAN).

The *HITRAN* database is the recognized international standard, used for a vast array of applications including terrestrial and planetary atmospheric remote sensing, transmission simulations, fundamental laboratory spectroscopy studies, industrial process monitoring, and pollution regulatory studies. An international *HITRAN* advisory committee, composed of a dozen experts in the field of spectroscopy, has been established under the auspices of NASA. This committee reviews and evaluates new data and makes recommendations for updates and replacements in the compilation.

Many recent developments have pushed the requirements of *HITRAN* in terms of accuracy and degree of completeness. Among these developments one can cite the retrievals that various satellite remote-sensing missions are now capable of due in part to the high signal-to-noise ratio of the spectra and to advances in retrieval algorithms. Notable satellite spectrometer instrumentation includes *MLS* (Microwave Limb Sounder) [2] and *TES* (Tropospheric Emission Spectrometer) [3] on the Aura platform, *MIPAS* (Michelson Interferometer for Passive Atmospheric Sounding) [4] on ENVISAT, *ACE-FTS* (Atmospheric Chemistry Experiment) [5] on SCISAT, *AIRS* (Atmospheric Infrared Sounder) [6] on Aqua, *IASI* (Infrared Atmospheric Sounding Interferometer) [7] on MetOP-A, *OCO* (Orbiting Carbon Observatory) [8], and *GOSAT* (Greenhouse gases Observing SATellite) [9]. These satellite instruments have put demands on *HITRAN* that include increased accuracy (by almost an order of magnitude in some cases) for the basic parameters: line position in vacuum wavenumbers, ν (in cm^{-1}), intensity of the line, S (in $cm^{-1}/(molecule\,cm^{-2})$), and line-shape parameters.[3] They also require more species, additional molecular bands, and weak lines throughout the spectral region covered by *HITRAN* (microwave through UV). In fact, the remote-sensing experiments have demonstrated that the basic Lorentz line-shape parameter for collisional broadening used in *HITRAN*, from which it is possible to calculate the Voigt line profile, is not satisfactory in many cases. To reduce the residuals between observation and simulation, it has often been necessary to invoke more sophisticated non-Voigt line shape functions such as Rautian or Galatry [10] and line mixing.

Section 2 of this paper presents the most significant of the improvements featured in this newly updated edition of *HITRAN* as it relates to the line-by-line parameters. Note that the line lists described here either include or supersede intermediate updates that were placed on the *HITRAN* web site after HITRAN2004. The status of the infrared cross-sections, sets of UV data, and the aerosol refractive indices of aerosols, are discussed in Sections 3–5.

2. Line-by-line parameters

This edition of *HITRAN* contains three new entries, methyl bromide (CH_3Br), methyl cyanide (CH_3CN), and tetrafluoromethane (CF_4). It is worth repeating that the number of transitions included in the database is limited by: (1) a reasonable minimum cutoff in absorption intensity (based on the sensitivity of instruments that observe absorption over extreme terrestrial atmospheric path lengths), (2) lack of sufficient experimental data, or (3) lack of calculated transitions.

The format for the line-by-line portion of the compilation remains the same as in the previous edition (see Table 1 of Ref. [1]), except that the self-broadened half-width parameter has now been written in a Fortran format of F5.3 rather than F5.4. The latter distinction is not significant unless the user employs the Fortran write function.

The molecules for which data are included in the line-by-line portion of *HITRAN* are mostly composed of small numbers of atoms and have low molecular weights. Large polyatomic molecules have many normal modes of vibration and "heavy" species have fundamentals at very low wavenumbers. For three of the molecules in this edition of *HITRAN*, SF_6, $ClONO_2$, and CF_4, we have kept the parameters for this edition in a supplemental folder (see Fig. 1 of Ref. [1]). The rationale for this is that the line-by-line parameters represent only a few bands, and neglect many significant hot bands for the "heavy" species. For most applications, the IR cross-sections of these molecules in the *HITRAN* compilation provide a better simulation.

[3] The HITRAN database does not adhere to SI units for both historical and application-specific reasons. We also employ the symbol ν throughout for line position in cm^{-1}, thereby dropping the tilde ($\tilde{\nu}$) that is the official designation of wavenumber. We normally express the HITRAN unit for intensity as $cm^{-1}/(molecule\,cm^{-2})$ rather than simplifying to the equivalent cm/molecule. In this way we emphasize the quantity as wavenumber per column density, which is consistent with the viewpoint of atmospheric radiative-transfer codes.

The user of the HITRAN line-by-line data and the cross-section data is encouraged to consult and cite the original sources of the data. In the case of the line-by-line parameters, there are indices pointing to the sources of six parameters: the transition wavenumber, ν; the intensity, S; the air- and self-broadened half-width parameters, γ_{air} and γ_{self}; the exponent for the temperature dependence of the air-broadened half-width parameter, n; and the air-pressure shift parameter, δ. The sources are contained in a separate file in the compilation.

The following subsections cover all molecules whose parameters have been updated since the last edition of *HITRAN* [1]. The descriptions are generally ordered by increasing wavenumber region, and we have attempted to describe the improvements in the line positions and intensities prior to those in the other parameters, when feasible. Future improvements are also mentioned where necessary.

2.1. H_2O (molecule 1)

Water vapor spectroscopy is of paramount importance to many applications. Not only are the spectroscopic parameters needed for studies of the climate and energy budget of the Earth, but also for the atmospheres of stars (see for example Ref. [11]) and now even exoplanets [12]. The recommended line list for water remains in a state of continued evolution. Substantial changes to the half-width parameters for the main isotopologue $H_2{}^{16}O$ and the addition of new data for isotopically substituted species are among the prominent recent modifications.

The 2004 edition of *HITRAN* [1] featured a major update in line positions and line intensities for all *HITRAN* water-vapor isotopologues between 500 and 8000 cm^{-1} based on the work of Toth [13], with the exception of the principal isotopologue which had calculated values from Coudert [14] up to 800 cm^{-1}. However, recently reported measurements of transitions in the ν_2 band in the 1000–2000 cm^{-1} range [15] suggest that Toth's data systematically underestimated the intensities of the strongest transitions in this region by between 5% and 10%. This conclusion is supported by independent *ab initio* calculations [16]. The intensities of the unblended strong lines have therefore been replaced using the new measurements; for four blended strong lines, those located at 1512.30732, 1539.05857, 1539.06079, and 1684.83515 cm^{-1}, the theoretical results are from variational calculations using an *ab initio* dipole surface [17]. There have been other recent measurements at shorter infrared wavelengths [15,18,19] as well as a comprehensive *ab initio* analysis of the line intensities [20]. The issue of whether or not adjustments are also needed for the line intensities at these wavelengths is currently being studied with a view to coming up with recommendations for a future edition of the database.

The region 9500–14 500 cm^{-1} for the main isotopologue has been updated using the new analysis by Tolchenov and Tennyson [21] who employed a novel fitting technique to reanalyze a series of Fourier transform absorption spectra of pure water vapor recorded by Schermaul et al. [22,23]. However, any data attributed to Brown et al. [24] that were in HITRAN2004 have been retained. Analogously, the 14 500- to 26 000-cm^{-1} region has been updated using the work of Tolchenov et al. [25] replacing the data from Coheur et al. [26] in HITRAN2004. Comparisons with previous studies on water-vapor absorption in this region suggest that the new parameters give a more consistent representation of the spectrum.

An update has also been made for the parameters of $H_2{}^{17}O$ and $H_2{}^{18}O$ isotopologues in the near-IR and visible region based on the work of Tanaka et al. [27]. This work is a reanalysis of long-path length Fourier transform spectra originally recorded at Kitt Peak by Chevillard et al. [28] and analyzed initially by Tanaka et al. [29]. The lines listed previously in this region for both isotopologues have been removed and replaced by 1087 lines of $H_2{}^{18}O$ spanning the range 12 400–14 520 cm^{-1} and 891 lines of $H_2{}^{17}O$ in the range 11 365–14 475 cm^{-1}. In addition, some misidentified lines that have now been attributed to oxygen, have been removed from the water-vapor line list.

A major addition has been made with 3528 monodeuterated water-vapor (HDO) transitions in the near infrared and visible, specifically 11 600–23 000 cm^{-1}. Previous editions of the database did not contain any HDO transitions in this region. The data are due to a re-analysis by Voronin et al. [30] of the long-path Fourier transform spectrum recorded by Bach et al. [31].

The pressure-broadened half-width parameters for the three most abundant isotopologues of water, $H_2{}^{16}O$, $H_2{}^{18}O$, and $H_2{}^{17}O$, have been completely updated. Air-broadened half-widths were updated in 2006 (an interim update) using an algorithm based on physical principles and statistics developed by Gordon et al. [32], which set a new criterion for the best available air-broadened half-width parameters using a mixture of measurements, calculated, and semi-empirical data. These new parameters have been tested for different remote-sensing applications and were found to give improved profiles for atmospheric constituents. The algorithm has been improved for the current release of *HITRAN*: additional measurements of γ_{air} and δ [18,33–39] and γ_{self} [18,38–45] have been added to the measurement databases. Additional data [46,47] have been added to the theoretical database of γ_{air}, n, and δ. The database of calculations of γ_{self} for water vapor now contains the data of Antony et al. [48,49] and Cazzoli et al. [44].

The temperature dependence of the air-broadened half-widths has now been added to all water-vapor transitions via an algorithm that first seeks values from CRB (Complex Robert–Bonamy) calculations [46,47,50]. If a CRB value for a transition is not found, the n values as a function of rotational quantum numbers from Table 7 of Ref. [1] are used.

2.2. CO_2 (molecule 2)

High-resolution spectroscopic monitoring of the evolution of carbon dioxide in the terrestrial atmosphere is obviously one of great importance for policy makers. Carbon dioxide is also prevalent in the atmospheres of some rocky planets, such

as Venus and Mars. With its many bands of very different intensity throughout the spectrum, carbon dioxide is also an excellent tool for probing atmospheres to different depths.

Since the last edition of the *HITRAN* database [1], there have been a large number of experimental and theoretical investigations of carbon dioxide spectra. A notable effort is the set of extensive Fourier transform spectroscopy (FTS) experiments carried out by the Jet Propulsion Laboratory (JPL) [51–58] in order to support the OCO mission [8]. The results of these efforts for the 4300–7000 cm^{-1} region have been compiled into a HITRAN-like database [57] with parameters for nine different isotopologues (including $^{13}C^{18}O_2$ which was not previously tabulated in *HITRAN*). The parameters listed in Ref. [57] cover a wide dynamic range (4×10^{-30}–1.29×10^{-21} cm^{-1}/(molecule cm^{-2}) at 296 K) which is substantially larger than the FTS experimental detection limit, i.e. parameters for some high-*J* lines as well as for lines of weak unobserved bands were theoretically extrapolated. Parallel experiments featuring the cavity ring down spectroscopy (CRDS) technique [59–64] in the 5851–7045 cm^{-1} region have shown that theoretical extrapolations of the FTS data in Ref. [57] deviate seriously from the CRDS line positions and line intensities for some of the higher-*J* lines, while some of the weaker bands, observed to be above 4×10^{-30} cm^{-1}/(molecule cm^{-2}) are missing completely from the predicted line list (see discussion in Refs. [62,65,66]). These discrepancies are thought to have a reliable basis because the CRDS technique allows the detection of lines with much weaker intensities than those with the FTS, although CRDS spectra are inferior to FTS spectra in terms of overall accuracy of determining line positions.

Simultaneously, great progress has been made in the global effective Hamiltonian (EH) model developed at the Université Pierre et Marie Curie (Paris, France) and the Institute of Atmospheric Optics (Tomsk, Russia) [67–70], which was used in the calculation of the theoretical Carbon Dioxide Spectroscopic Databank (CDSD) [71], significantly improving and extending the previous version [72] and achieving a pronounced agreement with the CRDS experiments. The improvement and extension of the CDSD databank have been achieved due to incorporating new measurements performed during the last five years into the global modeling. The above mentioned CRDS measurements in Grenoble and FTS measurements at JPL have had an especially strong impact on the quality of the modeling.

The present atmospheric version of CDSD consists of 419 610 lines belonging to $^{12}C^{16}O_2$, $^{13}C^{16}O_2$, $^{16}O^{12}C^{18}O$, $^{16}O^{12}C^{17}O$, $^{16}O^{13}C^{18}O$, $^{16}O^{13}C^{17}O$, and $^{12}C^{18}O_2$ covering a wavenumber range of 5–12 784 cm^{-1}. The intensity cutoff of CDSD was set to 10^{-30} cm^{-1}/(molecule cm^{-2}). On average, the residuals between CDSD calculated line positions and those observed are two times larger than measurement uncertainties. CDSD calculated line intensities are almost always within their measurement uncertainties.

The current atmospheric version of the databank is available via an anonymous ftp site ftp.iao.ru in the folder /pub/CDSD-2008/296. The same site also contains two other dedicated versions of the databank: a version for high-temperature applications (/pub/CDSD-2008/1000) and a version for studying the atmospheres of Venus and Mars (/pub/CDSD-2008/Venus).

The need for a sensible mixing of the experimental and theoretical data is obviously required in the 4300 to 7000 cm^{-1} region in order to support atmospheric remote sensing of the earth-like planets (Earth, Mars and Venus). In order to do that one has to consider the following caveats:

1. The database [57] (hereafter referred to as the OCO data set) is based on FTS measurements that are very accurate and, besides line positions and intensities, allow measurements of collision broadening parameters. However, theoretical extrapolations applied in the OCO data set for transitions weaker than 10^{-26} cm^{-1}/(molecule cm^{-2}) for the principal isotopologue and 10^{-27} cm^{-1}/(molecule cm^{-2}) for the other isotopologues have led to some very large deviations from subsequent observations in predicting line positions and especially intensities.
2. The data collected in the cavity ring down laser experiments (hereafter referred as CRDS data) is nearly complete for the lines stronger than 5×10^{-29} cm^{-1}/(molecule cm^{-2}). However, the typical accuracy of these line positions (1×10^{-3} cm^{-1}) is inferior to that of FTS experiments (4×10^{-5} cm^{-1}). Finally, CRDS measurements do not provide data below 5851 cm^{-1} and do not provide pressure-induced parameters. Note that the data set for $^{13}C^{16}O_2$, $^{16}O^{13}C^{18}O$, $^{16}O^{13}C^{17}O$, $^{13}C^{18}O_2$ and $^{18}O^{13}C^{17}O$ compiled in Ref. [65] provide experimental line positions supplemented with intensities calculated using the EH model and effective dipole moment parameters for completeness ($^{13}C^{18}O_2$ and $^{18}O^{13}C^{17}O$ isotopologues have not been tabulated in *HITRAN* before). For $^{12}C^{16}O_2$, $^{16}O^{12}C^{17}O$ and $^{16}O^{12}C^{18}O$ [62] only line positions are provided, although parameters for $^{12}C^{16}O_2$ are also tabulated in Ref. [61] where the experimental line positions and intensities are supplemented with the CDSD intensities.
3. The theoretical CDSD databank is quite complete, with intensities down to 1×10^{-30} cm^{-1}/(molecule cm^{-2}), at least for the majority of the *HITRAN* isotopologues. It has excellent predictive capabilities for line positions and intensities, although it is, of course, not as good as the accuracy achieved by experiment. In addition, a minor limitation of the EH method occurs when there are interpolyad anharmonic couplings. Four such occurrences have been observed for the asymmetric isotopologues, namely $^{16}O^{12}C^{18}O$ [62], $^{16}O^{13}C^{17}O$ [65] and $^{16}O^{13}C^{18}O$ [64,65]. Although these resonance interactions are not common for carbon dioxide, small deviations in the values of predicted line positions and line intensities values from their real values cannot be ruled out completely.

With this information in mind, a procedure, shown in a schematic diagram in Fig. 1, was developed in order to keep only the best parameters from the OCO, CRDS and CDSD data sets for compiling the *HITRAN*2008 CO_2 line list in the 4300 to

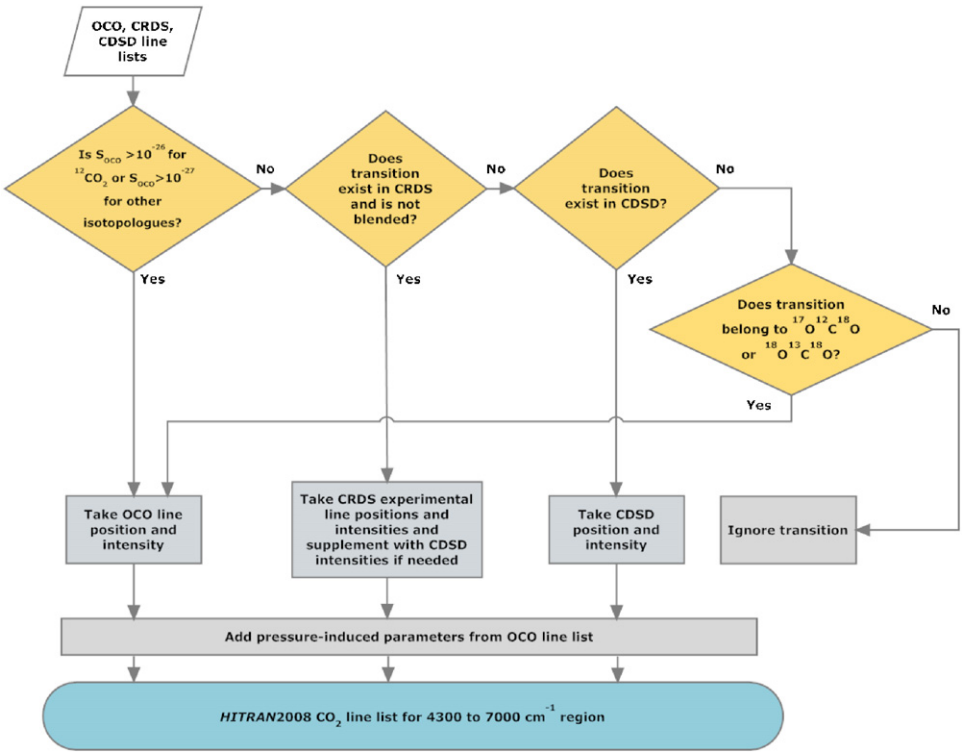

Fig. 1. Flow diagram outlining the assembly of the CO_2 HITRAN2008 line list in the 4300–7000 cm^{-1} region.

7000 cm^{-1} region, which completely replaces HITRAN2004 data in this wavenumber range. In this procedure, the CO_2 transitions that are critical for the OCO mission are always assumed to have superior quality within the FTS detection limit (lines stronger than 10^{-26} cm^{-1}/(molecule cm^{-2}) for the principal isotopologue and 10^{-27} cm^{-1}/(molecule cm^{-2}) for the other isotopologues. For the weaker lines in the 5851–7045 cm^{-1} region, the CRDS line positions are taken, wherever available, and supplemented with CDSD intensities. For the weak lines not present in the CRDS data set (this especially concerns lines below 5851 cm^{-1} and blended lines unobserved by CRDS due to overlapping with stronger lines), the CDSD line parameters were taken. The line positions and intensities for two rare isotopologues, $^{17}O^{12}C^{18}O$ and $^{18}O^{13}C^{18}O$, which are absent in CDSD, have been taken from the CO_2 list generated for OCO.

Finally, the γ_{air}, γ_{self}, n, and δ parameters, available in the OCO data set, have been included in this combined line list. Note that these parameters are slightly different from those listed in the supplementary file of Ref. [57], due to improvements accomplished through the newer work of Predoi-Cross et al. [73].

All combined (mixed) data sets are relatively new. The procedure suggested above is a temporary but necessary solution that has to be tested against atmospheric retrievals. As new, highly accurate measurement data sets become available, this procedure will have to be refined for future updates of the *HITRAN* database.

For the spectral regions below 4300 cm^{-1} and above 7000 cm^{-1} the following improvements have been made to the *HITRAN* database: (1) The four bands above 9650 cm^{-1} that were added to HITRAN2004 were found to have an error associated with an incorrect account of nuclear spin statistics. These bands have now been replaced with the lines from the CDSD databank above 9650 cm^{-1}, which includes several other additional bands. These data are important for the studies of the Venus atmosphere [74]. (2) In HITRAN2004 some of the bands of the principal isotopologue in the 2.8-μm region were based on extrapolations of limited experimental data. For example, the 23301–02201 band (centered at 3555 cm^{-1}) contained 188 lines which were extrapolated from 16 measured lines and the interaction between the vibrational levels 23301 and 12212 was not well accounted for at higher-J values. An analogous problem occurs in the 40002–11102 and the 30001–01101 bands (centered at 3543 and 3557 cm^{-1}, respectively). Thus, the line positions and intensities for these bands were replaced with the ones from the CDSD databank. (3) Recent FTS measurements [75] of the line intensities for the 11112–01101 band of the $^{13}C^{16}O_2$ isotopologue (centered at 3499 cm^{-1}) have shown differences up to 100% compared to HITRAN2004 (the error code in the former *HITRAN* indeed indicated problems for this band). The intensities of this band were previously calculated by the DND method of Wattson and Rothman [76], which did not fully account for perturbations. Therefore, the parameters for this band have been replaced with the ones from CDSD. (4) As was noted by Wang et al. [77], the HITRAN2004 line positions of the 30003–00001 band (at 3857 cm^{-1}) for $^{16}O^{12}C^{18}O$ differ from new experimental ones by −0.1 to 0.1 cm^{-1}. These line positions have now been replaced with line positions calculated using the EH method. (5) Although at this point the high-quality experimental data from Toth et al. [58] have not yet been

included into *HITRAN*, we note the remark in that work that experimental line intensities of the 10012–00001 band for $^{16}O^{13}C^{18}O$ (at 3490 cm^{-1}) differ from those in HITRAN2004 by amounts from −8% to 31%. Now the intensities of these lines have been replaced with those from CDSD, which agree very well with Ref. [58]. (6) In the 11112–11102 band of the principal isotopologue (at 2315 cm^{-1}), all HITRAN2004 line positions with uncertainty code 0 were replaced with the line positions and intensities from CDSD. (7) The intensity cutoff that was applied to earlier editions of the *HITRAN* database for CO_2 has been lowered and is now 4×10^{-30} cm^{-1}/(molecule cm^{-2}). Therefore, weak bands from the CDSD databank that did not appear previously in *HITRAN* [1] have been included in the new edition.

Finally, the parameters for broadening coefficients available from the OCO data set have been applied to all the bands, even outside the OCO spectral region. Although the line-shape parameters have been improved throughout the database, the improvements are only within the formalism of the Voigt line-shape profile, which is known to be inadequate to model the line shape given the precision of modern instruments used in atmospheric retrievals. In addition, the line mixing parameters have not been updated or extended in *HITRAN*, and this is one of the major issues that will be addressed in future updates.

2.3. O_3 (molecule 3)

Monitoring ozone in the atmosphere has been a major issue for two different respects: its deleterious effects in the troposphere as a pollutant and its protective effect in the upper-atmosphere layer. Furthermore, detection of ozone in the atmospheres of exosolar planets might be an indicator of oxygen, which is more difficult to observe spectroscopically.

A major update has been made for the first three isotopologues of ozone, $^{16}O^{16}O^{16}O$, $^{16}O^{16}O^{18}O$, and $^{16}O^{18}O^{16}O$. The line positions, intensities, and lower-state energies correspond to the S&MPO (Spectroscopy and Molecular Properties of Ozone) databank [78]. These results are based on the analyses of the absorption spectra recorded by the GSMA (Groupe de Spectrométrie Moléculaire et Atmosphérique) using the FTS of Reims University [79]. All these data have been published previously and are briefly described below. The list of the bands of $^{16}O^{16}O^{16}O$ included in *HITRAN* for the first time is shown in Table 1. The updated bands are listed in Table 2.

Calculation of the line positions of all bands was made by using Hamiltonian parameters for the lower energy levels from Ref. [96] for the (0 0 0), (1 0 0) and (0 0 1) vibrational states, from Ref. [87] for the (0 1 0) state, and from Ref. [88] for the (0 2 0) state.

The references for the newly included bands are given in Table 1 for the line positions (column 5) and for the line intensities (column 6). An additional detailed description of the improvements in the 2550–2900 cm^{-1} spectral region is given in a recent paper [100].

The upper-state energies of 24 bands listed in Table 2 (except $2\nu_2+2\nu_3-2\nu_2$ and $\nu_1+2\nu_2+\nu_3-2\nu_2$) were calculated using Hamiltonian parameters [89]. The transition moment parameters for the cold bands listed in this table (2590–3400 cm^{-1} spectral range) are given in Ref. [89]. Calculation of the hot-band line intensities was made with the transition moments of Refs. [92,95]. The main term of the dipole transition moment of the $3\nu_3-\nu_1$ band was estimated to be $\mu_1^{(0\,0\,3)\leftarrow(1\,0\,0)}=-1\times10^{-3}$ Debye [97]. The upper-state energies and line intensities of the $2\nu_2+2\nu_3-2\nu_2$ and $\nu_1+2\nu_2+\nu_3-2\nu_2$ bands were calculated using Hamiltonian parameters from Ref. [90] and transition moments from Ref. [95].

The least known part of the mid-infrared ozone ($^{16}O_3$) absorption spectrum is now in the range of 2.45–2.78 μm (3600–4080 cm^{-1}). First of all, the $\nu_2+3\nu_3$ and, especially, $\nu_1+\nu_2+2\nu_3$ bands must be updated in a future edition by the data reported by Bouazza et al. [94] for the 3600–3830 cm^{-1} region. Secondly, the $\nu_1+4\nu_3-\nu_3$ hot band must be taken into account for the 3865–3895 cm^{-1} region. The line positions of this band have been used by Flaud et al. [112] for determination of the rotational energies of the (1 0 4) vibrational state, but the line intensities have not been analyzed. According to an estimate of Barbe and Mikhailenko, the total band intensity $S_v(\nu_1+4\nu_3-\nu_3)$ can be of the order of 20% of $S_v(2\nu_1+\nu_2+\nu_3)$ (see Table 1). Thirdly, the region of the $\nu_1+3\nu_3$, $4\nu_3$, and $3\nu_1+\nu_2$ bands (3900–4080 cm^{-1}) analyzed by Perrin et al. [108] must be revisited. In particular, the R_R branch of the $4\nu_3$ band (4033–4065 cm^{-1}) is not reproduced by current data.

The lower-state energies of both ^{18}O enriched species have been calculated using the Hamiltonian parameters of Ref. [117]. The upper-state energies were calculated with Hamiltonian parameters of Refs. [118,119] for $^{16}O^{16}O^{18}O$ and $^{16}O^{18}O^{16}O$, respectively. Transition moment parameters reported by Barbe and De Backer-Barilly [120] were used for calculations of the line intensities of both species. Tables 3 and 4 list the updates for $^{16}O^{16}O^{18}O$ and $^{16}O^{18}O^{16}O$, respectively.

The new data cover bands in the spectral range 593–5786 cm^{-1}, thereby extending the short wavelength coverage of *HITRAN* as well (from 2.5 to 1.7 μm). The total number of transitions has increased significantly, from 311481 to 409686. In addition, an improved algorithm for incorporating the ozone line-shape parameters has been used for all ozone bands throughout the compilation.

The majority of HITRAN2004 air-broadened half-width parameters of ozone lines and their temperature dependences were calculated using polynomials derived by Wagner et al. [121] separately for the ν_1/ν_2 and ν_3 bands. The polynomials derived for the ν_3 band were applied for all the bands in the database except the ν_1 and ν_2 bands. This has been revised now and the ν_1/ν_2 polynomials from Wagner et al. [121] were used for all B-type bands and the ones from the ν_3 band were used for all A-type bands. For instance, the pure rotational band is a B-type band and the coefficients derived from the ν_1/ν_2 polynomials agree better with the values measured in the pure rotational band (for example with measurements in Ref. [122]) than those from ν_3 polynomials. In addition, a new polynomial was derived for γ_{air} in the B-type bands for the

Table 1
New ozone bands for the principal isotopologue $^{16}O^{16}O^{16}O$.

Band	Spectral range (cm^{-1})	Number of lines	Sum of line intensities (10^{-22} cm^{-1}/(molecule cm^{-2}))	References for line positions	References for line intensities
030–020	593–813	2897	19.640	[80,81]	[82]
121–021	956–991	15	0.004	[83–85]	[86]
030–010	1329–1480	804	0.403	[87,80]	[88]
102–011	1330–1378	210	0.057	[89,90]	[91]
111–020	1346–1409	221	0.090	[81,89]	[91]
201–110	1367–1406	71	0.016	[89,90]	[91]
022–011	1619–1687	660	0.396	[83,90]	[92]
121–110	1622–1678	297	0.096	[83,90]	[92]
031–020	1632–1711	1109	1.734	[81,93]	[92]
130–020	1722–1875	443	0.220	[81,89]	[92]
121–011	1735–1754	42	0.013	[83,90]	[92]
112–110	1886–2034	104	0.039	[90,94]	[95]
130–001	1992–2061	3	0.005	[96,89]	[97]
130–100	2040–2102	10	0.025	[96,89]	[97]
211–011	2043–2149	62	0.017	[90,98]	[95]
003–010	2255–2360	1809	11.908	[87,89]	[84]
102–010	2270–2407	479	0.400	[87,89]	[99]
201–010	2281–2325	11	0.003	[87,89]	[99]
031–010	2333–2407	742	0.474	[87,93]	[90]
130–010	2424–2552	487	0.185	[87,89]	[84]
013–100	2529–2607	659	0.394	[96,94]	[100]
013–001	2602–2724	775	0.455	[96,94]	[100]
022–010	2603–2769	1629	1.729	[87,83]	[89]
112–001	2630–2720	1432	4.414	[96,94]	[100]
112–100	2658–2718	68	0.025	[96,94]	[89]
131–020	2666–2741	899	0.828	[81,101]	[89]
221–110	2673–2727	311	0.102	[90,102]	[89]
121–010	2678–2774	1851	16.465	[87,83]	[89]
211–100	2681–2764	1242	2.522	[96,98]	[89]
211–001	2713–2768	48	0.014	[96,98]	[89]
202–100	3009–3093	365	0.155	[96,103]	[89]
031–000	3032–3111	689	0.417	[96,93]	[93]
202–001	3035–3117	662	0.392	[96,103]	[89]
211–010	3078–3166	876	0.878	[87,98]	[89]
130–000	3133–3249	384	0.126	[96,89]	[89]
022–000	3256–3511	1826	1.225	[96,83]	[83]
121–000	3286–3480	1764	7.430	[96,83]	[83]
131–010	3369–3440	910	0.689	[87,101]	[83]
113–100	3506–3566	466	0.195	[96,104]	[94]
014–001	3525–3605	992	1.306	[96,104]	[94]
014–100	3534–3538	9	0.002	[96,104]	[105]
113–001	3547–3605	11	0.004	[96,104]	[94]
212–001	3704–3755	326	0.102	[96,106]	[107]
221–010	3751–3821	895	0.772	[96,102]	[107]
211–000	3768–3866	1762	12.815	[96,98]	[107]
113–010	3864–3968	1466	4.367	[87,104]	[108]
014–010	3875–3968	183	0.076	[87,104]	[109]
320–010	3888–4000	279	0.173	[87,104]	[109]
202–000	4034–4207	1387	1.100	[96,103]	[103]
131–000	4065–4145	714	0.460	[96,101]	[101]
301–000	4179–4264	1213	2.471	[96,110]	[110]
230–000	4195–4263	14	0.009	[96,110]	[110]
221–000	4444–4525	1066	1.034	[96,102]	[102]
014–000	4522–4700	1998	1.626	[96,104]	[104]
123–010	4531–4600	783	0.649	[87,111]	[111]
330–010	4554–4602	47	0.018	[87,111]	[111]
113–000	4562–4668	1599	8.751	[96,104]	[104]
320–000	4586–4700	587	0.432	[96,104]	[104]
212–000	4700–4845	924	0.412	[96,106]	[106]
141–000	4760–4794	4	0.001	[96,106]	[106]
104–000	4805–4979	977	0.730	[96,112]	[112]
005–000	4807–4957	1579	5.350	[96,112]	[112]
311–000	4808–4952	1203	3.561	[96,112]	[112]
203–000	4997–5085	1086	1.255	[96,113]	[113]
132–000	5028–5085	27	0.014	[96,113]	[113]
123–000	5216–5301	784	0.586	[96,111]	[111]

Table 1 (*continued*)

Band	Spectral range (cm^{-1})	Number of lines	Sum of line intensities (10^{-22} cm^{-1}/(molecule cm^{-2}))	References for line positions	References for line intensities
401–000	5244–5319	896	0.809	[96,111]	[111]
330–000	5252–5302	43	0.015	[96,111]	[111]
024–000	5271–5316	2	0.001	[96,111]	[111]
015–000	5444–5526	947	0.975	[96,114]	[114]
213–000	5625–5705	622	0.344	[96,115]	[115]
420–000	5663–5706	10	0.003	[96,115]	[115]
312–000	5753–5786	14	0.004	[96,116]	[116]
Total		51781	124.407		

Table 2
Updated ozone bands for the principal isotopologue $^{16}O^{16}O^{16}O$.

Band	Spectral range (cm^{-1})	Number of lines	Sum of line intensities (10^{-21} cm^{-1}/(molecule cm^{-2}))
111–100	1613–1849	1271	0.267
012–001	1617–1826	1581	0.640
111–001	1629–1854	1557	0.130
012–100	1637–1706	85	0.004
210–100	1701–2051	1663	0.197
210–001	1719–2066	388	0.015
003–100	1848–2104	1920	1.175
003–001	1867–2098	2847	1.313
102–100	1869–2071	2206	0.426
012–010	1872–2120	3794	3.198
201–100	1888–2243	2831	10.902
201–001	1896–2289	2165	0.328
102–001	1901–2085	2965	15.675
022–020	1921–2067	1046	0.740
121–020	1984–2079	1817	1.424
111–010	1918–2220	3520	42.815
300–100	2021–2288	2508	0.472
210–010	2006–2353	3050	0.838
300–001	2012–2313	1804	0.915
012–000	2590–3025	3886	3.293
111–000	2626–3020	3604	24.909
210–000	2704–3156	3327	0.806
003–000	2906–3202	4512	140.140
201–000	2919–3274	2706	7.854
102–000	2924–3196	4646	12.683
300–000	2955–3398	2445	0.467

Table 3
New ozone bands for the $^{16}O^{16}O^{18}O$ isotopologue.

Band	Spectral range (cm^{-1})	Number of lines	Sum of line intensities (10^{-22} cm^{-1}/(molecule cm^{-2}))
002–000	1903–2143	6004	3.217
111–010	2010–2085	2413	1.334
101–000	2004–2182	8284	44.610
200–000	2020–2266	6117	1.660
111–000	2694–2768	2337	1.023
Total		25155	51.845

Note: The 101–000 band is an update.

cases where $J = K_a$ by fitting the data from Refs. [123,124]. This polynomial was applied to B-type transitions with $J'' \leqslant 12$. In HITRAN2004 a polynomial derived by Flaud et al. [125] was used to calculate γ_{air} for the transitions outside the range of applicability of the Wagner et al. polynomials [121]. These coefficients have been scaled by a factor of 1.05, as it was found that they are underestimated at higher J.

Table 4
New ozone bands for the $^{16}O^{18}O^{16}O$ isotopologue.

Band	Spectral range (cm^{-1})	Number of lines	Sum of line intensities (10^{-22} cm^{-1}/(molecule cm^{-2}))
002–000	1854–2082	3175	1.503
111–010	1962–2049	1375	0.749
101–000	1898–2149	3074	22.771
200–000	2020–2225	2450	0.378
111–000	2654–2739	1300	0.452
Total		11 374	25.853

Note: The 101–000 band is an update.

There is still a long way to go in order to improve the broadening parameters of ozone. This especially concerns the temperature exponents where the experimental measurements rarely agree with each other or with the theoretical calculations.

2.4. N_2O (molecule 4)

Concerning nitrous oxide, it was discovered that two strong P(1) lines (at 578.5261 and 1167.2943 cm^{-1}) were absent from the HITRAN2004 edition. These lines have been restored. In addition, 6 lines of a weak, highly perturbed band (06°0–10°0) around 4.6 μm have been added. Energy levels as well as the lower state levels of the perturbed state, 06°0, were computed from the coefficients given in Ref. [126] and the interaction parameters for intensities are presented in Ref. [127]. Only the strongly perturbed transitions were considered around and including $J = 47$.

2.5. CO (molecule 5)

The line parameters of carbon monoxide have not undergone a revision and remain the same as in HITRAN2004.

2.6. CH_4 (molecule 6)

The need for reliable high-resolution methane parameters throughout the spectrum is driven by many applications. Besides being a major greenhouse gas and absorber in the terrestrial atmosphere, it is a major component of the giant gas planets, (Jupiter, Saturn, Uranus, Neptune) and of the atmosphere of Saturn's main satellite, Titan [128]. It is also prominent in the atmospheres of brown dwarf stars, and has recently been identified by Swain et al. [129] in the atmosphere of an exosolar planet.

The parameters of $^{12}CH_4$ have been updated, and a few new bands of CH_3D were added, but no changes were made to the $^{13}CH_4$ parameters. The minimum intensity limit was set to 10^{-29} cm^{-1}/(molecule cm^{-2}) at 296 K to account for increasing sensitivity in remote-sensing instrumentation. Significant changes were made for γ_{air} between 5800 and 6180 cm^{-1}.

The $^{12}CH_4$ line positions and intensities were revised from 0 to 3300 cm^{-1} using calculated values from the new global analysis by Albert et al. [130] for the three lowest polyads (ground state, dyad from 900 to 1900 cm^{-1} and pentad from 1900 to 3400 cm^{-1}). Fig. 2 shows the polyad scheme for $^{12}CH_4$ and also demonstrates the increasing complexity as one progresses to higher wavenumber. In the far-IR, the intensities of ground-state transitions were adjusted by 16% to match the results of Wishnow et al. [131], but no change was required for the dyad–dyad hotbands. Some predicted pentad positions were replaced by semi-empirical upper-state energy levels obtained by adding calculated lower-state energies to observed positions. Because further intensity analyses are needed to meet required atmospheric remote-sensing accuracies, the semi-empirical *HITRAN* [1] parameters were retained for the hot bands in the dyad and pentad regions (900–3500 cm^{-1}); in the latter interval, a minimum intensity limit of hot bands was 10^{-27} cm^{-1}/(molecule cm^{-2}) at 296 K. For similar reasons, no change was made for the octad (3200–4900 cm^{-1}).

A number of improvements were made to the empirical linelist near 6000 cm^{-1}. First, the intensities and half-widths retrieved by Frankenberg et al. [132] replaced existing values for the 5860–6180 cm^{-1} region. During the format conversion for *HITRAN*2004 [1], the empirical lower-state energies of Margolis [133,134] given previously were corrupted. These values have been restored, and additional values from Gao et al. [135] were added. Misaligned fields in the near-IR quantum numbers were corrected, but only a few new assignments were entered to existing entries. However, weak lines with intensities less than 10^{-24} cm^{-1}/(molecule cm^{-2}) at 296 K are still missing between 5500 and 6180 cm^{-1}.

For broadening parameters, if there were no direct measurements of half-widths and pressure shifts [136,137], then estimated default values for γ_{air}, γ_{self}, n, and δ (similar to those used in *HITRAN* 2000 [138] and 2004 [139]) were used for most of the transitions up to 5860 cm^{-1}; the exceptions were approximately 4000 measured or theoretically predicted broadening coefficients inserted on a line-by-line basis. For the dyad, new measurements of γ_{air}, γ_{self}, n, and δ of about 500

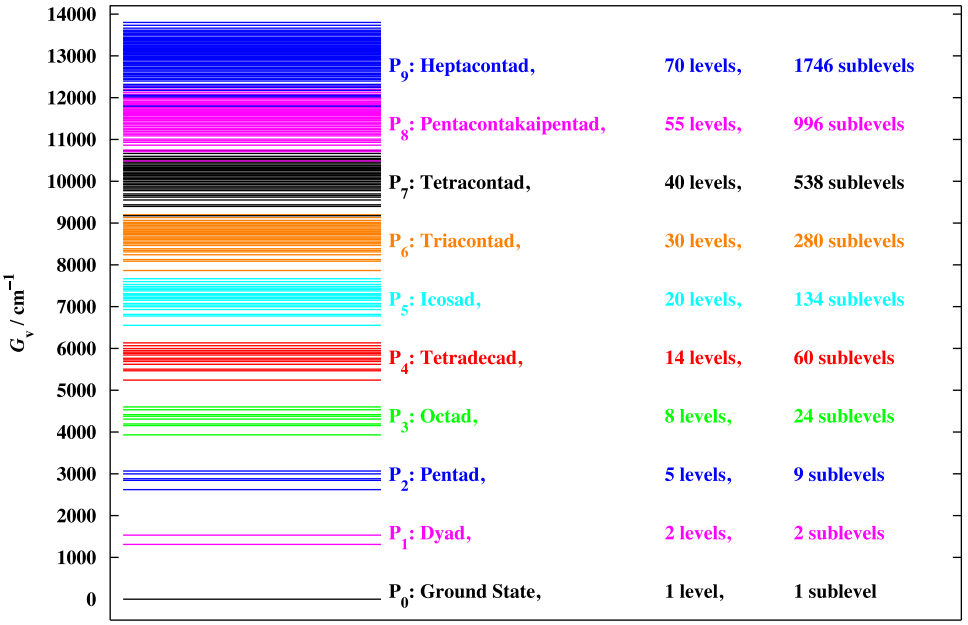

Fig. 2. Polyad energy-level structure for $^{12}CH_4$.

transitions were taken from Smith et al. [140,141]. For the pentad, about 500 prior measurements [138] were used along with approximately 3800 predicted values for γ_{air}, n, and δ of the ν_3 transitions from Antony et al. [142]. Scaled N_2-broadening from Frankenberg et al. [132] were inserted from 5860 to 6184 cm^{-1} and a few hundred values for γ_{air}, were entered between 5560 to 5860 cm^{-1} [143]. The value for the parameter n was set either to a default constant (0.75 below 5860 cm^{-1} or 0.85 above 5860 cm^{-1}) unless direct measurements were available [143].

There are a number of ongoing and recent studies [143,144] which can further improve the near-IR parameters (4800–7700 cm^{-1}). It is expected that an interim update of this region and a new semi-empirical list of the octad will be available within one year. Finally, the list described here is tailored for Earth remote sensing and will be inadequate to interpret high-temperature spectra (e.g. [145]). More extensive calculation of weaker transitions and partition functions [146] can be found at http://icb.u-bourgogne.fr/OMR/SMA/SHTDS. As usual, the predicted values beyond the range of measurements are expected to become very inaccurate because of extensive rovibrational interactions.

Most of the parameters for the monodeuterated form of methane, CH_3D, were retained from HITRAN2004. For the 2008 modifications, the positions and intensities of the far-IR (rotational) transitions were replaced with improved predictions, and a total of nine new bands were added at three different wavelengths (8, 2.9 and 1.56 μm). The far-IR prediction, based on the frequency analysis of Lattanzi et al. [147], was obtained from the *JPL* and Cologne Molecular Spectroscopy databases [148,149]. Because $^{13}CH_3D$ was detected in Titan's atmosphere [150], this species was added to the database for the first time. The prediction of the $^{13}CH_3D$ triad (ν_6, ν_3 and ν_5) near 8 μm used a program written for C_{3v} molecules by Tarrago and Delaveau [151]. This prediction was based on the position analysis by Ulenikov et al. [152] and employed the transition-moment parameters of the $^{12}CH_3D$ isotopologue from Brown et al. [153]. Six new $^{12}CH_3D$ vibrational bands were also added in the near-IR, using the analyzed positions and line intensities of $\nu_2+\nu_3$, $\nu_2+\nu_5$, $\nu_2+\nu_6$, $\nu_3+2\nu_6$ and $3\nu_6$ at 2.9 μm by Nikitin et al. [154] and empirical measurements of $3\nu_2$ at 1.56 μm reported by Boussin et al. [155]. The values for γ_{air} and γ_{self} were generally obtained using empirical formulae obtained from $^{12}CH_3D$ triad measurements [1,156]. However, γ_{air}, γ_{self}, and δ values observed by Boussin et al. [155] were used for $3\nu_2$. The temperature dependence of the half-widths, n, was crudely estimated in all bands using CH_4 values averaged by J [1]. The new mid- and near-IR parameters are considered to be preliminary and so rather conservative accuracies were set; this certainly indicates that additional laboratory and theoretical studies are needed.

2.7. O_2 (molecule 7)

The line positions, intensities, and pressure-broadening parameters (γ_{air}, γ_{air}, and δ) of the oxygen A-band ($b^1\Sigma_g^+ \leftarrow X^3\Sigma_g^-$) near 13100 cm^{-1} were modified for all three isotopologues ($^{16}O_2$, $^{16}O^{18}O$, and $^{16}O^{17}O$). The $^{16}O_2$ line positions and pressure shifts in HITRAN2004 in this region were replaced with values from Robichaud et al. [157] and intensities and the self- and air-broadened half-widths from Robichaud et al. [158]; these measurements obtained for the P branch using cavity ringdown spectroscopy [159] were extrapolated to the R branch. The value of the temperature

dependence of half-widths from Brown and Plymate [160] was retained, however. The positions and intensities of the two minor oxygen species were taken from Robichaud et al. [161]. For all three species, the half-widths were computed with the empirical formula derived from Yang et al. [162],

$$\gamma = A + B1 + c_1 J' + c_2 J'^2 + c_3 J'^4 \quad (1)$$

using the $^{16}O_2$ constants from Table 6 of Robichaud et al. [158]. The measured values of δ of the $b^1\Sigma_g^+ \leftarrow X^3\Sigma_g^-$ band were taken from Robichaud et al. [157] for the P Branch, but averages of shifts from Predoi-Cross et al. [163] were used for the R branch.

These modifications improve the accuracies of the parameters in several different aspects. The positions are now referenced to atomic potassium calibration standards [164], resulting in accuracies of 0.00006 cm^{-1} or better for $^{16}O_2$ and $^{16}O^{18}O$, and 0.0005 cm^{-1} for $^{16}O^{17}O$. The differences between HITRAN2004 and new positions are relatively small for the main and least abundant species (0.0007 cm^{-1} for $^{16}O_2$ and 0.002 cm^{-1} for $^{16}O^{17}O$), but much larger for $^{16}O^{18}O$ (up to 0.20 cm^{-1}); counter to the description given for HITRAN2004, the $^{16}O^{18}O$ positions were not updated in that edition, and the $^{16}O^{18}O$ upper-state levels were still based on results from 1948 [165]. Line intensities are only slightly different: −0.8% for $^{16}O_2$, +1% for $^{16}O^{18}O$, and ±5% for $^{16}O^{17}O$ (depending on the rotational quanta) [161]. The accuracies for intensities are thought to be ±1% or better for the first two species, but more analysis is needed for $^{16}O^{17}O$. For the half-widths, the values at high quantum numbers ($J>22$), previously in error by more than 40% near $J=30$, are now thought to be accurate to ±2%. Pressure shifts, however, are still rather uncertain (±0.003 cm^{-1}) because values from different studies do not agree (e.g. see Fig. 4 in Robichaud et al. [157] and the discussions in Predoi-Cross et al. [163,166]).

It should be emphasized that even with these improvements, the line parameters are not sufficient to reproduce atmospheric observations at 13,100 cm^{-1} because Voigt line shapes are inadequate. Tran and Hartmann [167] and Predoi-Cross et al. [163,166] have demonstrated the need to apply line mixing (and perhaps speed dependence) to the *A*-band. It is thus recommended that these improved line parameters be combined and tested with line-mixing results from Refs. [163,166,167].

The $a^1\Delta_g \leftarrow X^3\Sigma_g^-$ band at 1.27 μm has not been updated in some time. This band is very important partly because it is being used as a benchmark in some remote-sensing applications. A new line list is described in Washenfelder et al. [168] which is based on laboratory measurements published by Newman et al. [169,170]. These data will be considered for an impending update.

Finally, it was discovered that due to a programming error, some of the Einstein *A*-coefficients and statistical weights for oxygen in HITRAN2004 were in error; they have been recalculated.

2.8. NO (molecule 8)

The Einstein *A*-coefficients and statistical weights were recalculated for the three isotopologues in *HITRAN*, due to a programming error in HITRAN2004. In the process, it was noted that hyperfine splitting for the microwave and far infrared lines was not included in the HITRAN2004 edition. To include hyperfine spitting for the principal isotopologue, $^{14}N^{16}O$, we have adapted data generated in the course of work summarized in Goldman et al. [171]. These data also include magnetic-dipole transitions between spin components of the ground electronic state, previously absent in *HITRAN*. The magnetic-dipole transitions obey different parity selection rules and have been identified by the letter "m" in the first field for upper-state rotational quantum numbers in the *HITRAN* database.

In addition, we included lines with resolved hyperfine structure from the *JPL* catalog [148] if these lines were not available from Ref. [171].

2.9. SO_2 (molecule 9)

Because of its presence in interstellar clouds and in the atmosphere of Venus, sulfur dioxide is well known to be both of astrophysical and planetary importance. In the terrestrial atmosphere, SO_2 is produced by both anthropogenic and natural sources, and is responsible for the production of acid rain. Strong volcanic eruptions, such as the Mount Pinatubo eruption in the Philippines in June 1991, can deposit a large amount of SO_2 in the atmosphere. Once in the stratosphere, sulfur dioxide is converted into sulfate aerosols which affect both stratospheric chemistry and climate. The HITRAN2004 database [1] provided SO_2 parameters in seven different spectral regions, which correspond to transitions within the ground vibrational state, and the 19.3- , 8.6- , 7.3- , 4- , 3.7- and 2.5-μm spectral regions. However, as stated in Ref. [1], there were considerable differences in the 19.3-, 8.6- and 7.3-μm spectral regions between HITRAN2004 and published papers [172–175]. The 8.6- and 7.3-μm regions are important for atmospheric detection of SO_2. The 7.3-μm region corresponds indeed to the strongest SO_2 infrared band but unfortunately it has the disadvantage of being overlapped with the strong ν_3 band of water vapor, preventing measurements of SO_2 in this infrared region from the ground. On the other hand, the ν_1 band, although about nine times weaker than ν_3, corresponds to a rather clear atmospheric window. Finally the 19.3-μm region can be used for retrieving SO_2 in the atmosphere of planets.

For all these reasons it was decided to generate a new line list based on the recent published results. It includes not only the cold bands ν_2, ν_1, and ν_3 but also the corresponding hot bands $2\nu_2-\nu_2$, $3\nu_2-2\nu_2$, $\nu_1+\nu_2-\nu_2$ and $\nu_3+\nu_2-\nu_2$ as well as the ν_3 band of $^{34}SO_2$.

As far as the air-broadened parameters are concerned, a survey of the literature [176–178] has shown that it was only possible to estimate an average value for this parameter. In fact no variation of this parameter with respect to the lower quantum numbers J or K_a of the transitions could be determined. As an example, Fig. 3 shows the measured parameters with respect to the lower quantum numbers K_a of the transitions. It is clearly difficult to derive any clear variation (the same is true when these parameters are plotted versus the quantum number J) so only an average value of $0.1025\,cm^{-1}\,atm^{-1}$ could be determined.

The situation is completely different for the self-broadening parameters since many measurements spanning a wide range of quantum numbers J and K_a are available [176,177,179–182]. While no variation with respect to the quantum number J could be determined, a clear variation with respect to the quantum number K_a could be observed as shown in Fig. 4. Following these results, it was decided to include in the database the following values for γ_{self} (in HITRAN2004 in general a fixed value of $0.4\,cm^{-1}\,atm^{-1}$ was used): $\gamma_{self} = 0.4\,cm^{-1}\,atm^{-1}$ for $K_a \leqslant 5$, $\gamma_{self} = 0.156\,cm^{-1}\,atm^{-1}$ for $K_a \geqslant 21$, and γ_{self} calculated through a linear interpolation for $6 \leqslant K_a \leqslant 20$.

The accuracy for line positions is estimated to be better than $0.001\,cm^{-1}$. For line intensities, it is estimated to be on the order of 2–3%, degrading up to about 15% for high J or K_a transitions. Finally, an accuracy of 10–15% for γ_{air} and γ_{self} seems a reasonable estimate. Note that for consistency the new broadening parameters have been used for all the SO_2 lines included in the *HITRAN* database since in the previous version different values, the origin of which is not immediately

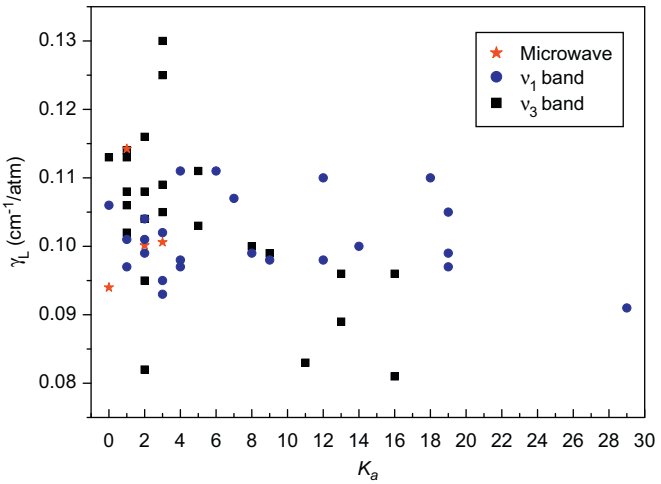

Fig. 3. $^{32}SO_2$ air-broadened half-width parameters.

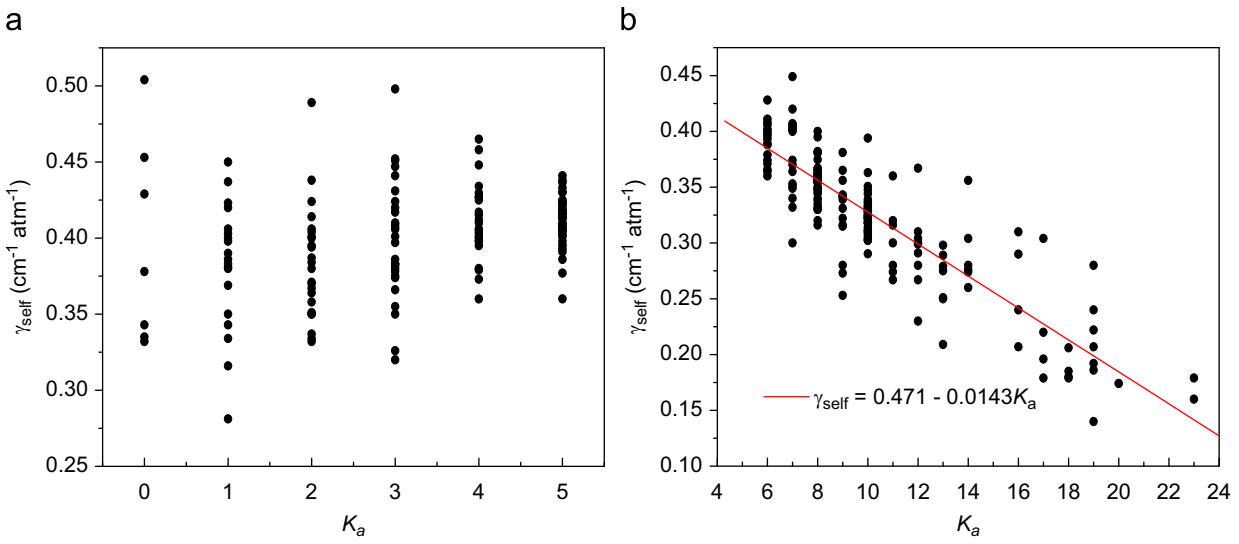

Fig. 4. SO_2 self-broadened half-width parameters: (a) for $K_a \leqslant 5$ and (b) for $K_a \geqslant 6$.

transparent, were used. Also a "standard" value of 0.75 has been used for the temperature-dependence of the air-broadened half-width parameter, *n*.

It is worth noticing that recently a series of papers [183–185] has been devoted to the high-resolution study of the absorption of the $^{34}SO_2$ isotopologue in the infrared. They will provide in the future much better spectral parameters which should be included in a future *HITRAN* database.

2.10. NO_2 (molecule 10)

Unchanged.

2.11. NH_3 (molecule 11)

Unchanged.

2.12. HNO_3 (molecule 12)

Using new and accurate experimental results concerning line positions and line intensities as well as sophisticated theoretical methods, it has been possible to generate an improved set of line positions, line intensities, and line-shape parameters for the nitric acid molecule in the infrared spectral region. The present update was performed in two steps described in Refs. [186,187], respectively.

The first study [186] was performed in the 820–1770 cm^{-1} spectral range covered by the Michelson Interferometer for Passive Atmospheric Sounding (*MIPAS*) instrument and the results of this first update are summarized in Table 5 of Ref. [186]. The line positions have been improved for the ν_5 and $2\nu_9$ cold bands and the $\nu_5+\nu_9-\nu_9$ hot band around 11.2 μm, and for the $\nu_8+\nu_9$ and $\nu_6+\nu_7$ bands around 8.3 μm (see details in Refs. [186,188] and in the references therein). In addition, the line intensities were updated in the 11.3-, 8.3- and 7.6-μm spectral ranges by making use of the cross-section measurements performed in Ref. [189]. Finally the air-broadened half-width parameters were updated using an empirical law describing the rotational dependence of these parameters.

The results of the second update are described in Table 1 of Ref. [187]. At 11.3 μm, approximate parameters for the $\nu_5+\nu_7-\nu_7$ and $\nu_5+\nu_6-\nu_6$ hot bands have been added for the first time to the line list. The intensities for the ν_6 and ν_8 bands centered at 646.826 and 763.154 cm^{-1}, respectively, were decreased by about 20–30% as compared to the previous *HITRAN* version [1]. Also following recent line-broadening calculations [190], a complete update of the γ_{air} parameters was performed in the 11-μm region. It is to be noticed that the γ_{air} parameters implemented in the narrow Q branches of the ν_8 and $\nu_5+\nu_9-\nu_9$ bands at 763.154 and 885.425 cm^{-1}, respectively, account empirically for line-mixing effects as evidenced by laboratory measurements.

The validation of these updates in the new line list was performed during several satellite, ground-based or balloon-borne measurement of atmospheric HNO_3 [186,191,192]. Furthermore, the microwave line intensities, which were overestimated by ~30% [191], have been updated using the newer HNO_3 listing in the *JPL* catalog [148].

Future studies should concentrate on the improvements of HNO_3 line parameters in several spectral regions:

1. The far infrared region needs a revision. Indeed the present line list which is derived from a 2004 version of the JPL catalog includes only transitions within the ground vibrational state. The updated line list should also include rotational transitions within the first vibrational states of HNO_3 [193,194].
2. In HITRAN2004 [1], the $\nu_5-\nu_9$ and $2\nu_9-\nu_9$ hot bands were added to the existing ν_9 line list in the 22-μm region. In Ref. [194], the hot bands intensities were scaled with respect to the ν_9 intensity from Sirota et al. [195]. The net result is that there could be an inconsistency between the intensities of these two hot bands and the intensity of the ν_9 band since this last band intensity was scaled using the work of Goldman et al. [196]. Indeed, the ν_9 intensities in Ref. [195] are about 28% weaker than the intensity reported in Ref. [196]. Therefore, it is clear that new line intensity data are needed for HNO_3 in the 22-μm region.
3. The 7.6-μm region, which corresponds to the ν_3 and ν_4 bands located at 1325.7354 and 1303.5182 cm^{-1}, respectively, needs significant updates in term of line positions and intensities. The previous studies in this region [197] did not consider resonances due to several dark states which perturb the 3^1 and 4^1 energy levels.

Future updates in the 11-μm region should include the linelist for the $H^{15}NO_3$ isotopologue of nitric acid [198], which is the second-most abundant isotopic variant with a concentration of 3.7‰ in relative concentration. This isotopologue was first detected in MIPAS/ENVISAT atmospheric spectra [199]; it has significance in the determination of the atmospheric profile of the nitrogen isotopes.

Table 5
J_{max} values for OH term values.

Vibrational level	J_{max} Ref. [201]	J_{max} HITRAN2004	J_{max} HITRAN2008
0	49.5	45.5	45.5
1	47.5	45.5	45.5
2	46.5	44.5	44.5
3	44.5	44.5	44.5
4	36.5	44.5	36.5
5	22.5	44.5	22.5
6	23.5	44.5	23.5
7	23.5	42.5	23.5
8	17.5	40.5	17.5
9	18.5	38.5	18.5
10	16.5	35.5	16.5

2.13. OH (molecule 13)

Following the work of Colin et al. [200], Bernath and Colin [201] have reanalyzed all the published experimental data for the electronic ground state of the hydroxyl radical, to which they added a pure rotational constants of the $v = 4$ level determined from a solar spectrum [201]. They produced a new set of term values for $v = 0,\ldots,10$, extrapolated to five J values above the last observed one.

These results were used to revise all the OH transitions (where hyperfine structure was not resolved) in the *HITRAN* database with updated positions and ground-state energy values. However, the line list has been reduced to lower J_{max} values, thus eliminating high-J extrapolations used in the work [202] upon which *HITRAN* was previously based (see Table 5). The new (unextrapolated) term values [201] agree with the observed data within the experimental error. All the other line parameters were kept the same.

A small format change for the quantum numbers has been made that now shows both the upper and lower Λ-doubling e and f parity labels instead of only the lower label (we found that in some publications only the upper state is listed, not the lower state as used in *HITRAN*). The lines with hyperfine splitting listed in *HITRAN* remain unchanged.

Due to a programming error in HITRAN2004, the Einstein A-coefficients and statistical weights have been recalculated for all OH lines in the new database. Also, it was found that there were mistakes in parity assignments (e and f) in the pure-rotation bands in HITRAN2004; these have now been corrected.

2.14. HF (molecule 14)

Unchanged.

2.15. HCl (molecule 15)

It was mentioned quite some time ago by Rinsland et al. [203] that the hydrochloric acid line positions in previous editions of *HITRAN* were lacking accuracy, especially when compared to experiments at higher rotational lines. The line positions of all HCl bands in *HITRAN* have now been recalculated using the most recent complete set of constants from Coxon and Hajigeorgiu [204]. The new line positions are in excellent agreement with available experimental measurements. An effort is planned to extend the number of bands of HCl in *HITRAN* and increase the coverage in J.

2.16. HBr (molecule 16)

Unchanged.

2.17. HI (molecule 17)

Unchanged.

2.18. ClO (molecule 18)

The Einstein A-coefficients in the HITRAN2004 data set for chlorine monoxide were found to be $\frac{1}{4}$ of the correct values; this is now corrected.

The microwave region has been updated with the latest data from the *JPL* catalog [148], which includes rotational transitions within the first vibrational state, $v = 1$, for both isotopes of chlorine, previously unavailable in *HITRAN*. The total number of lines of ClO is now 11,501, as compared to 7230 in HITRAN2004.

The parameters γ_{air} and n for the pure-rotational transitions have been revisited. In HITRAN2004, the default values of $0.085\,cm^{-1}\,atm^{-1}$ for γ_{air} and 0.5 for n were used for all pure rotational transitions. We have now adopted values based on the $J' = 5.5 \leftarrow J'' = 4.5$, $J' = 13.5 \leftarrow J'' = 12.5$, and $J' = 17.5 \leftarrow J'' = 16.5$ transitions measured by Oh and Cohen [205] and Bauer et al. [206]. For all other transitions with $J'' < 20.5$, we used linear extrapolation of the above measurements:

$$\gamma_{air} = 0.09206 - 0.00111J'', \tag{2}$$

$$n = 0.5259 + 0.01768J''. \tag{3}$$

Although this represents a rough approximation, it was deemed better than a constant value, especially for the case of temperature dependence where the previous default value of 0.5 was somewhat low. For all transitions with $J'' \geqslant 20.5$, default values of $0.075\,cm^{-1}\,atm^{-1}$ and 0.6 were used for γ_{air} and n, respectively.

2.19. OCS (molecule 19)

In the HITRAN2004 edition, the intensities of the v_3 band of the principal isotopologue (the region around 5 μm) were increased by 15.79% to match the average of the measurements reported by Régalia-Jarlot et al. [207] and Vander Auwera and Fayt [208]. However, for the sake of consistency, such a scaling should also have been applied to the other $\Delta v_3 = 1$ transitions. They are the hot bands of v_3 involving v_1, v_2 and $2v_2$ of the $^{16}O^{12}C^{32}S$, $^{16}O^{12}C^{34}S$, $^{16}O^{12}C^{33}S$, and $^{18}O^{12}C^{32}S$ isotopologues (622, 624, 623, and 822 in the old AFGL abbreviation), and the v_3 band of $^{16}O^{12}C^{34}S$, $^{16}O^{12}C^{33}S$, and $^{18}O^{12}C^{32}S$. This situation has been corrected in the current edition. The line intensities of the v_3 fundamental of $^{16}O^{13}C^{32}S$ in HITRAN2004 were found to agree within 5% with the measurements of Vander Auwera and Fayt [208]. They were therefore not changed.

Compared to the HITRAN2004 database, which gave about 1100 OCS transitions in the 3800–4200 cm^{-1} region for seven bands ($2v_3$ of the five isotopologues and the $v_2+2v_3-v_2$ of $^{16}O^{12}C^{32}S$ and $^{16}O^{12}C^{34}S$), substantial updates were made for 2008. The new database now includes 10,425 transitions of 51 bands involving the five isotopologues $^{16}O^{12}C^{32}S$, $^{16}O^{12}C^{34}S$, $^{16}O^{13}C^{32}S$, $^{16}O^{12}C^{33}S$, and $^{18}O^{12}C^{32}S$. Of these, two are forbidden bands, 15 are allowed cold bands arising from the ground state, and the remaining 34 are hot bands arising from various vibrational states.

The line positions in this region were calculated using the effective rovibrational energy constants based on the global analysis [209–213]. Although the accuracy in line position was reported to be $5 \times 10^{-5}\,cm^{-1}$ [209], conservative values for the *HITRAN* uncertainty criteria were assigned, depending on J value and line intensity.

Intensities were taken from new FTIR measurements [214,215] performed at JPL to support Venus studies. Sung et al. [214] measured line intensities of the $2v_3$ band at 4101.387 cm^{-1}, $v_1+2v_2+v_3$ at 3937.421 cm^{-1}, and $4v_2+v_3$ at 4141.212 cm^{-1} of $^{16}O^{12}C^{32}S$. The new $2v_3$ band intensity of $6.315(13) \times 10^{-19}\,cm^{-1}/(molecule\,cm^{-2})$ for 100% abundance of $^{16}O^{12}C^{32}S$ was within 1.3% of the average of two earlier measurements, $6.528(96) \times 10^{-19}$ and $6.27 \times 10^{-19}\,cm^{-1}/molecule\,cm^{-2}$, respectively, by Bermejo et al. [216] and Naïm et al. [209]. The band intensities corresponding to 100% abundance of isotopologue $^{16}O^{12}C^{32}S$ for the $v_1+2v_2+v_3$ and $4v_2+v_3$ bands were also in similar agreement (1%) with those from Naïm et al. [209]. Intensities of all the other 43 bands of the five isotopologues in this region were taken from the exhaustive work by Toth et al. [215], in which many bands were measured for the first time. Uncertainties of the line intensities in this region were adopted from measurement precisions, which range from 1% to 6% depending on the bands. However, conservative values coupled with evaluation depending on the line intensities were assigned for the *HITRAN* uncertainty criteria. The line intensities vary through five orders of magnitude, but very weak unassigned features were omitted from the database pending further analysis.

The γ_{self} in the pure-rotation band have been updated using a recent improvement [217] to the work of Matton et al. [218], while γ_{air} and γ_{self} in the rest of the database have been updated using a Padé approximation from Ref. [219]. Air-pressure induced frequency shifts, δ, for OCS were given for the first time based on the $2v_3$ work of Domenech et al. [220].

A separate file, with CO_2-broadened half-widths rather than γ_{air}, based on the measurements of Bouanich et al. [221] in the v_1 band of OCS, is available from the authors [214,215] on request. This second database is intended to support remote sensing of Venus at 2.5 μm.

2.20. H_2CO (molecule 20)

For formaldehyde, the major update in the infrared region for the line positions and line parameters involved the complete replacement of the line list at 3.6 μm and the addition of a list at 5.7 μm [222]. Indeed both spectral regions are now used for the infrared measurements of this molecule in the atmosphere [223,224]. The 5.7-μm region corresponds to the v_2 band together with three dark bands. In the 3.6-μm region, the lines belong to the v_1 and v_5 bands together with nine dark bands.

The line positions were generated using the models and the parameters described in detail in Refs. [225–227] for the 5.7- and 3.6-μm regions, respectively. In addition, a consistent set of line intensity parameters was generated [222] for both

the 5.7- and 3.6-μm spectral regions using high-resolution Fourier transform spectra recorded for the whole 1600–3200 cm^{-1} spectral range. The calculated band intensities derived for the 5.7- and 3.6-μm bands are in excellent agreement with the values achieved recently by medium resolution band intensity measurements [228–230].

Details giving the description of the new database which involves 3713 and 31,796 transitions at 5.7 and 3.6 μm, respectively, are given in Table 9 of the accompanying paper [222]. As compared to the HITRAN2004 line list, which involves only 1161 lines at 3.6 μm, the quality of the line parameters is significantly improved in terms of the positions and intensities.

A subsequent and complementary study dealing with measurements and calculations of formaldehyde self- and N_2-broadened half-width parameters is in progress.

2.21. HOCl (molecule 21)

Unchanged.

2.22. N_2 (molecule 22)

Improvements to the *HITRAN* molecular nitrogen line parameters include intensities and half-widths. The new intensities are based on the work of Goldman et al. [231], which used a semi-empirical Herman–Wallis formulation of the vibration–rotation effects on the intensities with a final scaling based on observed spectra, and the work by Li and LeRoy [232] who used ab initio methods. The values derived by Li and LeRoy [232] are very similar to those of Goldman et al. [231]. However, it can be expected that the Herman–Wallis formulation of Goldman et al. yields less accurate values with increasing J, and thus the ab initio matrix elements of Ref. [232] have been adopted for the *HITRAN* line listing. It should also be noted that the *HITRAN* database is presently limited to only the (1–0) N_2 band; Li and LeRoy [232] can provide line parameters for other bands that may be of atmospheric importance. Li and LeRoy estimate that their intensities have an absolute accuracy of about 1% and their new values are still being validated.

The new half-widths are based on available experimental and theoretical studies as described in Ref. [231]. Further extensions are anticipated in the near future [231].

2.23. HCN (molecule 23)

The air-broadened half-width parameters have been recalculated using a polynomial expression derived in Ref. [233] by fitting together parameters from ν_1 [234], ν_2 [235] and pure rotational [233] bands. This polynomial provides better prediction of γ_{air} for the lines involving higher-lying rotational states. The new polynomial was applied for all the lines with $|m| \leqslant 40$ (the previous polynomial used in HITRAN2004 was applicable only up to $m = 29$). The lines with $|m| > 40$ were assigned a constant half-width parameter of 0.0518 $cm^{-1}\,atm^{-1}$, which corresponds to the new polynomial value at $|m| = 40$.

2.24. CH_3Cl (molecule 24)

In the region from 650 to 2650 cm^{-1} HITRAN2004 data have been completely replaced with lines from the work of Nikitin et al. [236]. The line positions in this list are based on the significantly larger (than previously used) experimental information from cold and hot bands. The standard deviation of about 3×10^{-4} cm^{-1} is close to the experimental precision including perturbed series which were treated separately in previous works. The use of monoisotopic samples synthesized in Ref. [236] was a major advantage. The line intensities are based on the approximate dipole moment parameters as no precise analyses on the transition intensities have been carried out yet. Further intensity work is desirable. However, the most pressing need for ground-based observations is a complete analysis of the 3.3 μm region where weak CH_3Cl features are routinely encountered.

Note that there are four duplicate lines present in the new data set. These are in fact different lines but in some cases (perturbed hot-band levels) the traditional quantum assignments based on approximate quantum numbers become ambiguous. The line-shape parameters were filled in the same way as in HITRAN2004.

2.25. H_2O_2 (molecule 25)

The earlier hydrogen peroxide data previously reported in *HITRAN* for the ν_6 band in the 7.9-μm region have been completely replaced, leading to improved line positions and intensities. The previous version of the H_2O_2 line list in the spectral range of the ν_6 band involved only the two main torsional components of the ν_6 band (in the $n = 0$, $\tau = 1$ and $n = 0$, $\tau = 3$ torsional quantum numbers), and the line positions were not always accurate. The new list is more precise in terms of line positions because the numerous resonances coupling the energy levels from the $\nu_6 \leftrightarrow \nu_2$, $\nu_6 \leftrightarrow \nu_3$, and $\nu_6 \leftrightarrow$ ground interacting torsion–vibrational states have now been taken into account [237]. The present linelist is also more complete since it includes several hot torsion–vibration subbands of the ν_6 band (up to the $n = 2$ torsional quantum numbers),

together with contributing lines from the dark ν_2 and ν_3 torsion–vibration bands. As a result, the new linelist contains many more lines (126 983 instead of 100 781) than the previous one.

In addition, the line intensities of the ν_6 band have been determined more accurately than the torsion–rotation bands [238].

2.26. C_2H_2 (molecule 26)

In the period after the release of HITRAN2004, new bands of acetylene were added to *HITRAN* in the 2.5- and 3.8-μm regions. The parameters (line positions and intensities) are from the work of Lyulin et al. [239] and Jacquemart et al. [240], respectively.

Updates have also been included for the $^{12}C_2H_2$ isotopologue: spectroscopic data have been noticeably enhanced in nine spectral regions, namely, in the regions around 3, 2.2, 1.9, 1.7, 1.5, 1.4, 1.3, 1.2, and 1 μm. Among these regions, only those data at 3 and 1.5 μm were partially reported in the *HITRAN* database. The new line lists are described in detail in Refs. [241,242]. Corrections of the updates of *HITRAN* for the 2.5- and 3.8-μm spectral regions of $^{12}C_2H_2$ have also been performed and described in Ref. [241]. Table 6 summarizes the number of bands and transitions of the spectral regions now available in the new *HITRAN* database, together with the intensity ranges and spectral domains. Fig. 5 is a plot of the $^{12}C_2H_2$ lines now available in *HITRAN* and illustrates the noticeable improvement the new data bring to the database, especially in extending the coverage of the database towards shorter wavelengths.

These data summarize the improvements in current experimental spectroscopic knowledge on acetylene. Several of the spectral regions involved are of atmospheric, planetary, astrophysical, and metrology interest (e.g. at 3, 2.2, 1.5, and 1 μm). A study of the 7.7-μm region, very useful for astrophysics applications, is in progress. For example, the acetylene molecule has been observed in the circumstellar envelopes of carbon-rich stars. Using the Infrared Spectrograph (*IRS*) on board the Spitzer Space Telescope (*SST*), Matsuura et al. [243] detected acetylene bands at 7 and 14 μm in carbon-rich asymptotic giant branch stars in the Large Magellanic Cloud. Around 7 μm, *HITRAN* only contains line positions and intensities that Vander Auwera calculated from his absolute measurements in the $(\nu_4+\nu_5)^0_+$ band [244], for the rotational quantum number J up to 35. But intensities measured in Ref. [244] for some lines of the $(\nu_4+\nu_5)^2$ band are not reported in the database. The temperature of interest for applications being around 500 K [243], the knowledge of intensities in the remaining hot bands is also important. In the quoted paper [243], Matsuura et al. could not reproduce the spectra that they observed in their *IRS-SST* observations around 7 μm because of the lack of data in *HITRAN*.

In addition, some values of the temperature-dependence exponents that were inadvertently set to zero in HITRAN2004 have been set to a default value of 0.75. The total number of lines for C_2H_2 has more than tripled, increasing from 3517 to 11 340.

Table 6
Summary of the bands and transitions now available for the $^{12}C_2H_2$ molecule.

Spectral region (μm)	Number of bands[a]		Number of transitions[a]		Spectral range (cm^{-1})	Intensity range (cm^{-1}/(molecule cm^{-2})) at 296 K
	Cold	Hot	Cold	Hot		
13.6[b]	1	5	150	1038	604–870	10^{-18}–10^{-26}
7.7[b]	1	0	71	0	1248–1415	10^{-19}–10^{-22}
5[b]	3	15	283	1212	1810–2255	10^{-22}–10^{-25}
3.8[c]	2	3	90	331	2499–2769	10^{-21}–10^{-25}
3[b]	2	0	125	0	3204–3359	10^{-19}–10^{-21}
3[d]	0	18	77[e]	1971	3139–3398	10^{-20}–10^{-26}
2.5[c]	4	5	450	720	3762–4226	10^{-21}–10^{-27}
2.2[d]	4	4	254	392	4421–4798	10^{-22}–10^{-25}
1.9[d]	7	0	539	0	5032–5567	10^{-24}–10^{-26}
1.7[d]	2	4	175	350	5692–6032	10^{-23}–10^{-26}
1.5[b]	2	2	129	224	6448–6685	10^{-20}–10^{-24}
1.5[d]	4	16	200	1443	6277–6865	10^{-23}–10^{-28}
1.4[d]	4	0	347	0	7042–7476	10^{-22}–10^{-25}
1.3[f]	1	0	51	0	7671–7791	10^{-25}–10^{-24}
1.2[f]	2	0	132	0	8407–8612	10^{-26}–10^{-23}
1.0[f]	3	1	193	108	9516–9890	10^{-25}–10^{-22}

[a] $^{12}C^{13}CH_2$ data are not in this table.
[b] HITRAN2004.
[c] *HITRAN* updates of 2007.
[d] New data from Ref. [241].
[e] New high-J lines added to the two cold bands already present in HITRAN2004.
[f] New data from Ref. [242].

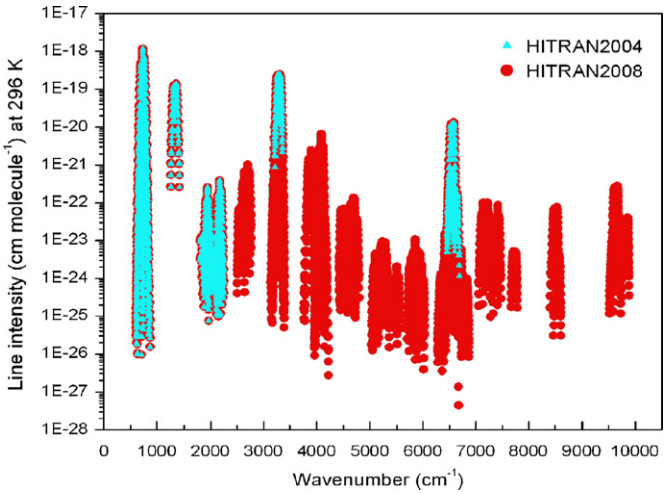

Fig. 5. Extension of data now available in *HITRAN* for the $^{12}C_2H_2$ isotopologue of acetylene.

2.27. C_2H_6 (molecule 27)

The data for the ν_9 fundamental band of $^{12}C_2H_6$ in the 12-μm region, introduced with the 1982 edition of HITRAN [245], have been completely replaced with a new line list including the ν_9, $3\nu_4$, $\nu_9+\nu_4-\nu_4$, and $\nu_9+2\nu_4-2\nu_4$ bands. It was generated by Vander Auwera et al. [246] using a spectrum of the ν_9 band recorded at the Pacific Northwest National Laboratory [228], and results from a global analysis of data involving the four lowest vibrational states of ethane [247] and measurements of pressure-broadening parameters [248,249]. Note that the quantum number notation for representing rotation–torsion states has been converted to *HITRAN* formalism. In Ref. [246], the levels are identified by the quantum numbers J, associated with the total angular momentum of the molecule, K, its projection along the top 3-fold symmetry axis, ℓ, the vibrational angular momentum associated with the degenerate mode ν_9, and $\sigma = 0$–3, the torsional index. In *HITRAN*, the latter is replaced by the symmetry species A_{1s} (6), A_{2s} (10), A_{3s} (6), A_{4s} (10), E_{1s} (4), E_{2s} (4), E_{3s} (2), E_{4s} (6), and G_s (16) in the G_{36}^+ extended permutation-inversion group (the nuclear-spin statistical weights are given in parentheses). Because the symmetry occupies three characters only, the letter 's' is omitted (all the allowed species are s-species): for instance, E_{1s} symmetry is given as ' E1', and $A_{1s}+A_{2s}$ is given as 'A12'.

With this edition, estimated line parameters for the ν_{12} band of $^{13}C^{12}CH_6$ have also been added. The line positions, intensities and assignments (J, K, ℓ, and symmetry in the G_{18}^+ extended permutation-inversion group; see above) are from the work of Kurtz et al. [250] and Weber et al. [251–253]. Since no line-shape parameter measurements have been reported for this isotopologue, γ_{air}, γ_{self}, and n have been set to the values used for the main isotopologue [246].

In the HITRAN2004 edition, the empirical parameters for a number of Q branches were inadvertently excluded from the ν_7 band around 3.3 μm while updating one of the branches. The missing Q branches have now been restored. In addition, in this update numerous multiplets (due to internal rotation tunneling) have been uniquely identified. Note that this band is sorely in need of improvement, especially since the incorporation of the one Q branch in the ν_7 band around 3.3 μm in HITRAN2004 was inconsistent with the intensities of the rest of the band. However, similar to the situation for CH_3Cl, there are weak C_2H_6 features of P and R branch lines that should be included in future updates to support tropospheric monitoring.

2.28. PH_3 (molecule 28)

Phosphine is a constituent of the lower troposphere at very low and highly variable concentrations. Its sources could be bacterial reduction of phosphate in decaying organic matter, its use as a fumigant, and processes related to corrosion of metals containing phosphorus impurities. It is a significant contributor to the continuum opacity in the 5-μm window in the atmosphere of Jupiter, which can be used as a means of probing the deeper atmospheric structure [254].

Spectral line parameters for new bands of PH_3 have been added in the region from 2724 to 3602 cm^{-1}, based on the work of Butler et al. [255]. In addition, the collision-broadened parameters of the previously existing data in *HITRAN* from 770 to 2472 cm^{-1} have been updated using Ref. [255]. A recent global study of PH_3 [256] has confirmed the need to improve and normalize the calculated intensities for the bands at 5 and 3 μm.

2.29. COF_2 (molecule 29)

Unchanged.

2.30. SF_6 (molecule 30)

A totally new line list for sulfur hexafluoride has been created. This line list not only replaces the former ν_3 band that was in *HITRAN*, but includes the ν_4 band and the $\nu_4+\nu_6-\nu_6$ hot band.

The new $^{32}SF_6$ line list has been calculated based upon the EH parameters resulting from the latest analyses. The intense ν_3 stretching fundamental has been the subject of numerous studies (see Ref. [257] for a review). The best fit results are from the simultaneous analysis of various high-precision data (FTIR but also saturated absorption and IR–IR double resonance). The resulting accuracy for line positions is estimated to be better than 0.001 cm^{-1} up to $J = 100$. Measurements of hot bands in this region, although of great importance to atmospheric applications, are still to be investigated. The high line density and only partial knowledge of the inactive ν_6 fundamental have thus far prevented a reliable analysis of the main hot band, namely $\nu_3+\nu_6-\nu_6$. The ν_4 and $\nu_4+\nu_6-\nu_6$ bending region has been investigated in detail in Ref. [258]. Its much lower line density allows an easier analysis compared to the crowded ν_3 region. For the ν_4 fundamental, the accuracy for line positions is $\sim$0.001 cm^{-1} up to $J = 100$ and for the $\nu_4+\nu_6-\nu_6$ hot band it is $\sim$0.002 cm^{-1} up to $J = 65$ (highest assigned lines). The accuracy may decrease quickly when extrapolating to higher J values, although this is difficult to estimate quantitatively.

The determination of reliable dipole-moment parameters, allowing an accurate calculation of line intensities, is a difficult problem in the case of heavy molecules like sulfur hexafluoride. In fact, most spectra do not show any isolated lines but rather unresolved clusters of many transitions (up to several tens for high J values). The present calculation uses the best known, although rather old, dipole-moment derivatives for the ν_3 and ν_4 fundamentals taken from Refs. [259,260]. In the case of the ν_2 fundamental, the intensities of those lines that were listed in the previous *HITRAN* edition have been checked and confirmed to be the same. The new calculation extends the measurements to somewhat higher J values for ν_3 and also includes the ν_4 and $\nu_4+\nu_6-\nu_6$ bands and clearly represents a significant improvement. However, the accuracy in intensities should be considered with some caution and may not be better than 20%, especially for the high-J regions.

Analyses and calculations have been performed with the Highly-spherical Top Data System (*HTDS*) software [261]. The new line list for SF_6 contains 2,889,065 transitions (actually reasonably reduced from the University of Burgundy original list by applying an intensity cutoff of 10^{-30} $cm^{-1}/(molecule\,cm^{-2})$ at 296 K), and covers the spectral range 580–996 cm^{-1}. Since SF_6 has low-lying vibrational modes, most applications will require hot bands that are not present in this list. Therefore, it is the *HITRAN* policy to relegate this list to a supplemental folder, similar to what was done for SF_6 and $ClONO_2$ in the 2004 edition of *HITRAN*.

2.31. H_2S (molecule 31)

Unchanged.

2.32. HCOOH (molecule 32)

This edition of HITRAN constitutes a major update of the information provided for formic acid: the 9-μm region has been completely replaced [262,263], and there is the first inclusion of the 5.6-μm region [264]. These regions correspond to the strong ν_6 and ν_3 bands, respectively. They are both used to probe this species in the troposphere [265,266]. The line parameters for the ν_6 band of $H^{12}C^{16}O^{16}OH$ near 1105 cm^{-1} available in the editions of *HITRAN* earlier than 2004 [1] originate from the work of Goldman and Gillis [267]. The sum of the line intensities was equal to 1.757×10^{-17} $cm^{-1}/(molecule\,cm^{-2})$ at 296 K, determined using a Fourier transform laboratory spectrum recorded at the University of Denver [267]. With the 2004 edition of *HITRAN*, the ν_6 band line positions and intensities were improved according to the work of Perrin et al. [268]. However, absolute line intensities were still derived by scaling the calculated total band intensity to the sum of line intensities obtained in Ref. [267]. Recently, Vander Auwera et al. [262] reported absolute line intensities measurements for the ν_6 and ν_8 bands using FTS, taking the dimer $(HCOOH)_2$ into account in the analysis. They showed that the intensities reported by Goldman and Gillis [267], and therefore in *HITRAN*, were a factor of about 2 lower than the average of the other existing laboratory measurements, and also lower than theoretical calculations. Relying on results of that work, Perrin and Vander Auwera generated a new list of line parameters and showed that it provides a vastly improved modeling of the 9-μm spectral region of formic acid [263]. In the present edition of HITRAN, this list completely replaces previous information for that spectral range of HCOOH.

Using high-resolution Fourier transform spectra of *trans*-HCOOH recorded at 5.6 μm, Perrin et al. [264] carried out an extensive analysis of the strong ν_3 fundamental band at 1776.83 cm^{-1}, significantly perturbed by resonances due to numerous dark bands. That work also involved the determination of absolute line intensities with an accuracy estimated to 15%. A list of line parameters was generated for the first time for this spectral region of *trans*-formic acid. Details can be found in the accompanying article [264]. This line list has been incorporated into the present edition of *HITRAN*, constituting the first inclusion of the 5.6-μm spectral region of formic acid into the database.

2.33. HO_2 (molecule 33)

Unchanged.

Table 7
Dunham constants (in cm^{-1}) for the $X^1\Sigma^+$ ground electronic state of NO^+.

Dunham coefficient	Value (cm^{-1})
$Y_{1,0}$	2376.5568(85)
$Y_{2,0}$	−16.2603(46)
$Y_{3,0}$	−0.00480(55)
$Y_{0,1}$	1.997365(33)
$Y_{1,1}$	−0.018804(22)
$Y_{2,1}$	$-4.90(53)\times10^{-5}$
$Y_{0,2}$	$-5.580(99)\times10^{-6}$
$Y_{1,2}$	$6.(3)\times10^{-8}$

Note: Number in parentheses is approximately 2σ.

2.34. O ("molecule" 34)

Unchanged.

2.35. $ClONO_2$ (molecule 35)

Unchanged.

2.36. NO^+ (molecule 36)

As was pointed out in López-Puertas et al. [269], there were significant inaccuracies in the line positions in HITRAN2004 when compared against *MIPAS* spectra.

Therefore, new line positions corresponding to $J'' \leqslant 40$ for all vibration bands of the nitric oxide ion in the database have been generated using constants derived from a global fit of microwave [270], infrared [269,271,272], and UV spectra [273]. The excited electronic state in the UV data was fit to individual term values because of the perturbations. The resultant Dunham constants are given in Table 7. The fit was performed using the DParFit program of LeRoy [274].

Lines with J'' greater than 40 were left untouched as the new constants cannot predict accurate frequencies for high-J values. One should keep in mind that the *HITRAN* data above $J'' = 40$ will still be of mediocre accuracy. Note that the spectrum of this molecule is often used for upper atmospheric research and hence there is a large dynamic range in intensities in the line list.

2.37. HOBr (molecule 37)

Hypobromous acid is formed in the Earth's atmosphere by gas-phase reactions (e.g. HO_2+BrO) [275] and also by heterogeneous chemistry on aerosol particles (e.g. $BrONO_2$+H_2O) [276,277]. It is an important reservoir for active bromine and is particularly important in the lower stratosphere where it can contain a significant part of the total bromine [277,278]. It also plays an important role in the marine troposphere [279,280]. For atmospheric detection of HOBr, the far-infrared is probably the most promising spectral region [281]. HOBr exists in two main isotopic species ($HO^{79}Br$ and $HO^{81}Br$) with nearly the same natural abundance and mass.

Recent high-resolution studies in the far- and mid-infrared [282,283] have been used to produce a new line list, including (for the far-infrared region) the rotational dependence of the molecular dipole moment and also the rotational transitions in the $v_3 = 1$ state. This line list was not available in time for the new edition of HITRAN; it will be included as an update. A high-resolution line-by-line analysis of the near-infrared $2v_1$ bands of $HO^{79}Br$ and $HO^{81}Br$ is currently in progress [284].

2.38. C_2H_4 (molecule 38)

Spectral line parameters for two isotopologues of ethylene, $^{12}C_2H_4$ and $^{13}C^{12}CH_4$, have been included in *HITRAN* as of the 2000 edition [285]. Recently, Rotger et al. [286] carried out an experimental and theoretical study of the v_{12} band of $^{12}C_2H_4$ near 6.93 μm. Experimental line positions and intensites obtained using FTS were analyzed with a tensorial formalism developed in Dijon, and a list of line parameters was generated for that band. The line positions, intensities, and lower state energies are calculated using the results of that work. The values of γ_{air}, γ_{self}, and n are based on Refs. [287–290] (see [286] for details). This v_{12} band line list has been added to the present edition.

2.39. CH_3OH (molecule 39)

A misassignment of the vibrational levels for the pure-rotation lines of methanol has been fixed (the levels previously labeled as v_1 are now correctly assigned to v_{12}). At the same time, some corrections were made to the list by Xu [291]. These corrections include deleting two duplicate lines, and updating two unresolved doublets.

2.40. CH_3Br (molecule 40)

Methyl bromide is the major contributor to bromine in the stratosphere and the main organobromide in the lower atmosphere. This molecule contributes significantly to ozone depletion since it is dissociated by UV radiation producing Br radicals that catalyze the destruction of ozone [292]. These bromine atoms are 50–60 times more destructive of ozone than the chlorine atoms coming from the chlorofluorocarbon compounds (CFCs) [293]. For this reason, since 2005 the use of CH_3Br is being phased out under the Montreal protocol.

CH_3Br spectroscopic line parameters have been included for the first time in the 2008 *HITRAN* edition. Methyl bromide is composed of 50.099% of $^{12}CH_3{}^{79}Br$ and 48.743% of $^{12}CH_3{}^{81}Br$ in natural abundance. Isotopologue numbers 1 and 2 have been assigned for these two isotopologues, respectively. Two line lists of both isotopologues have been generated, one around 10 μm for the v_6 band, and the other around 7 μm for the interacting v_2 and v_5 bands. Several works published recently for this molecule have been used to build these line lists. The works of Kwabia Tchana et al. have been used for the line positions [294] and intensities [295] in the 7-μm spectral region. In the 10-μm spectral region, line positions, intensities, self- and N_2-broadened half-width parameters have been studied in Ref. [296]. The line list now present in *HITRAN* is the one provided as supplementary material of Ref. [296]. The model for self- and N_2-broadened half-width parameters obtained in Ref. [296], showing a J and K rotational dependence, has been used both for the 10- and 7-μm spectral regions. Because atmospheric needs are concerned with air-broadened half-width parameters, we deduced γ_{air} by scaling γ_{N_2} by a factor of 0.96. Similar approximations have been done for many molecules in the various editions of the *HITRAN* database. For the H_2O molecule, air-broadened half-width parameters could be estimated by multiplying N_2-broadened half-width parameters by the value 0.9 as suggested in Refs. [297–299]. For CH_3Cl, the ratio is found to be around 0.96 due to the ratio $\gamma_{N_2}/\gamma_{O_2} = 1.25$ obtained by averaging measurements of CH_3Cl from Refs. [300,301]. Note that this result is quite similar to what has been proposed for ozone in Ref. [302]. Because CH_3Br is similar to CH_3Cl, the scaling factor $\gamma_{air}/\gamma_{N_2} = 0.96$ has been used. This procedure, although approximate since $\gamma_{N_2}/\gamma_{O_2}$ varies from line to line, is expected to be precise within a few percent. Also, the temperature-dependence parameter n has been added in both spectral regions, based on the N_2-width temperature dependence measurements of Jacquemart and Tran [303] (see Eq. (5) of Ref. [303]). Accuracies or details for the line-parameter calculation can be found in Refs. [294–296,303]. Note also that line mixing has been observed and analyzed in the strong Q-branches between 220 and 300 K [304,305]; line mixing parameters are available on request to the authors [304,305].

2.41. CH_3CN (molecule 41)

Line parameters of methyl cyanide (also called acetonitrile) have been included in *HITRAN* for the first time. A total of 3572 features between 890 and 946 cm^{-1} has been given for the v_4 region near 920 cm^{-1}. Published line positions and intensities from Rinsland et al. [306] have been supplemented by unpublished measurements from the same data set, as well as selected values from preliminary Hamitonian calculations. Only lines with intensities greater than 10^{-24} $cm^{-1}/(molecule\,cm^{-2})$ at 296 K have been included. The spectral region from 918.5 to 920.3 cm^{-1} (containing the Q branch and the P1 and P2 manifolds) proved too dense to measure directly and so these parameters are represented by 326 calculated transitions of v_4. Some 2243 lines are given without quantum identifications; many are thought to be hot band lines involving as yet unanalyzed upper-state levels of v_4+v_8. The lower state energy of these unidentified lines is set to 410.0000 cm^{-1}. It should be noted that a number of hot-band lines are not included in the list; this is most noticeable at the hot band Q branch near 924 cm^{-1}.

Measured self-broadened half-width parameters were available [306], and identified lines with the same K quantum number and the same or very close m were assigned approximately the same or interpolated values. The total number of lines with self-broadening assigned in this manner is 2185. The air-broadened half-width parameters were estimated using the reported N_2 broadening [306] and extension to unmeasured identified lines in the same manner as self-broadening for a total of 2279. Previously, Fabian et al. [307] reported N_2 and O_2 broadening of 11 microwave lines and the mean ratio of their O_2-broadened to the N_2-broadened half-width parameters was 0.67. Assuming the standard 79% N_2 and 20% O_2 in air, this implies that γ_{air} is 0.93 times the corresponding N_2-broadened value, and so this factor was applied for the database. For the lines lacking measured Lorentz half-width parameters for air and self-broadening, default values of 0.14 and 1.5 $cm^{-1}\,atm^{-1}$ at 296 K were used, respectively (obtained as an approximate average of measured values).

The measured N_2 shifts [306], where available, were inserted for air shifts. Unmeasured pressure shifts have been set to zero, the approximate average of the measured values. There are no measurements of the temperature dependence of the Lorentz half-width in air and only one in N_2 [308], so the default n was set to the single measured N_2 value of 0.72.

The error codes have been set based upon an uncertainty of five times the formal fitting uncertainty. The one exception is the air-broadened Lorentz half-width parameter for which an additional 2% was added to account for the uncertainty in the air-to-N_2 ratio of these parameters. Furthermore, a calculation of the total internal partition function sum has been performed for four isotopologues, $^{12}CH_3{}^{12}CN$, $^{13}CH_3{}^{12}CN$, $^{12}CH_3{}^{13}CN$, and $^{13}CH_3{}^{13}CN$, and those results have been made available for the *HITRAN* compilation.

2.42. CF_4 (molecule 42)

Tetrafluorocarbon (CFC-14) is a strong greenhouse gas of both anthropogenic and natural origin [309,310]. It has been increasing in the atmosphere [311,312]. Its infrared spectrum is dominated by the intense ν_3 band at 1282 cm^{-1} [313]. However, high-resolution infrared spectroscopy of this molecule has received only a limited interest up to now with its atmospheric identification first reported from balloon-borne measurements [313]. The previous editions of the *HITRAN* database for CF_4 were only represented by cross-sections (referenced as CFC 14) [314], but contained no line list.

The strongly absorbing ν_4 (around 15.8 μm) and $2\nu_4/\nu_3$ regions (around 7.3 μm) have been recently reinvestigated, thanks to several new Fourier transform infrared spectra recorded at a resolution of 0.003 cm^{-1}. Following the previous work of Gabard et al. [315], a simultaneous analysis of the ground state, ν_4, ν_3, $2\nu_4$ and $\nu_3-\nu_3$ bands was performed, making use of the XTDS and SPVIEW programs [316] developed by the Dijon group. Compared to Ref. [310], the present work extends the analysis to much higher J values (70 instead of 40 for ν_4 and 63 instead of 32 for the $2\nu_4/\nu_3$ dyad). Absorption intensities were used to fit the ν_4 and ν_3 dipole-moment derivatives and the results compare very well to the calculated values of Papoušek et al. [317]. The details of this new analysis will be given in a forthcoming paper [318].

The analysis allowed for the first time the generation of a reliable line list for $^{12}CF_4$ that is included in the present *HITRAN* edition, tetrafluorocarbon becoming molecule number 42. The estimated precision for line positions is 0.001 cm^{-1}, up to $J = 60$. The accuracy of intensities, however, should be considered with some care and may not be better than 20%, especially for the high-J regions. The list covers the spectral ranges 600–670 cm^{-1} (ν_4) and 1276–1290 cm^{-1} ($2\nu_4/\nu_3$).

The γ_{air} parameter was fixed to a constant value 0.078 cm^{-1} atm^{-1} (at 296 K) based on the averaged value from tunable diode laser experiments [319]. Note that at higher J values the air-broadened half-width parameters will most likely be lower than this fixed value; further experiments are desirable. The temperature dependence of the air-broadened half-width parameter, n, was set to 0.66 also based on Ref. [319]. There is no experimental (or theoretical) information about the self-broadened half-width parameter; this parameter was estimated to be 0.08 cm^{-1} atm^{-1}.

Just as for SF_6 (Section 2.30 above), CF_4 has low-lying vibrational modes and, as most applications will require hot bands that are not present in this list, this line list has been placed into the supplemental folder.

3. Infrared cross-sections

Infrared cross-sections for this edition of the *HITRAN* compilation are listed in Table 8. This portion of the database supplies cross-sections of molecules for which line-by-line spectral parameters are not yet available or are incomplete. With the exception of the HFC-143a and HFC-125 cross-sections, all of the cross-sections are similar to those discussed by Rothman et al. [1] and Massie and Goldman [320]. The cross-sections of each molecule are specified in separate files, labeled with the chemical symbol of the molecule followed by an underscore and IRxx, where xx stands for the edition that the data was introduced or updated. A file extension of .xsc is used. Files may have many temperature–pressure sets for different spectral regions, as indicated by headers throughout the file. Headers indicate the molecule name, the range of wavenumber for the band, number of data points, temperature (K) and pressure (Torr) of the laboratory measurements, the maximum cross-section in the band (cm^2 $molecule^{-1}$), and the resolution (cm^{-1}) of the measurements.

In previous editions, the cross-sections from the original laboratory data sets were set to zero if they were negative. Wavelength ranges were chosen such that there are positive valued cross-sections in the far wings of the various bands at all of the measurement temperatures. In HITRAN2008 we also provide complete original laboratory data. Original files of HFC125 and HFC143a (discussed below) are included in a new subdirectory called "Original Data". Using these data requires special care since there are instrumental distortions and wide intervals of oscillating values near zero that are present in the data files.

Di Lonardo and Masciarelli [321] measured HFC-143a cross-sections at six temperatures between 203 and 293 K, similar to those of Smith et al. [322], and at a similar resolution of 0.03 cm^{-1}. Integrated band intensities at room temperature and at 203 K differ by 6% and 16%, respectively, while the maximum cross-sections near the 1281 cm^{-1} Q branch differ by 30%. This difference points out the need for additional measurements, especially of the strong Q-branch features of molecules that play a predominant role in atmospheric remote sensing. The data of Smith et al. [322] are currently in the main directory, while those of Di Lonardo and Masciarelli [321] are in the Original Data subdirectory. Both data sets should be consulted until the differences are resolved.

Di Lonardo and Masciarelli [321] also measured HFC-125 cross-sections at six temperatures between 203 and 293 K and pressures between 50 and 800 hPa at a resolution of 0.03 cm^{-1}. Integrated band intensities of the Clerbaux et al. [323] and Di Lonardo and Masciarelli [321] measurements agree to 3.4% when the same molecular bands are intercompared.

Table 8
Summary of molecules represented by IR cross-section data in *HITRAN*.

Molecule	Common Name	Temperature Range (K)	Pressure Range (torr)	Number of T,P sets	Spectral Coverage (cm^{-1})
SF_6	Sulfur hexafluoride	180–295	20–760	32	925–955
$ClONO_2$	Chlorine nitrate	189–297	0–117	25	750–830
		189–297	0–117	25	1260–1320
		213–296	0	2	1680–1790
CCl_4	Carbon tetrachloride	208–297	8–760	32	750–812
N_2O_5	Dinitrogen pentoxide	205–293	0	5	540–1380
HNO_4	Peroxynitric acid	220	0	1	780–830
C_2F_6	Hexafluoroethane, CFC-116	181–296	25–760	43	1061–1165
		181–296	25–760	43	1220–1285
CCl_3F	CFC-11	190–296	8–760	55	810–880
		190–296	8–760	55	1050–1120
CCl_2F_2	CFC-12	190–296	8–760	52	850–950
		190–296	8–760	52	1050–1200
$CClF_3$	CFC-13	203–293	0	6	765–805
		203–293	0	6	1065–1140
		203–293	0	6	1170–1235
CF_4	CFC-14	180–296	8–761	55	1250–1290
$C_2Cl_2F_3$	CFC-113	203–293	0	6	780–995
		203–293	0	6	1005–1232
$C_2Cl_2F_4$	CFC-114	203–293	0	6	815–860
		203–293	0	6	870–960
		203–293	0	6	1030–1067
		203–293	0	6	1095–1285
C_2ClF_5	CFC-115	203–293	0	6	955–1015
		203–293	0	6	1110–1145
		203–293	0	6	1167–1260
$CHCl_2F$	HCFC-21	296	1	1	785–840
$CHClF_2$	HCFC-22	181–297	0–765	29	760–860
		181–296	22–761	31	1070–1195
		253–287	0	3	1060–1210
		253–287	0	3	1275–1380
$CHCl_2CF_3$	HCFC-123	253–287	0	3	740–900
		253–287	0	3	1080–1450

Table 8 (*continued*)

Molecule	Common Name	Temperature Range (K)	Pressure Range (torr)	Number of T,P sets	Spectral Coverage (cm^{-1})
$CHClFCF_3$	HCFC-124	287	0	1	675–715
		287	0	1	790–920
		287	0	1	1035–1430
CH_3CCl_2F	HCFC-141b	253–287	0	3	710–790
		253–287	0	3	895–1210
		253–287	0	3	1325–1470
CH_3CClF_2	HCFC-142b	253–287	0	3	650–705
		253–287	0	3	875–1265
		253–287	0	3	1360–1475
$CHCl_2CF_2CF_3$	HCFC-225ca	253–287	0	3	695–865
		253–287	0	3	1010–1420
$CClF_2CF_2CHClF$	HCFC-225cb	253–287	0	3	715–1375
CH_2F_2	HFC-32	203–297	0–750	17	995–1236
		203–297	0–750	17	1385–1475
CHF_2CF_3	HFC–125	287	0	1	700–745
		287	0	1	840–890
		287	0	1	1060–1465
CHF_2CHF_2	HFC–134	203–297	0–750	9	600–1700
CFH_2CF_3	HFC–134a	253–287	0	3	815–865
		190–296	20–760	32	1035–1130
		190–296	20–760	33	1135–1340
		253–287	0	3	935–1485
CF_3CH_3	HFC–143a	203–297	0–750	9	580–630
		203–297	0–750	9	750–1050
		203–297	0–750	9	1100–1500
CH_3CHF_2	HFC–152a	253–287	0	3	840–995
		253–287	0	3	1050–1205
		253–287	0	3	1320–1490
SF_5CF_3	Trifluoromethyl sulfur pentafluoride	213–323	760	5	599–624
		213–323	760	5	676–704
		213–323	760	5	740–766
		213–323	760	5	860–920
		213–323	760	5	1150–1280
		213–323	760	5	1280–2600
New or modified data added after the HITRAN2004 edition					
$CH_3C(O)OONO_2$	PAN (Peroxyacetal nitrate)	295	0.08	1	550–1450
		295	0.08	1	1650–1901

Table 8 (*continued*)

Molecule	Common Name	Temperature Range (K)	Pressure Range (torr)	Number of T,P sets	Spectral Coverage (cm^{-1})
CH_3CN	Acetonitrile (methyl cyanide)	276–324	760	3	624–784
		276–324	760	3	867–1159
		276–324	760	3	1175–1687
		276–324	760	3	2217–2343
		276–324	760	3	2786–3261
		276–324	760	3	3881–4574
CHF_2CF_3	HFC–125	203–293	0–600	16	494–1503

Infrared cross-section data for methyl cyanide (CH_3CN) became available soon after the release of HITRAN2004, and were first placed in the update section of the *HITRAN* web site. The source of the data is Rinsland et al. [324]. This molecule is emitted from incomplete combustion of plant matter, for example in forest fires. It is relatively non-reactive in the troposphere and is thus a tracer of troposphere-stratosphere transport.

Infrared cross-section data for peroxyacetyl nitrate-PAN ($CH_3C(O)OONO_2$) also became available after the release of the HITRAN2004 database. The source of the data is Allen et al. [325,326]. This organic compound is formed in photochemical smog, for example. It is thermally quite stable, and can contribute to pollution in areas away from its source. It is an irritant to the eyes and breathing. *HITRAN* cross-sections have been used for measurements of short-lived organic compounds including PAN and acetone in a biomass burning upper tropospheric plume measured by *MIPAS*-B limb emission spectra [327] and in *ACE* Fourier transform spectrometer solar occultation spectra as reported by Coheur et al. [265].

Pressure-broadened (1 atm N_2) laboratory spectra of benzene vapor (in natural abundance) were recorded at 278, 298, and 323 K, covering 600–6500 cm^{-1} [328] and added to *HITRAN*. The spectra were recorded at a resolution of 0.112 cm^{-1} using a commercial Fourier transform spectrometer. The pressure of each benzene vapor sample was measured using high precision capacitance manometers, and a minimum of nine sample pressures were recorded for each temperature. The samples were introduced into a temperature-stabilized static cell (19.94(1) cm pathlength) that was hard-mounted into the spectrometer. From these data, a fitted composite spectrum was calculated for each temperature. The number density for the three composite spectra was normalized to 296 K. The spectra give the absorption coefficient (cm^2 $molecule^{-1}$, naperian units) as a function of wavenumber. From these spectra, integrated band intensities (cm $molecule^{-1}$ and atm^{-1} cm^{-2}) for intervals corresponding to the stronger benzene bands were calculated and were compared with previously reported values. Error sources and estimated systematic (NIST Type-B) errors were found to be 3% for the stronger bands. The measured absorption coefficients and integrated band intensities are useful for remote sensing applications such as measurements of planetary atmospheres and assessment of the environmental impact of terrestrial oil fire emissions.

4. UV data sets

4.1. Line-by-line data

4.1.1. O_2

A new line list has been created for the oxygen Herzberg bands. Corrections have also been made to the Schumann–Runge line list.

The line list for the Herzberg bands ($A^3\Sigma_u^+ \leftarrow X^3\Sigma_g^-$, $c^1\Sigma_u^- \leftarrow X^3\Sigma_g^-$, $A'^3\Delta_u \leftarrow X^3\Sigma_g^-$) is based on the data from Mérienne et al. [329]. Fig. 6 shows an overall view of the bands. The file was created in a format different from former oxygen line lists in *HITRAN* in order to distinguish different spin-components of the $A'^3\Delta_u$ state of the Herzberg III band. The only difference is in the presentation of the "global" quanta identification which is closer now to Class 3 of Table 3 in Ref. [1]. The new format (in FORTRAN descriptors) is shown in the bottom of Table 9. The description of all the oxygen electronic energy levels that are now in *HITRAN*, and their presentation in the new format, is also illustrated in Table 9.

In addition, the assignments of lines in the Schumann–Runge bands ($B^3\Sigma_u^- \leftarrow X^3\Sigma_g^-$) have been corrected from previous editions of *HITRAN*. The associated parameters such as Einstein *A*-coefficients and statistical weights were recalculated. The uncertainty and reference indices were fixed as well. The self-broadened half-width parameter field is used for predissociation widths at zero pressure. In the previous editions of *HITRAN*, FWHM (full width at half maximum) was listed for the Schumann–Runge bands, where now it has been changed to HWHM (half width at half maximum) to make it consistent with the rest of *HITRAN*. The Schumann–Runge bands employ the new format for the "global" quanta identifications.

The spectral range covered by the Herzberg bands is 34 014–41 261 cm^{-1}, while the Schumann–Runge bands cover 44 606–57 028 cm^{-1}. The total number of lines in the combined UV file is 15 466.

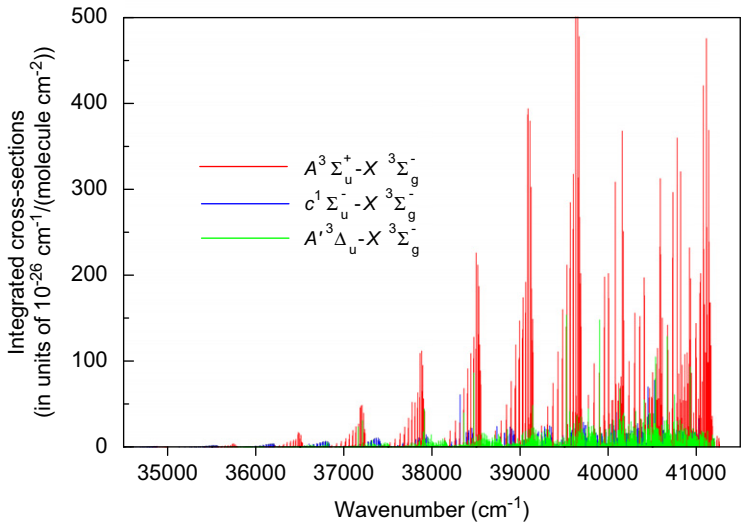

Fig. 6. Line intensities of the O_2 Herzberg bands now in *HITRAN*.

Table 9
Energy levels for oxygen currently in *HITRAN* with their vibrational range and descriptors.

Electronic state	X	Ω	υ (range)
$X^3\Sigma_g^-$	X		0–2
$a^1\Delta_g$	a		0–1
$b^1\Sigma_g^-$	b		0–2
$A^3\Sigma_u^+$	A		0–12
$c^1\Sigma_u^-$	c		2–19
$A'^3\Delta_u$	A'	1, 2, or 3	2–12
$B^3\Sigma_u^-$	B		0–19
FORTRAN descriptor	A8	A3	I4

Note: X is the character describing the electronic state, Ω are values defining the spin components, and υ is an integer specifying the vibrational level. Note that the Ω-value is given only for states with $\Lambda \neq 0$.

4.2. UV cross-sections

UV cross-sections for a number of molecules were introduced in the 2004 edition of HITRAN [1]. They were intended to represent the most useful data for analysis of atmospheric measurements, including ground-based and satellite-based spectroscopic measurements of the atmosphere [330]. Several updates are included in the present version of HITRAN, as presented here. Several current studies with potential implications for near-future updates are also discussed.

4.2.1. O_3

The Hartley–Huggins bands of ozone, adopted from Bass and Paur [331], with wavelength correction as discussed in [1] remain the HITRAN2008 choice. There is now substantial indication that shifting to new cross-sections will soon be warranted [332], with the likely choice being those from Ref. [333].

4.2.2. BrO

Bromine oxide cross-sections have been re-measured in the UV at five different temperatures between 203 and 298 K [334]. At present, these are being evaluated by research groups analyzing satellite spectra to see whether they present an improvement over those currently used [335].

4.2.3. H_2CO

It has recently been demonstrated [229] that the UV cross-sections for H_2CO implemented in *HITRAN* may be as much as 20% too low, leading to overestimates of atmospheric H_2CO by up to 20%. Other cross-section measurements currently in use include those of Meller and Moortgat [336]. These data, however, are at lower spectral resolution and in air wavelengths. For the present, corrections may be made to fitted atmospheric concentrations when the cross-sections of

Ref. [337] are used. We recommend, however, that the cross-sections be systematically re-measured, simultaneously with infrared line parameters using FTS.

4.2.4. IO

Cross-sections for iodine oxide [338], which have recently been successfully measured in the visible in both ground-based and satellite spectra [339], have now been added to *HITRAN*.

4.2.5. SO_2

Sulfur dioxide absorption cross-sections have already been extensively investigated in the 250 to 345 nm region at room temperature [340–354]. The temperature dependence was mainly investigated by looking at temperatures lower than room temperature [349,350,353]. Only a couple of measurements have been performed at higher temperatures [343,344]. Recently, Danielache et al. [355] investigated the effect of the isotopes of S on the absorption cross-sections of SO_2. Measurements of the SO_2 absorption cross-sections above 345 nm are scarce: Manatt and Lane [348], who did a compilation of absorption cross-sections existing in the literature, have digitalized the data of Sidebottom et al. [356] from the figures in their paper. However, they introduced some modifications to the original data by shifting them by 0.67 nm to the red after comparison with peak positions from measurements performed by Clements [357] and by correcting for the sinking baseline at the short wavelength side of the Sidebottom et al. data [356]. Sprague and Joens [358] report measurements of SO_2 in the 320–405 nm region at a temperature of 298 K and a resolution of 0.1 nm.

Recently, the SO_2 absorption cross-sections were investigated in the 225–425 nm region with FTS [359,360]. This study provides cross-sections at relatively high spectral resolution ($2\,cm^{-1}$) with high wavelength accuracy at several temperatures (298, 318, 338, and 358 K). At room temperature, these data compare fairly well with the previous measurements of Vandaele et al. [341], Bogumil et al. [353] and of Rufus et al. [347]. At higher temperatures, there are very few literature data to compare with. These data, which cover a wide spectral interval and include temperature dependence, have now been included in *HITRAN*.

4.2.6. Aromatic species

Aromatic hydrocarbons in the atmosphere are mainly of anthropogenic origin with major emissions due to motor vehicles and solvent use. Minor sources are biomass burning and biogenic emissions. They play an important role in the chemistry of tropospheric ozone and in urban air pollution problems because of their carcinogenic and mutagenic properties [361,362]. However, the quality of atmospheric detections is not very good and is partly attributed to the poor spectral resolution of the reference absorption cross-sections [363]. These species are also of importance for astronomical studies: benzene has been detected in the north polar auroral region of Jupiter [364] and in the stratospheres of Jupiter and Saturn [365] as well as in Titan's atmosphere [366]. The need for laboratory spectroscopic data to study organic chemistry in planetary atmospheres was highlighted in Refs. [367–369], in particular the low-temperature dependence in the UV range.

Benzene (C_6H_6) is a planar oblate symmetric top molecule with D_{6h} point group symmetry. Such a high symmetry allows a total of thirty normal modes of vibration among which ten are doubly degenerate. The UV absorption spectrum of benzene is attributed to the S_1 ($^1B_{2u}$)$\leftarrow S_0$ ($^1A_{1g}$) electronic transition which is electronically forbidden but vibrationally induced, and it is dominated by the 6^1_0 vibronic progression involving the symmetrical ring-breathing vibration ν_1. This band system becomes more allowed and therefore more intense as the D_{6h} symmetry is broken in methyl and dimethyl-substituted benzene, i.e. toluene and xylene, respectively. The UV bands of benzene have been studied in the past by high-resolution spectroscopy and their rotational structure has been completely analyzed by Okruss et al. [370].

Measurements of the absorption cross-sections of gaseous benzene (C_6H_6), toluene (C_7H_8), ortho-, meta-, and para-xylene (or the three isomers of dimethyl-benzene $C_6H_4(CH_3)_2$) have been performed with a Fourier transform spectrometer at the resolution of $1\,cm^{-1}$ (MOPD = 0.9 cm) over the 30 000–42 000 cm^{-1} spectral range (238–333 nm) and at temperatures ranging from 253 to 293 K. This systematic study of five organic molecules is presented in detail in Fally et al. [371]. The complete data set comprises the absorption cross-sections of: (i) benzene at 253, 263, 273, 283 and 293 K, (ii) toluene at 263, 273, 283 and 293 K, and (iii) the three isomers of xylene at 273, 283 and 293 K. Wavenumbers are given by increments of $0.2\,cm^{-1}$ and the non-systematic error of the absorption cross-section (to which a total systematic uncertainty of 8% must be added) is also reported in a separate column.

Compared to recent studies in the same UV region [372–374], this work provides absorption cross-sections (cm^2 $molecule^{-1}$) at several atmospheric temperatures with a better spectral resolution and an accurate wavelength scale. It also proposes a parameterization for the temperature effect in support of tropospheric and astronomical studies. These data, which appear in *HITRAN* for the first time, are also available in digital form from the web site of the Belgian Institute for Space Aeronomy (http://www.aeronomie.be/spectrolab/).

5. Aerosol refractive indices

Refractive indices of water, ice, aqueous sulfuric and nitric acid, solid hydrates (i.e. nitric acid mono-, di-, and tri-hydrate), organic non-volatile aerosol, and crustal material (e.g. quartz, hematite, and sand) in the previous version of

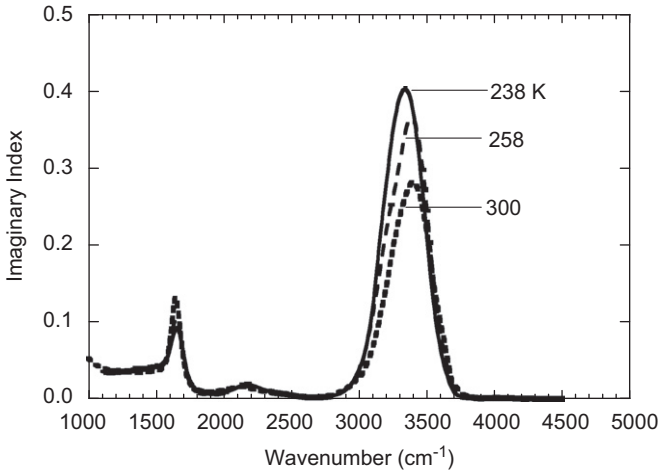

Fig. 7. Temperature dependence of the supercooled water imaginary indices of Wagner et al. [375]. The 300 K indices are from Downing and Williams [376].

HITRAN are discussed by Rothman et al. [1] and Massie and Goldman [320]. There is a separate ASCII file for each refractive-index data set. The header of each file describes the data, cites a journal reference, specifies an email contact, and provides the format specification of the tabulation. Additions to HITRAN2008 include indices of supercooled water, ice, and ternary $H_2SO_4/HNO_3/H_2O$ droplets at low temperatures.

Real and imaginary indices of supercooled water at 238, 252, 258, and 269 K from 1101 to 4503 cm^{-1} are tabulated by Wagner et al. [375]. These data are based upon expansion experiments conducted in the Karlsruhe AIDA coolable aerosol chamber, followed by a Mie inversion technique. The influence of temperature on the optical constants was analyzed previously only down to 274 K. The supercooled optical constants are notably different from room temperature indices. Fig. 7 compares room temperature indices of Downing and Williams [376] and the supercooled indices. Notable differences are apparent in the O–H stretching mode near 3400 cm^{-1}. These indices will help to improve retrievals of the ratio of supercooled water droplets to ice crystals in mixed phase clouds.

Warren and Brandt [377] have updated the 1984 Warren [378] compilation of ice indices. Indices from 0.044 to 2×10^6 μm at 266 K are specified. There are notable differences in the two data sets. Imaginary indices in the 1.4- to 5-μm range are larger or smaller than those in Ref. [378] by a factor up to two, depending upon the specific wavelength. In the 7- to 10-μm range, the new imaginary indices are 30% lower than those in Warren [378]. Temperature dependence is strong in the 15–30 μm range. While *HITRAN* includes the Clapp et al. [379] indices of ice from 2.5- to 12.5-μm in 10 K steps from 130 to 210 K, there is a need for new measurements in the 8–30 μm range from 200 to 273 K. The far-infrared 45 μm peak in Ref. [377] is stronger than in the 1984 compilation. Warren [377] recommends that researchers should consult the formulas of Matzler [380] if they require microwave indices at temperatures other than 266 K.

Ternary $H_2SO_4/HNO_3/H_2O$ indices at low temperature are important in the interpretation of infrared spectra of Polar Stratospheric Clouds (PSCs) since ternary solution droplets are observed in PSCs. Lund Myhre et al. [381] measured indices between 12 and 81 wt% H_2SO_4 from 220 to 300 K. Lund Myhre et al. [382] measured indices of HNO_3/H_2O (at 30, 54, and 64 wt% HNO_3) and three mixtures of $H_2SO_4/HNO_3/H_2O$ between 183 and 293 K. Prior to Ref. [381], only two other sets of measurements of the ternary indices, Norman et al. [383] and Biermann et al. [384], have been made, both of which are included in the *HITRAN* database. HITRAN2008 contains all of these data sets since the measurement temperatures differ, and because there are important differences in the indices of the various data sets. The specification of the indices of the ternary mixture is considered incomplete, since there is not yet available a definitive way to combine (i.e. mix) the binary HNO_3/H_2O and H_2SO_4/H_2O indices to derive ternary indices for PSC studies.

6. Global data and software

There are some data that are needed to accompany HITRAN that are of a global nature. One such file, called molparam.txt, is included with the compilation. It is a table listing the abundances, partition sum at 296 K, and the molecular weight of each of the isotopologues contained in HITRAN. There is also a file of all the sources used for the parameters in HITRAN, as well as a file giving the partition sums at temperatures from 70 to 3000 K.

As in previous editions, there is software, called JavaHAWKS, included in the compilation that provides a functional and flexible set of tools for managing the database. This software can be installed on a wide set of platforms, running for example Windows, UNIX, Solaris, LINUX, and Mac OS. However, the JavaHAWKS software has not yet been updated to be

able to completely work on the newest additional molecules (beyond molecule 39). Likewise there are some new bands of molecules that have not been implemented in the band selection feature.

In the future we plan to restructure the whole of the *HITRAN* compilation into an internet-based browsing platform. A possible prototype for this system is the W@DIS database being produced by the IUPAC (International Union of Pure and Applied Chemistry) Water Vapor task group [385].

7. Conclusions

The details of the updates and enhancements of the new HITRAN2008 compilation have been described. The compilation consists of several parts: (1) the traditional high-resolution, line-by-line portion where fundamental spectroscopic parameters required for calculation of radiative transfer are archived; (2) files of infrared cross-sections primarily for large or heavy polyatomic molecules; (3) UV line-by-line parameters and cross-sections; (4) tables of aerosol refractive indices; and (5) generalized tables and references that relate to *HITRAN*.

In addition to adding some new molecules, many vibration–rotation bands for the previously included species have been updated or extended. One can highlight the vast improvement for H_2O, CO_2, O_3, CH_4, O_2, and most of the trace-gas species. Emphasis has been on increased accuracy and completeness of line positions, intensities, and line-shape parameters. Recent atmospheric remote-sensing experiments have placed very demanding requirements on the accuracy of intensities and broadening parameters. Indeed, various field experiments have now demonstrated the need (by lowering the residuals between observed and simulated spectra) for more sophisticated models of line shape beyond the Voigt profile currently accessible through *HITRAN*. This extension will be the topic of future editions of *HITRAN*.

Continuing efforts to improve and extend the database are ongoing. As critical new data become available, they will be evaluated by the international HITRAN committee. These approved data will be posted as interim updates on the internet before a total new edition is released. The compilation is free; access instructions can be obtained at http://www.cfa.harvard.edu/HITRAN.

Acknowledgments

The *HITRAN* molecular database has been a project with strong international cooperation during its development. Laboratories throughout the world have contributed both experimental data and theoretical calculations. We greatly appreciate the major efforts of S. Albert, M. Barber, S. Bauerecker, C. Boone, S.A. Clough, R. Colin, M.R. DeBacker-Barilly, L. Daumont, B.J. Drouin, C. Frankenberg, J.-M. Hartmann, F. Hindle, J.T. Hodges, K. Jucks, A. Laraia, R.J. Le Roy, M. Loëte, O. Lyulin, H.S.P. Müller, M. Okumura, B. Perevalov, M. Quack, L. Régalia-Jarlot, D.J. Robichaud, F. Rohart, M.W. Shephard, R. Tolchenov, V.G. Tyuterev, G. Wagner, C. Wenger, L.-H. Xu, and L.Y. Yeung in support of this new edition. The constructive suggestions by G. Toon of JPL for improving the manuscript are also gratefully acknowledged.

Appendix A. Converting intensities from the JPL or CDMS catalogs to HITRAN intensities

This appendix provides users with the steps needed for the conversion of intensities between the *HITRAN* database [1] and the *JPL* [148] or Cologne Database for Molecular Spectroscopy (*CDMS*) [149] spectral databases. The *JPL* and *CDMS* lists, which are identical in their intensity formalisms, provide base-10 logarithms of the integrated intensity at 300 K (in nm^2 MHz), while *HITRAN* gives the intensity at 296 K (in $cm^{-1}/(molecule\,cm^{-2})$). Apart from these differences, there are certain differences in the formalism of intensities and this appendix provides steps for the most accurate conversion. If accuracy better than 2% is not required, it is fairly safe to use an approximation given in Section A.5. Some other intensity unit conversions are described in the textbook of Bernath [386]. Appendix B gives definitions of some of the quantities in the databases.

A.1. Unit conversion

The *JPL* [148] and *CDMS* [149] catalogs use nm^2 MHz as units of intensity. In order to convert to *HITRAN* [1] units ($cm^{-1}/(molecule\,cm^{-2})$), one has to divide the *JPL* intensity (*not its logarithm*) by a factor related to the speed of light, namely $2.99792458\times10^{10}\,cm\,s^{-1}$. It should be recalled that the *HITRAN* units were constructed with application to atmospheric transmission calculations in mind, hence the emphasis on writing the units as *wavenumber per column density* and not simplifying it to the equivalent $cm\,molecule^{-1}$:

$$I_{JPL}(cm^{-1}/(molecule\times cm^{-2})) = \frac{I_{JPL}(nm^2\,MHz)}{2.99792458\times10^{18}}. \tag{A.1}$$

A.2. Isotopic abundance

The *JPL* and *CDMS* catalogs assume 100% abundance of every isotopologue, whereas the *HITRAN* database incorporates a terrestrial abundance scaling. Therefore, one has to multiply the *JPL* (*CDMS*) intensity by the isotopologue abundance value

(I_a) adopted by *HITRAN*. For the isotopic abundances used in *HITRAN*, see for example Table 1 in Ref. [387].

$$S_{JPL} = I_a \frac{I_{JPL}(\mathrm{nm^2\,MHz})}{2.99792458 \times 10^{18}}. \tag{A.2}$$

A.3. Scaling of the partition sum

After conversion to $\mathrm{cm^{-1}/(molecule\,cm^{-2})}$ and scaling by isotopic abundance, one needs to consider the intensity defined in the *JPL* catalog, S_{JPL}, which is given by

$$S_{JPL}(T) = \frac{g'_{JPL}}{Q_{JPL}(T)} \frac{A}{8\pi c \nu_0^2} \mathrm{e}^{-hcE''/k_B T}(1 - \mathrm{e}^{-hc\nu_0/k_B T}), \tag{A.3}$$

where g' is a statistical weight of the upper level and $Q(T)$ is a total partition sum. The other terms in Eq. (A.3) are defined in the appendix of Ref. [388]. The labels "*JPL*" refer to the fact that in some cases in the *JPL* and *CDMS* catalogs the common factors are factored out in g' and $Q(T)$. This common factor is a state-independent statistical weight g_i, which is not ignored in the *HITRAN* database. Nevertheless it is obvious that

$$\frac{g'_{JPL}}{Q_{JPL}(T)} \approx \frac{g'_{HIT}}{Q_{HIT}(T)}. \tag{A.4}$$

The use of the "$\approx$" refers to the fact that partition sums are not calculated exactly the same way in the *JPL* catalog and *HITRAN*. Unlike *HITRAN*, the partition sums in the *JPL* catalog do not include the "vibrational" contribution in most cases. However, this contribution may be significant for molecules possessing low vibrational modes. Therefore, it is recommended that one should scale the intensities obtained at *JPL* to *HITRAN* formalism in the following manner:

$$S_{HIT}(T) = S_{JPL}(T) \frac{Q_{JPL}(T)}{Q_{HIT}(T)} \frac{g'_{HIT}}{g'_{JPL}}. \tag{A.5}$$

Since 300 K is the reference temperature in both the *JPL* and *CDMS* databases,

$$S_{HIT}(300) = I_a \frac{I_{JPL}(\mathrm{nm^2\,MHz})}{2.99792458 \times 10^{18}} \frac{Q_{JPL}(300)}{Q_{HIT}(300)} \frac{g'_{HIT}}{g'_{JPL}}. \tag{A.6}$$

It is not always immediately obvious whether or not $g'_{JPL} = g'_{HIT}$. Therefore, it is always useful to obtain a ratio between partition sums in *JPL* and *HITRAN* at the same temperature and then round that ratio to an integer, which will be the ratio between statistical weights in *HITRAN* and *JPL*.

The partition sums for *HITRAN* database are available in the file parsum.dat that is distributed with the database. The partition sums for 296 K are also listed in Table 1 of Ref. [387]. The partition sums (or their logarithms) for the *JPL* and *CDMS* catalogs are provided in the following websites: http://spec.jpl.nasa.gov/ftp/pub/catalog/catdir.cat and http://www.ph1.uni-koeln.de/vorhersagen/catalog/partition_function.html.

A.4. Temperature adjustment

All intensities in the *JPL* and *CDMS* catalogs are calculated at 300 K, whereas *HITRAN* gives intensities at 296 K. By definition:

$$S_{HIT}(300) = \frac{g'_{HIT}}{Q_{HIT}(300)} \frac{A}{8\pi c \nu_0^2} \mathrm{e}^{-hcE''/k_B 300}(1 - \mathrm{e}^{-hc\nu_0/k_B 300}) \tag{A.7}$$

and

$$S_{HIT}(296) = \frac{g'_{HIT}}{Q_{HIT}(296)} \frac{A}{8\pi c \nu_0^2} \mathrm{e}^{-hcE''/k_B 296}(1 - \mathrm{e}^{-hc\nu_0/k_B 296}). \tag{A.8}$$

Combining the last two equations one obtains

$$S_{HIT}(296) = S_{HIT}(300)\, exp\left[\frac{hcE''}{k_B}\left(\frac{1}{300} - \frac{1}{296}\right)\right]\left[\frac{1 - \mathrm{e}^{-hc\nu_0/k_B 296}}{1 - e^{-hc\nu_0/k_B 300}}\right]\frac{Q_{HIT}(300)}{Q_{HIT}(296)}, \tag{A.9}$$

or using Eq. (A.5):

$$\begin{aligned} S_{HIT}(296) &= I_a \frac{I_{JPL}(\mathrm{nm^2\,MHz})}{2.99792458 \times 10^{18}} \frac{Q_{JPL}(300)}{Q_{HIT}(300)} \frac{g'_{HIT}}{g'_{JPL}} \exp\left[\frac{hcE''}{k_B}\left(\frac{1}{300} - \frac{1}{296}\right)\right]\left[\frac{1 - \mathrm{e}^{-hc\nu_0/k_B 296}}{1 - \mathrm{e}^{-hc\nu_0/k_B 300}}\right]\frac{Q_{HIT}(300)}{Q_{HIT}(296)} \\ &= I_a \frac{I_{JPL}(\mathrm{nm^2\,MHz})}{2.99792458 \times 10^{18}} \exp\left[\frac{hcE''}{k_B}\left(\frac{1}{300} - \frac{1}{296}\right)\right]\left[\frac{1 - \mathrm{e}^{-hc\nu_0/k_B 296}}{1 - \mathrm{e}^{-hc\nu_0/k_B 300}}\right]\frac{Q_{JPL}(300)}{Q_{HIT}(296)} \frac{g'_{HIT}}{g'_{JPL}}. \end{aligned} \tag{A.10}$$

A.5. Approximate temperature adjustment

It should be noted that in the majority of cases in the literature, step 3 is omitted and the last equation in step 4 can be approximated by

$$S_{HIT}(296) \cong I_a \frac{I_{JPL}(\mathrm{nm^2\,MHz})}{2.99792458\times10^{18}} \exp\left[\frac{hcE''}{k_B}\left(\frac{1}{300}-\frac{1}{296}\right)\right]\left[\frac{1-e^{-hc\nu_0/k_B296}}{1-e^{-hc\nu_0/k_B300}}\right]\left(\frac{300}{296}\right)^n, \tag{A.11}$$

where $n=1$ for linear molecules and $n=3/2$ for nonlinear molecules. Sometimes an even coarser approximation is used:

$$S_{HIT}(296) \cong I_a \frac{I_{JPL}(\mathrm{nm^2\,MHz})}{2.99792458\times10^{18}} \exp\left[\frac{hcE''}{k_B}\left(\frac{1}{300}-\frac{1}{296}\right)\right]\left(\frac{300}{296}\right)^{n+1}. \tag{A.12}$$

Appendix B. Definitions and units used in *HITRAN*

The *HITRAN* database does not strictly use the International System of Units (SI). The units have been chosen for historical, transmission-algorithm structure, and/or instrument-related reasons. Table 10 gives the units for the spectroscopic parameters and related constants in *HITRAN*.

Table 10
Definitions and units associated with the *HITRAN* database.

Variable	Definition	Units	Comments
Mol	Molecule number	Unitless	Chronological assignment
I_a	Isotopologue number	Unitless	Ordering based on terrestrial values of atoms given in Ref. [389]
ν	Transition wavenumber	$\mathrm{cm^{-1}}$	Line position in vacuum
S	Intensity	$\mathrm{cm^{-1}/(molecule\,cm^{-2})}$	At 296 K
A	Einstein A-coefficient	$\mathrm{s^{-1}}$	See Ref. [387]
γ_{air}	Air-broadened half-width	$\mathrm{cm^{-1}\,atm^{-1}}$	HWHM at 296 K
γ_{self}	Self-broadened half-width	$\mathrm{cm^{-1}\,atm^{-1}}$	HWHM at 296 K
E''	Lower-state energy	$\mathrm{cm^{-1}}$	Referenced to zero for lowest possible level
n_{air}	Temperature-dependence exponent of γ_{air}	Unitless	
δ_{air}	Air pressure-induced shift	$\mathrm{cm^{-1}\,atm^{-1}}$	At 296 K
ν',ν''	Upper- and lower-state "global" quanta	Unitless	See Table 3 of Ref. [1]
q',q''	Upper- and lower-state "local" quanta	Unitless	See Table 4 of Ref. [1]
ierr	Uncertainty indices	Unitless	See Table 5 of Ref. [1]
iref	Reference indices	Unitless	Pointers to sources in *HITRAN*
g',g''	Upper- and lower-state statistical weights	Unitless	Includes state-independent factors in *HITRAN*, see Ref. [387]
Other properties or constants			
Q	Partition sum	Unitless	Function of temperature
h	Planck constant	erg s	$6.62606896(33)\times10^{-27}$
c	Speed of light	$\mathrm{cm\,s^{-1}}$	2.99792458×10^{10}
k_B	Boltzmann constant	$\mathrm{erg\,K^{-1}}$	$1.3806504(24)\times10^{-16}$
T	Temperature	K	

References

[1] Rothman LS, Jacquemart D, Barbe A, Chris Benner D, Birk M, Brown LR, et al. The HITRAN 2004 molecular spectroscopic database. JQSRT 2005;96:139–204.
[2] Waters JW, Froidevaux L, Harwood RS, Jarnot RF, Pickett HM, Read WG, et al. The earth observing system microwave limb sounder (EOS MLS) on the Aura Satellite. IEEE Trans Geosci Remote Sensing 2006;44:1075–92.
[3] Beer R. TES on the aura mission: scientific objectives, measurements, and analysis overview. IEEE Trans Geosci Remote Sensing 2006;44:1102–5.
[4] Fischer H, Birk M, Blom C, Carli B, Carlotti M, von Clarmann T, et al. MIPAS: an instrument for atmospheric and climate research. Atmos Chem Phys 2008;8:2151–88.
[5] Bernath PF, McElroy CT, Abrams MC, Boone CD, Butler M, Camy-Peyret C, et al. Atmospheric chemistry experiment (ACE): mission overview. Geophys Res Lett 2005;32:5.
[6] Aumann HH, Chahine MT, Gautier C, Goldberg MD, Kalnay E, McMillin LM, et al. AIRS/AMSU/HSB on the aqua mission: design, science objectives, data products, and processing systems. IEEE Trans Geosci Remote Sensing 2003;41:253–64.
[7] Clerbaux C, Hadji-Lazaro J, Turquety S, George M, Coheur PF, Hurtmans D, et al. The IASI/MetOp1 mission: first observations and highlights of its potential contribution to GMES2. Space Res Today 2007;168:19–24.
[8] Crisp D, Atlas RM, Breon FM, Brown LR, Burrows JP, Ciais P, et al. The orbiting carbon observatory (OCO) mission. Adv Space Res 2004;34:700–9.
[9] Yokomizo M. Greenhouse gases observing SATellite (GOSAT) ground systems. Fujitsu Sci Techn J 2008;44:410–7.
[10] Hartmann JM, Boulet C, Robert D. Collisional effects on molecular spectra, laboratory experiments and models, consequences for applications. Amsterdam: Elsevier; 2008.

[11] Shiba H, Sato S, Yamashita T, Kobayashi Y, Takami H. Detection of water vapor in T Tauri stars. Astrophys J Suppl Ser 1993;89:299–319.
[12] Tinetti G, Vidal-Madjar A, Liang MC, Beaulieu JP, Yung Y, Carey S, et al. Water vapour in the atmosphere of a transiting extrasolar planet. Nature 2007;448:169–71.
[13] Toth RA. Linelists of water vapor parameters from 500 to 8000 cm^{-1}. See: 〈http://mark4sun.jpl.nasa.gov/data/spec/〉.
[14] Coudert LH. Line frequency and line intensity analyses of water vapour. Mol Phys 1999;96:941–54.
[15] Coudert LH, Wagner G, Birk M, Baranov YI, Lafferty WJ, Flaud JM. The $H_2{}^{16}O$ molecule: line position and line intensity analyses up to the second triad. J Mol Spectrosc 2008;251:339–57.
[16] Lodi L, Tennyson J. A line list of allowed and forbidden rotational transition intensities for water. JQSRT 2008;109:1219–33.
[17] Barber RJ, Tennyson J, Harris GJ, Tolchenov RN. A high-accuracy computed water line list. Mon Not R Astron Soc 2006;368:1087–94.
[18] Jenouvrier A, Daumont L, Régalia-Jarlot L, Tyuterev VG, Carleer M, Vandaele AC, et al. Fourier transform measurements of water vapor line parameters in the 4200–6600 cm^{-1} region. JQSRT 2007;105:326–55.
[19] Mikhailenko SN, Wang L, Kassi S, Campargue A. Weak water absorption lines around 1.455 and 1.66 μm by CW-CRDS. J Mol Spectrosc 2007;244:170–8.
[20] Lodi L, Tolchenov RN, Tennyson J, Lynas-Gray AE, Shirin SV, Zobov NF, et al. A new ab initio ground-state dipole moment surface for the water molecule. J Chem Phys 2008;128:044304.
[21] Tolchenov R, Tennyson J. Water line parameters from refitted spectra constrained by empirical upper state levels: study of the 9500–14500 cm^{-1} region. JQSRT 2008;109:559–68.
[22] Schermaul R, Learner RCM, Newnham DA, Williams RG, Ballard J, Zobov NF, et al. The water vapor spectrum in the region 8600–15 000 cm^{-1}: experimental and theoretical studies for a new spectral line database: I. Laboratory measurements. J Mol Spectrosc 2001;208:32–42.
[23] Schermaul R, Learner RCM, Canas AAD, Brault JW, Polyansky OL, Belmiloud D, et al. Weak line water vapor spectra in the region 13 200–15 000 cm^{-1}. J Mol Spectrosc 2002;211:169–78.
[24] Brown LR, Toth RA, Dulick M. Empirical line parameters of $H_2{}^{16}O$ near 0.94 μm: positions, intensities and air-broadening coefficients. J Mol Spectrosc 2002;212:57–82.
[25] Tolchenov RN, Naumenko O, Zobov NF, Shirin SV, Polyansky OL, Tennyson J, et al. Water vapour line assignments in the 9250–26 000 cm^{-1} frequency range. J Mol Spectrosc 2005;233:68–76.
[26] Coheur PF, Fally S, Carleer M, Clerbaux C, Colin R, Jenouvrier A, et al. New water vapor line parameters in the 26 000–13 000 cm^{-1} region. JQSRT 2002;74:493–510.
[27] Tanaka M, Naumenko O, Brault JW, Tennyson J. Fourier transform absorption spectra of $H_2^{18}O$ and $H_2^{17}O$ in the $3\nu+\delta$ and 4ν polyad region. J Mol Spectrosc 2005;234:1–9.
[28] Chevillard JP, Mandin JY, Flaud JM, Camy-Peyret C. $H_2{}^{18}O$ line positions and intensities between 9500 and 11 500 cm^{-1}. The (0 4 1), (2 2 0), (1 2 1), (3 0 0), (2 0 1), (1 0 2), and (0 0 3) interacting states. Can J Phys 1987;65:777–89.
[29] Tanaka M, Brault JW, Tennyson J. Absorption spectrum of $H_2{}^{18}O$ in the 12 400–14 520 cm^{-1} range. J Mol Spectrosc 2002;216:77–80.
[30] Voronin BA, Naumenko OV, Carleer M, Coheur PF, Fally S, Jenouvrier A, et al. HDO absorption spectrum above 11 500 cm^{-1}: assignment and dynamics. J Mol Spectrosc 2007;244:87–101.
[31] Bach M, Fally S, Coheur PF, Carleer M, Jenouvrier A, Vandaele AC. Line parameters of HDO from high-resolution Fourier transform spectroscopy in the 11 500–23 000 cm^{-1} spectral region. J Mol Spectrosc 2005;232:341–50.
[32] Gordon IE, Rothman LS, Gamache RR, Jacquemart D, Boone C, Bernath PF, et al. Current updates of the water-vapor line list in HITRAN: a new "Diet" for air-broadened half-widths. JQSRT 2007;108:389–402.
[33] Cazzoli G, Puzzarini C, Buffa G, Tarrini O. Experimental and theoretical investigation on pressure-broadening and pressure-shifting of the 22.2 GHz line of water. JQSRT 2007;105:438–49.
[34] Durry G, Zeninari V, Parvitte B, Le Barbu T, Lefevre F, Ovarlez J, et al. Pressure-broadening coefficients and line strengths of H_2O near 1.39 μm: application to the in situ sensing of the middle atmosphere with balloonborne diode lasers. JQSRT 2005;94:387–403.
[35] Liu X, Zhou X, Jeffries JB, Hanson RK. Experimental study of H_2O spectroscopic parameters in the near-IR (6940–7440 cm^{-1}) for gas sensing applications at elevated temperature. JQSRT 2007;103:565–77.
[36] Liu X, Jeffries JB, Hanson RK. Measurements of spectral parameters of water-vapour transitions near 1388 and 1345 nm for accurate simulation of high-pressure absorption spectra. Meas Sci Technol 2007:1185–94.
[37] Seta T, Hoshina H, Kasai Y, Hosako I, Otani C, Loßow S, et al. Pressure broadening coefficients of the water vapor lines at 556.936 and 752.033 GHz. JQSRT 2008;109:144–50.
[38] Golubiatnikov GY, Koshelev MA, Krupnov AF. Pressure shift and broadening of 110–101 water vapor lines by atmosphere gases. JQSRT 2008;109: 1828–33.
[39] Toth RA. Measurements and analysis (using empirical functions for widths) of air- and self-broadening parameters of H_2O. JQSRT 2005;94:1–50.
[40] Cazzoli G, Puzzarini C, Buffa G, Tarrini O. Pressure-broadening in the THz frequency region: the 1.113 THz line of water. JQSRT 2008;109:1563–74.
[41] Koshelev MA, Tretyakov MY, Golubiatnikov GY, Parshin VV, Markov VN, Koval IA. Broadening and shifting of the 321-, 325- and 380-GHz lines of water vapor by pressure of atmospheric gases. J Mol Spectrosc 2007;241:101–8.
[42] Ibrahim N, Chelin P, Orphal J, Baranov YI. Line parameters of H_2O around 0.8 μm studied by tuneable diode laser spectroscopy. JQSRT 2008; 109:2523–36.
[43] Lisak D, Rusciano G, Sasso A. An accurate comparison of lineshape models on H_2O lines in the spectral region around 3 μm. J Mol Spectrosc 2004;227:162–71.
[44] Cazzoli G, Puzzarini C, Buffa G, Tarrini O. Pressure-broadening of water lines in the THz frequency region: improvements and confirmations for spectroscopic databases. Part I. JQSRT 2008;109:2820–31.
[45] Bruno A, Pesce G, Rusciano G, Sasso A. Self-, Nitrogen-, and Oxygen-broadening coefficient measurements in the ν_1 band of H_2O using a difference frequency generation spectrometer at 3 μm. J Mol Spectrosc 2002;215:244–50.
[46] Gamache RR, Laraia A. N_2-, O_2-, and air-broadened half-widths, their temperature dependence, and line shifts for the rotation band of $H_2{}^{16}O$. J Mol Spectrosc 2009, submitted.
[47] Lynch R, Gamache RR, Neshyba SP. N_2 and O_2 induced halfwidths and line shifts of water vapor transitions in the (3 0 1)←(0 0 0) and (2 2 1)←(0 0 0) bands. JQSRT 1998;59:595–613.
[48] Antony BK, Neshyba S, Gamache RR. Self-broadening of water vapor transitions via the complex Robert–Bonamy theory. JQSRT 2007;105:148–63.
[49] Antony BK, Gamache RR. Self-broadened half-widths and self-induced line shifts for water vapor transitions in the 3.2–17.76 μm spectral region via complex Robert–Bonamy theory. J Mol Spectrosc 2007;243:113–23.
[50] Gamache RR. Lineshape parameters for water vapor in the 3.2–17.76 μm region for atmospheric applications. J Mol Spectrosc 2005;229:9–18.
[51] Toth RA, Brown LR, Miller CE, Devi VM, Benner DC. Line strengths of $^{12}C^{16}O_2$: 4550–7000 cm^{-1}. J Mol Spectrosc 2006;239:221–42.
[52] Toth RA, Brown LR, Miller CE, Devi VM, Benner DC. Self-broadened widths and shifts of $^{12}C^{16}O_2$: 4750–7000 cm^{-1}. J Mol Spectrosc 2006;239:243–71.
[53] Toth RA, Miller CE, Brown LR, Devi VM, Benner DC. Line positions and strengths of $^{16}O^{12}C^{18}O$, $^{18}O^{12}C^{18}O$ and $^{17}O^{12}C^{18}O$ between 2200 and 7000 cm^{-1}. J Mol Spectrosc 2007;243:43–61.
[54] Toth RA, Miller CE, Malathy Devi V, Benner DC, Brown LR. Air-broadened halfwidth and pressure shift coefficients of $^{12}C^{16}O_2$ bands: 4750–7000 cm^{-1}. J Mol Spectrosc 2007;246:133–57.
[55] Malathy Devi V, Benner DC, Brown LR, Miller CE, Toth RA. Line mixing and speed dependence in CO_2 at 6348 cm^{-1}: positions, intensities, and air- and self-broadening derived with constrained multispectrum analysis. J Mol Spectrosc 2007;242:90–117.

[56] Devi VM, Benner DC, Brown LR, Miller CE, Toth RA. Line mixing and speed dependence in CO_2 at 6227.9 cm^{-1}: constrained multispectrum analysis of intensities and line shapes in the 30013←00001 band. J Mol Spectrosc 2007;245:52–80.
[57] Toth RA, Brown LR, Miller CE, Malathy Devi V, Benner DC. Spectroscopic database of CO_2 line parameters: 4300–7000 cm^{-1}. JQSRT 2008;109:906–21.
[58] Toth RA, Miller CE, Brown LR, Devi VM, Benner DC. Line strengths of $^{16}O^{13}C^{16}O$, $^{16}O^{13}C^{18}O$, $^{16}O^{13}C^{17}O$ and $^{18}O^{13}C^{18}O$ between 2200 and 6800 cm^{-1}. J Mol Spectrosc 2008;251:64–89.
[59] Ding Y, Macko P, Romanini D, Perevalov VI, Tashkun SA, Teffo JL, et al. High sensitivity CW-cavity ringdown and Fourier transform absorption spectroscopies of $^{13}CO_2$. J Mol Spectrosc 2004;226:146–60.
[60] Majcherova Z, Macko P, Romanini D, Perevalov VI, Tashkun SA, Teffo JL, et al. High-sensitivity CW-cavity ringdown spectroscopy of $^{12}CO_2$ near 1.5 μm. J Mol Spectrosc 2005;230:1–21.
[61] Perevalov BV, Campargue A, Gao B, Kassi S, Tashkun SA, Perevalov VI. New CW-CRDS measurements and global modeling of $^{12}C^{16}O_2$ absolute line intensities in the 1.6 μm region. J Mol Spectrosc 2008;252:190–7.
[62] Perevalov BV, Kassi S, Perevalov VI, Tashkun SA, Campargue A. High sensitivity CW-CRDS spectroscopy of $^{12}C^{16}O_2$, $^{16}O^{12}C^{17}O$ and $^{16}O^{12}C^{18}O$ between 5851 and 7045 cm^{-1}: line positions analysis and critical review of the current databases. J Mol Spectrosc 2008;252:143–59.
[63] Perevalov BV, Deleporte T, Liu AW, Kassi S, Campargue A, Vander Auwera J, et al. Global modeling of $^{13}C^{16}O_2$ absolute line intensities from CW-CRDS and FTS measurements in the 1.6 and 2.0 μm regions. JQSRT 2008;109:2009–26.
[64] Perevalov BV, Kassi S, Romanini D, Perevalov VI, Tashkun SA, Campargue A. Global effective Hamiltonians of $^{16}O^{13}C^{17}O$ and $^{16}O^{13}C^{18}O$ improved from CW-CRDS observations in the 5900–7000 cm^{-1} region. J Mol Spectrosc 2007;241:90–100.
[65] Perevalov BV, Perevalov VI, Campargue A. A (nearly) complete experimental linelist for $^{13}C^{16}O_2$, $^{16}O^{13}C^{18}O$, $^{16}O^{13}C^{17}O$, $^{13}C^{18}O_2$ and $^{17}O^{13}C^{18}O$ by high-sensitivity CW-CRDS spectroscopy between 5851 and 7045 cm^{-1}. JQSRT 2008;109:2437–62.
[66] Campargue A, Perevalov BV. Comment on "Spectroscopic database of CO_2 line parameters: 4300–7000 cm^{-1}". JQSRT 2008;109:2261–71.
[67] Teffo JL, Sulakshina ON, Perevalov VI. Effective Hamiltonian for rovibrational energies and line intensities of carbon dioxide. J Mol Spectrosc 1992;156:48–64.
[68] Perevalov VI, Lobodenko EI, Lyulin OM, Teffo JL. Effective dipole moment and band intensities problem for carbon dioxide. J Mol Spectrosc 1995;171:435–52.
[69] Tashkun SA, Perevalov VI, Teffo JL, Rothman LS, Tyuterev VG. Global fitting of $^{12}C^{16}O_2$ vibrational-rotational line positions using the effective Hamiltonian approach. JQSRT 1998;60:785–801.
[70] Tashkun SA, Perevalov VI, Teffo JL, Tyuterev VG. Global fit of $^{12}C^{16}O_2$ vibrational-rotational line intensities using the effective operator approach. JQSRT 1999;62:571–98.
[71] Perevalov VI, Tashkun SA. CDSD-296 (Carbon Dioxide Spectroscopic Databank): updated and enlarged version for atmospheric applications. In: 10th HITRAN database conference, Cambridge, MA, USA, 2008.
[72] Tashkun SA, Perevalov VI, Teffo JL, Bykov AD, Lavrentieva NN. CDSD-296, the carbon dioxide spectroscopic databank: version for atmospheric applications. In: 14th international symposium on high resolution molecular spectroscopy, Krasnoyarsk, Russia, 2003.
[73] Predoi-Cross A, McKellar ARW, Chris Benner D, Malathy Devi V, Gamache RR, Miller CE, et al. Temperature dependences for air-broadened Lorentz half width and pressure-shift coefficients in the 30013←00001 and 30012←00001 bands of CO_2 near 1600 nm. Can J Phys 2009; accepted.
[74] Pollack JB, Dalton JB, Grinspoon D, Wattson RB, Freedman R, Crisp D, et al. Near-infrared light from venus' nightside: a spectroscopic analysis. Icarus 1993;103:1–42.
[75] Vander Auwera J, Claveau C, Teffo JL, Tashkun SA, Perevalov VI. Absolute line intensities of $^{13}C^{16}O_2$ in the 3090–3920 cm^{-1} region. J Mol Spectrosc 2006;235:77–83.
[76] Wattson RB, Rothman LS. Direct numerical diagonalization: wave of the future. JQSRT 1992;48:763–80.
[77] Wang L, Perevalov VI, Tashkun SA, Song KF, Hu SM. Fourier transform spectroscopy of $^{12}C^{18}O_2$ and $^{16}O^{12}C^{18}O$ in the 3800–8500 cm^{-1} region and the global modeling of the absorption spectrum of $^{12}C^{18}O_2$. J Mol Spectrosc 2008;247:64–75.
[78] Mikhailenko S, Barbe A, Babikov Y, Tyuterev VG. S&MPO-a databank and information system for ozone spectroscopy on the WEB. See: 〈http://smpo.iao.ru〉.
[79] Plateaux JJ, Barbe A, Delahaigue A. Reims high resolution Fourier transform spectrometer—data reduction for ozone. Spectrochim Acta Part A 1995;51:1153–69.
[80] See: 〈http://smpo.iao.ru/ru/lev/par/1/6/〉 (December 2007).
[81] See: 〈http://smpo.iao.ru/en/lev/par/1/4/〉 (June 2000).
[82] Pickett HM, Cohen EA, Brown LR, Rinsland CP, Smith MAH, Devi VM, et al. The vibrational and rotational spectra for ozone for (0,1,0) and (0,2,0) states. J Mol Spectrosc 1988;128:151–71.
[83] Bouazza S, Barbe A, Mikhailenko S, Plateaux JJ. Line positions and intensities of the $\nu_1+2\nu_2+\nu_3$ and $2\nu_2+2\nu_3$ bands of $^{16}O_3$. J Mol Spectrosc 1994;166:365–71.
[84] Barbe A, Sulakshina O, Plateaux JJ, Hamdouni A, Bouazza S. High-resolution infrared spectra of ozone in the 2300–2600 cm^{-1} region. J Mol Spectrosc 1995;170:244–50.
[85] Sulakshina O, Institute of Atmospheric Optics, Tomsk, Russia, private communication, 1998. See: 〈http://smpo.iao.ru/en/lev/par/1/7/〉.
[86] Flaud JM, Wagner G, Birk M, Camy-Peyret C, Claveau C, De Backer-Barilly MR, et al. Ozone absorption around 10 μm. J Geophys Res 2003;108(D9):4269.
[87] Flaud JM, Camy-Peyret C, Rinsland CP, Smith MAH, Malathy Devi V. Line parameters for $^{16}O_3$ bands in the 7-μm region. J Mol Spectrosc 1989;134:106–12.
[88] Barbe A, Chichery A, Tyuterev VG, Tashkun S, Mikhailenko S. The $2\nu_2$ and $3\nu_2-\nu_2$ bands of ozone. Spectrochim Acta Part A 1998;54A:1935–45.
[89] Mikhailenko S, Barbe A, Tyuterev VG. Extended analysis of line positions and intensities of ozone bands in the 2900–3400 cm^{-1} region. J Mol Spectrosc 2002;215:29–41.
[90] De Backer-Barilly MR. Université de Reims, Reims, France, private communication, 2002. See: 〈http://smpo.iao.ru/ru/lev/par/1/5/〉.
[91] Chichery A, Barbe A, Tyuterev VG, Sulakshina O, Borkov Y. Intensities of the difference bands $\nu_1+\nu_3-\nu_2$ and $2\nu_3-\nu_2$ of ozone. Comparison with theoretical predictions. J Mol Struct 2000;517:165–70.
[92] Malathy Devi V, Flaud JM, Camy-Peyret C, Rinsland CP, Smith MAH. Line positions and intensities for the $\nu_1+\nu_2$ and $\nu_2+\nu_3$ bands of $^{16}O_3$. J Mol Spectrosc 1987;125:174–83.
[93] Barbe A, Mikhailenko S, Plateaux JJ, Tyuterev VG. First study of the $\nu_2=3$ dyad (1 3 0)/(0 3 1) of ozone through the analysis of hot bands in the 2300–2600 cm^{-1} region. J Mol Spectrosc 1998;187:70–4.
[94] Bouazza S, Mikhailenko S, Barbe A, Regalia L, Tyuterev VG, Plateaux JJ. The $\nu_1+\nu_2+2\nu_3$ and $\nu_2+3\nu_3$ bands of $^{16}O_3$. J Mol Spectrosc 1995;174:510–9.
[95] Barbe A, Plateaux JJ, Bouazza S, Sulakshina O, Mikhailenko S, Tyuterev VG, et al. Experimental and theoretical study of absolute intensities of ozone spectral lines in the range 1850–2300 cm^{-1}. JQSRT 1994;52:341–55.
[96] Flaud JM, Camy-Peyret C, Devi VM, Rinsland CP, Smith MAH. The ν_1 and ν_3 Bands of $^{16}O_3$: line positions and intensities. J Mol Spectrosc 1987;124:209–17.
[97] Transition moment parameters. See: 〈http://smpo.iao.ru/ru/tran/par/1/8-3/〉.
[98] Hamiltonian parameters. See: 〈http://smpo.iao.ru/ru/lev/par/1/12/〉.
[99] Transition moment. See: 〈http://smpo.iao.ru/ru/tran/par/1/8-2/〉.
[100] Mikhailenko S, Barbe A, De Backer-Barilly MR, Tyuterev VG. Update of line parameters of ozone in the 2590–2900 cm^{-1} region. Appl Opt 2008;47:4612–8.

[101] Barbe A, Mikhailenko S, Plateaux JJ. First observation of the $v_2 = 3$ state of ozone: the (1 3 1) state through analysis of cold and hot bands. Study of v_2 behavior. J Mol Spectrosc 1997;184:448–53.
[102] Barbe A, Mikhailenko S, Tyuterev VG, Hamdouni A, Plateaux JJ. Analysis of the $2v_1+2v_2+v_3$ band of ozone. J Mol Spectrosc 1995;171:583–8.
[103] Barbe A, Plateaux JJ. Analysis of the $2v_1+2v_3$ band of ozone: Line positions and intensities. JQSRT 1996;55:449–55.
[104] Mikhailenko S, Barbe A, Tyuterev VG, Regalia L, Plateaux JJ. Line positions and intensities of the $v_1+v_2+3v_3$, v_2+4v_3, and $3v_1+2v_2$ bands of ozone. J Mol Spectrosc 1996;180:227–35.
[105] SMPO. See: 〈http://smpo.iao.ru/ru/tran/par/1/17-3/〉.
[106] Barbe A, Mikhailenko S, Plateaux JJ, Tyuterev VG. Analysis of the $2v_1+v_2+2v_3$ band of ozone. J Mol Spectrosc 1997;182:333–41.
[107] Bouazza S, Barbe A, Plateaux JJ. Line positions and intensities for the $2v_1+v_2+v_3$ band of $^{16}O_3$. J Mol Spectrosc 1995;171:86–90.
[108] Perrin AM, Vasserot AM, Flaud JM, Camy-Peyret C, Devi VM, Smith MAH, et al. The 2.5 μm bands of ozone: line positions and intensities. J Mol Spectrosc 1991;149:519–29.
[109] Mikhailenko S, Barbe A, Tyuterev VG, Plateaux JJ. New analysis of the (2 1 1)/(1 4 0)/(3 1 0)/(0 0 4)/(1 0 3) interacting states of ozone. In: VIII joint international symposium "atmospheric and ocean optics, atmospheric physics," Irkutsk, Russia, 2001.
[110] Barbe A, Sulakshina O, Plateaux JJ, Tyuterev VG, Bouazza S. Line positions and intensities of the $3v_1+v_3$ band of ozone. J Mol Spectrosc 1996;175:296–302.
[111] Barbe A, Plateaux JJ, Mikhailenko SN, Tyuterev VG. Infrared spectrum of ozone in the 4600 and 5300 cm^{-1} regions: high order accidental resonances through the analysis of $v_1+2v_2+3v_3-v_2$, $v_1+2v_2+3v_3$, and $4v_1+v_3$ bands. J Mol Spectrosc 1997;185:408–16.
[112] Flaud JM, Barbe A, CamyPeyret C, Plateaux JJ. High resolution analysis of the $5v_3$, $3v_1+v_2+v_3$, and v_1+4v_3 bands of $^{16}O_3$: Line positions and intensities. J Mol Spectrosc 1996;177:34–9.
[113] Barbe A, Plateaux JJ, Tyuterev VG, Mikhailenko S. Analysis of high resolution measurements of the $2v_1+3v_3$ band of ozone: coriolis interaction with the $v_1+3v_2+2v_3$ band. JQSRT 1998;185–94.
[114] Barbe A, Chichery A, Tyuterev VG, Taskhun SA, Mikhailenko SN. Infrared high-resolution spectra of ozone in the range 5500–5570 cm^{-1}: analysis of v_2+5v_3 and $v_1+v_2+4v_3$ bands. J Phys B At Mol Opt Phys 1998;31:2559–69.
[115] Barbe A, Chichery A. The $2v_1+v_2+3v_3$ band of $^{16}O_3$: Line positions and intensities. J Mol Spectrosc 1998;192:102–10.
[116] Barbe A, Chichery A, Tyuterev VG, Plateaux JJ. Analysis of high resolution measurements of the v_1+5v_3 band of ozone: coriolis interactions with the $6v_3$ and $3v_1+v_2+2v_3$ bands. Mol Phys 1998;94:751–7.
[117] Flaud JM, Camy-Peyret C, Ngom A, Devi VM, Rinsland CP, Smith MAH. The n_2 bands of $^{16}O^{18}O^{16}O$ and $^{16}O^{16}O^{18}O$: line positions and intensities. J Mol Spectrosc 1989;133:217–23.
[118] Chichery A, Barbe A, Tyuterev VG, Tashkun S. High resolution IR spectra of ^{18}O-enriched ozone: band centers of $^{16}O^{16}O^{18}O$, $^{16}O^{18}O^{18}O$, $^{18}O^{16}O^{18}O$, and $^{16}O^{18}O^{16}O$. J Mol Spectrosc 2001;205:347–9.
[119] De Backer-Barilly MR, Barbe A, Tyuterev VG, Chichery A, Bourgeois MT. High-resolution infrared spectra of the $^{16}O^{18}O^{16}O$ ozone isotopomer in the range 900–5000 cm^{-1}: line positions. J Mol Spectrosc 2002;216:454–64.
[120] De Backer-Barilly MR. Université de Reims, Reims, France, private communication, 2007.
[121] Wagner G, Birk M, Schreier F, Flaud JM. Spectroscopic database for ozone in the fundamental spectral regions. J Geophys Res 2002;107(D22):4626.
[122] Drouin BJ, Gamache RR. Temperature dependent air-broadened linewidths of ozone rotational transitions. J Mol Spectrosc 2008;251:194–202.
[123] Devi VM, Benner DC, Smith MAH, Rinsland CP. Air-broadening and shift coefficients of O_3 Lines in the v_2 band and their temperature dependence. J Mol Spectrosc 1997;182:221–38.
[124] Larsen RW, Nicolaisen FM, Sørensen GO. Determination of self-, air-, and oxygen-broadening coefficients of pure rotational absorption lines of ozone and of their temperature dependencies. J Mol Spectrosc 2001;210:259–70.
[125] Flaud JM, Camy-Peyret C, Rinsland CP, Devi VM, Smith MAH, Goldman A. Improved line parameters for ozone bands in the 10 μm spectral region. Appl Opt 1990;29:3667–71.
[126] Toth RA. Line frequency measurements and analysis of N_2O between 900 and 4700 cm^{-1}. Appl Opt 1991;30:5289–315.
[127] Toth RA. Line strengths (900–3600 cm^{-1}), self-broadened linewidths and frequency shifts (1800–2630 cm^{-1}) of N_2O. Appl Opt 1993;32:7326–65.
[128] Negrão A, Hirtzig M, Coustenis A, Gendron E, Drossart P, Rannou P, et al. The 2-μm spectroscopy of Huygens probe landing site on Titan with very large telescope/nasmyth adaptive optics system near-infrared imager and spectrograph. J Geophys Res 2007;112:E02S92.
[129] Swain MR, Vasisht G, Tinetti G. The presence of methane in the atmosphere of an extrasolar planet. Nature 2008;452:329–31.
[130] Albert S, Bauerecker S, Boudon V, Brown LR, Champion JP, Loëte M, et al. Global analysis of the high resolution infrared spectrum of methane $^{12}CH_4$ in the region from 0 to 4800 cm^{-1}. Chem Phys 2009;356:131–46.
[131] Wishnow EH, Orton GS, Ozier I, Gush HP. The distortion dipole rotational spectrum of CH_4: a low temperature far-infrared study. JQSRT 2007;103:102–17.
[132] Frankenberg C, Warneke T, Butz A, Aben I, Hase F, Spietz P, et al. Pressure broadening in the $2v_3$ band of methane and its implication on atmospheric retrievals. Atmos Chem Phys 2008;8:5061–75.
[133] Margolis JS. Measured line positions and strengths of methane between 5500 and 6180 cm^{-1}. Appl Opt 1988;27:4038–51.
[134] Margolis JS. Empirical values of the ground state energies for methane transitions between 5500 to 6150 cm^{-1}. Appl Opt 1990;29:2295–302.
[135] Gao B, Kassi S, Campargue A. Empirical low energy values for methane transitions in the 5852–6181 cm^{-1} region by absorption spectroscopy at 81 K. J Mol Spectrosc 2009;253:55–63.
[136] Predoi-Cross A, Brown LR, Devi VM, Brawley-Tremblay M, Benner DC. Multispectrum analysis of self-broadening and pressure-shifting coefficients of $^{12}CH_4$ from 4100 to 4635 cm^{-1}. J Mol Spectrosc 2005;232:231–46.
[137] Predoi-Cross A, Brawley-Tremblay M, Brown LR, Devi VM, Benner DC. Multispectrum analysis of $^{12}CH_4$ from 4100 to 4635 cm^{-1}: II. Air-broadening coefficients (widths and shifts). J Mol Spectrosc 2006;236:201–15.
[138] Brown LR, Benner DC, Champion JP, Devi VM, Fejard L, Gamache RR, et al. Methane line parameters in HITRAN. JQSRT 2003;82:219–38.
[139] Brown LR. Empirical line parameters of methane from 1.1 to 2.1 μm. JQSRT 2005;96:251–70.
[140] Smith MAH, Benner DC, Predoi-Cross A, Malathy Devi V. Multispectrum analysis of $^{12}CH_4$ in the v_4 band: I. Air-broadened half widths, pressure-induced shifts, temperature dependences and line mixing. JQSRT 2009; this issue, doi:10.1016/j.jqsrt.2009.02.015.
[141] Smith MAH, Benner DC, Predoi-Cross A, Malathy Devi V. Multispectrum analysis of $^{12}CH_4$ in the v_4 band: II. Self-broadened half widths, pressure-induced shifts, temperature dependences and line mixing. JQSRT 2009, to be submitted.
[142] Antony BK, Niles DL, Wroblewski SB, Humphrey CM, Gabard T, Gamache RR. N_2-, O_2- and air-broadened half-widths and line shifts for transitions in the v_3 band of methane in the 2726- to 3200-cm^{-1} spectral region. J Mol Spectrosc 2008;251:268–81.
[143] Lyulin OM, Nikitin AV, Perevalov VI, Morino I, Yokota T, Kumazawa R, et al. Measurements of N_2- and O_2-broadening and -shifting parameters of the methane spectral lines in the 5550–6236 cm^{-1} region. JQSRT 2009, this issue, doi:10.1016/j.jqsrt.2009.02.012.
[144] Kassi S, Gao B, Romanini D, Campargue A. The near-infrared (1.30–1.70 μm) absorption spectrum of methane down to 77 K. Phys Chem Chem Phys 2008;10:4410.
[145] Thiévin J, Georges R, Carles S, Benidar A, Rowe B, Champion JP. High-temperature emission spectroscopy of methane. JQSRT 2008;109:2027–36.
[146] Wenger C, Champion JP, Boudon V. The partition sum of methane at high temperature. JQSRT 2008;109:2697–706.
[147] Lattanzi V, Walters A, Pearson JC, Drouin BJ. THz spectrum of monodeuterated methane. JQSRT 2008;109:580–6.
[148] Pickett HM, Poynter RL, Cohen EA, Delitsky ML, Pearson JC, Müller HSP. Submillimeter, millimeter and microwave spectral line catalog. JQSRT 1998;60:883–90.
[149] Müller HSP, Schlöder F, Stutzki J, Winnewisser G. The cologne database for molecular spectroscopy, CDMS: a useful tool for astronomers and spectroscopists. J Mol Struct 2005;742:215.

[150] Bézard B, Nixon CA, Kleiner I, Jennings DE. Detection of $^{13}CH_3D$ on Titan. Icarus 2007;191:397–400.
[151] Tarrago G, Delaveau M. Triad $\nu_n(A_1)$, $\nu_t(E)$, $\nu_{t'}(E)$, in C_{3v} molecules: energy and intensity formulation (computer programs). J Mol Spectrosc 1986;119:418–25.
[152] Ulenikov ON, Onopenko GA, Tyabaeva NE, Anttila R, Alanko S, Schroderus J. Rotational analysis of the ground state and the lowest fundamentals v_3, v_5, and v_6 of $^{13}CH_3D$. J Mol Spectrosc 2000;201:9–17.
[153] Brown LR, Nikitin A, Benner DC, Devi VM, Smith MAH, Fejard L, et al. Line intensities of CH_3D in the Triad region: 6–10 μm. J Mol Struct 2004;695–696:181–8.
[154] Nikitin AV, Champion JP, Brown LR. Preliminary analysis of CH_3D from 3250 to 3700 cm^{-1}. J Mol Spectrosc 2006;240:14–25.
[155] Boussin C, Lutz BL, de Bergh C, Hamdouni A. Line intensities and self-broadening coefficients for the $3v_2$ band of monodeuterated methane. JQSRT 1998;60:501–14.
[156] Malathy Devi V, Chris Benner D, Smith MAH, Rinsland CP, Brown LR. Self- and N_2-broadening, pressure induced shift and line mixing in the v_5 band of $^{12}CH_3D$ using a multispectrum fitting technique. JQSRT 2002;74:1–41.
[157] Robichaud DJ, Hodges JT, Maslowski P, Yeung LY, Okumura M, Miller CE, et al. High-accuracy transition frequencies for the O_2 A-band. J Mol Spectrosc 2008;251:27–37.
[158] Robichaud DJ, Hodges JT, Brown LR, Lisak D, Maslowski P, Yeung LY, et al. Experimental intensity and lineshape parameters of the oxygen A-band using frequency-stabilized cavity ring-down spectroscopy. J Mol Spectrosc 2008;248:1–13.
[159] Robichaud DJ, Hodges JT, Lisak D, Miller CE, Okumura M. High-precision pressure shifting measurement technique using frequency-stabilized cavity ring-down spectroscopy. JQSRT 2008;109:435–44.
[160] Brown LR, Plymate C. Experimental line parameters of the oxygen A band at 760 nm. J Mol Spectrosc 2000;199:166–79.
[161] Robichaud DJ, Yeung LY, Long DA, Havey DK, Hodges JT, Lisak D, et al. Experimental line parameters of the A-band of oxygen isotopologues at 760 nm using frequency-stabilized cavity ring-down spectroscopy. J Phys Chem A 2009, submitted for publication.
[162] Yang Z, Wennberg PO, Cageao RP, Pongetti TJ, Toon GC, Sander SP. Ground-based photon path measurements from solar absorption spectra of the O_2 A-band. JQSRT 2005;90:309–21.
[163] Predoi-Cross A, Holladay C, Heung H, Bouanich JP, Mellau GC, Keller R, et al. Nitrogen-broadened lineshapes in the oxygen A-band: experimental results and theoretical calculations. J Mol Spectrosc 2008;251:159–75.
[164] Falke S, Tiemann E, Lisdat C, Schnatz H, Grosche G. Transition frequencies of the D lines of K39, K40, and K41 measured with a femtosecond laser frequency comb. Phys Rev A 2006;74:32503.
[165] Babcock HD, Herzberg L. Fine structure of the red system of atmospheric oxygen bands. Astrophys J 1948;108:167.
[166] Predoi-Cross A, Hambrook K, Keller R, Povey C, Schofield I, Hurtmans D, et al. Spectroscopic lineshape study of the self-perturbed oxygen A-band. J Mol Spectrosc 2008;248:85–110.
[167] Tran H, Hartmann JM. An improved O_2 A band absorption model and its consequences for retrievals of photon paths and surface pressures. J Geophys Res 2008:113.
[168] Washenfelder RA, Toon GC, Blavier JF, Yang Z, Allen NT, Wennberg PO, et al. Carbon dioxide column abundances at the Wisconsin Tall Tower site. J Geophys Res 2006;111:D22305.
[169] Newman SM, Lane IC, Orr-Ewing AJ, Newnham DA, Ballard J. Integrated absorption intensity and Einstein coefficients for the O_2 $a\ ^1\Delta_g$–$X\ ^3\Sigma_g^-$ (0,0) transition: a comparison of cavity ringdown and high resolution Fourier transform spectroscopy with a long-path absorption cell. J Chem Phys 1999;110:10749–57.
[170] Newman SM, Orr-Ewing AJ, Newnham DA, Ballard J. Temperature and pressure dependence of line widths and integrated absorption intensities for the O_2 $a\ ^1\Delta_g$–$X\ ^3\Sigma_g^-$ (0,0) transition. J Phys Chem A 2000;104:9467–80.
[171] Goldman A, Brown LR, Schoenfeld WG, Spencer MN, Chackerian Jr. C, Giver LP, et al. Nitric oxide line parameters: review of 1996 HITRAN update and new results. JQSRT 1998;60:825–38.
[172] Chu PM, Wetzel SJ, Lafferty WJ, Perrin A, Flaud JM, Arcas P, et al. Line intensities for the 8-μm bands of SO_2. J Mol Spectrosc 1998;189:55–63.
[173] Flaud JM, Perrin A, Salah LM, Lafferty WJ, Guelachvili G. A reanalysis of the (0 1 0), (020), (1 0 0) and (0 0 1) rotational levels of $^{32}S^{16}O_2$. J Mol Spectrosc 1993;160:272–8.
[174] Spencer JR, Lellouch E, Richter MJ, López-Valverde MA, Lea Jessup K, Greathouse TK, et al. Mid-infrared detection of large longitudinal asymmetries in Io's SO_2 atmosphere. Icarus 2005;176:283–304.
[175] Henningsen J, Barbe A, De Backer-Barilly MR. Revised molecular parameters for $^{32}SO_2$ and $^{34}SO_2$ from high resolution study of the infrared spectrum in the 7–8 μm wavelength region. JQSRT 2008;109:2491–510.
[176] Sumpf B, Schöne M, Kronfeldt HD. Self- and air-broadening in the v_3 band of SO_2. J Mol Spectrosc 1996;179:137–41.
[177] Sumpf B, Fleischmann O, Kronfeldt HD. Self-, air-, and nitrogen-broadening in the v_1 band of SO_2. J Mol Spectrosc 1996;176:127–32.
[178] Ball CD, Dutta JM, Goyette TM, Helminger P, De Lucia FC. The pressure broadening of SO_2 by N_2, O_2, He, and H_2 between 90 and 500 K. JQSRT 1996;56:109–17.
[179] Sumpf B. Experimental investigation of the self-broadening coefficients in the v_1+v_3 band of SO_2 and the $2v_2$ Band of H_2S. J Mol Spectrosc 1997;181:160–7.
[180] Sumpf B. Line intensity and self-broadening investigations in the 19 μm v_2 band of SO_2. Spectrochim Acta Part A 1999;55:1931–9.
[181] Sumpf B. Line intensity and self-broadening investigations in the v_1 and v_3 bands of SO_2. J Mol Struct 2001;599:39–49.
[182] Pine AS, Suenram RD, Brown ER, McIntosh KA. A terahertz photomixing spectrometer: application to SO_2 self broadening. J Mol Spectrosc 1996;175:37–47.
[183] Lafferty WJ, Flaud JM, Ngom EHA, Sams RL. $^{34}S^{16}O_2$: high-resolution analysis of the (0 3 0), (1 0 1), (1 1 1), (0 0 2) and (2 0 1) vibrational states; determination of equilibrium rotational constants for sulfur dioxide and anharmonic vibrational constants. J Mol Spectrosc 2009;253:51–4.
[184] Lafferty WJ, Flaud JM, Sams RL, Abib Ngom EH. High resolution analysis of the rotational levels of the (0 0 0), (0 1 0), (1 0 0), (0 0 1), (0 2 0), (1 1 0) and (0 1 1) vibrational states of $^{34}S^{16}O_2$. J Mol Spectrosc 2008;252:72–6.
[185] Flaud JM, Lafferty WJ, Sams RL. Line intensities for the v_1, v_3 and v_1+v_3 bands of $^{34}SO_2$. JQSRT 2009; this issue, doi:10.1016/j.jqsrt.2009.12.003.
[186] Flaud JM, Brizzi G, Carlotti M, Perrin A, Ridolfi M. MIPAS database: validation of HNO_3 line parameters using MIPAS satellite measurements. Atmos Chem Phys 2006;6:5037–48.
[187] Gomez L, Tran H, Perrin A, Gamache RR, Laraia A, Orphal J, et al. Some improvements of the HNO_3 spectroscopic parameters in the spectral region from 600 to 950 cm^{-1}. JQSRT 2009; this issue, doi:10.1016/j.jqsrt.2008.07.004.
[188] Perrin A, Orphal J, Flaud JM, Klee S, Mellau G, Mäder H, et al. New analysis of the v_5 and $2v_9$ bands of HNO_3 by infrared and millimeter wave techniques: line positions and intensities. J Mol Spectrosc 2004;228:375–91.
[189] Chackerian C, Sharpe SW, Blake TA. Anhydrous nitric acid integrated absorption cross sections: 820–5300 cm^{-1}. JQSRT 2003;82:429–41.
[190] Laraia A, Gamache RR, Perrin A, Hartmann JM, Gomez L. Theoretical calculations of N_2-broadened half-widths of v_5 transitions of HNO_3. JQSRT 2009; this issue, doi:10.1016/j.jqsrt.2009.02.003.
[191] Mencaraglia F, Bianchini G, Boscaleri A, Carli B, Ceccherini S, Raspollini P, et al. Validation of MIPAS satellite measurements of HNO_3 using comparison of rotational and vibrational spectroscopy. J Geophys Res 2006;111:D19305.
[192] Tran H, Brizzi G, Gomez L, Perrin A, Hase F, Ridolfi M, et al. Validation of HNO_3 spectroscopic parameters using atmospheric absorption and emission measurements. JQSRT 2009;110:109–17.
[193] Petkie DT, Helminger P, Butler RAH, Albert S, De Lucia FC. The millimeter and submillimeter spectra of the ground state and excited v_9, v_8, v_7, and v_6 vibrational states of HNO_3. J Mol Spectrosc 2003;218:127–30.

[194] Petkie DT, Helminger P, Winnewisser BP, Winnewisser M, Butler RAH, Jucks KW, et al. The simulation of infrared bands from the analyses of rotational spectra: the $2\nu_9-\nu_9$ and $\nu_5-\nu_9$ hot bands of HNO_3. JQSRT 2005;92:129–41.
[195] Sirota JM, Weber M, Reuter DC, Perrin A. HNO_3: absolute line intensities for the ν_9 fundamental. J Mol Spectrosc 1997;184:140–4.
[196] Goldman A, Bonomo FS, Williams WJ, Murcray DG. Statistical-band model analysis and integrated intensities for the 21.8 μm bands of HNO_3 vapor. J Opt Soc Am 1975;65:10–2.
[197] Perrin A, Lado-Bordowski O, Valentin A. The ν_3 and ν_4 interacting bands of HNO_3. Mol Phys 1989;67:249–70.
[198] Perrin A, Mbiaké R. The ν_5 and $2\nu_9$ bands of the ^{15}N isotopic species of nitric acid ($H^{15}NO_3$): line positions and intensities. J Mol Spectrosc 2006;237:27–35.
[199] Brizzi G, Carlotti M, Flaud JM, Perrin A, Ridolfi M. First observation of $H^{15}NO_3$ in atmospheric spectra. Geophys Res Lett 2007;34:L03802.
[200] Colin R, Coheur PF, Kiseleva M, Vandaele AC, Bernath PF. Spectroscopic constants and term values for the $X^2\Pi_i$ state of OH ($v = 0$–10). J Mol Spectrosc 2002;214:225–6.
[201] Colin R. University of Brussels, Brussels, Belgium, private communication, 2008.
[202] Goldman A, Schoenfeld WG, Goorvitch D, Chackerian Jr. C, Dothe H, Mélen F, et al. Updated line parameters for OH $X\,^2\Pi$–$X\,^2\Pi$ (v'',v') transitions. JQSRT 1998;59:453–69.
[203] Rinsland CP, Smith MAH, Goldman A, Devi VM, Benner DC. The fundamental bands of $H^{35}Cl$ and $H^{37}Cl$: line positions from high-resolution laboratory data. J Mol Spectrosc 1993;159:274–8.
[204] Coxon JA, Hajigeorgiou PG. The radial Hamiltonians for the $X\,^1\Sigma^+$ and $B\,^1\Sigma^+$ states of HCl. J Mol Spectrosc 2000;203:49–64.
[205] Oh JJ, Cohen EA. Pressure broadening of ClO by N_2 and O_2 near 204 and 649 GHz and new frequency measurements between 632 and 725 GHz. JQSRT 1994;52:151–6.
[206] Bauer A, Birk M, Bühler S, Colmont JM, von Engeln A, Künzi K, et al. Study on a spectroscopic database for millimeter and submillimeter wavelength. Final report of ESA no. 11581/95/NL/CN, 1998.
[207] Régalia-Jarlot L, Hamdouni A, Thomas X, Von der Heyden P, Barbe A. Line intensities of the: ν_3, $4\nu_2$, $\nu_1+\nu_3$, $3\nu_1$ and $2\nu_1+2\nu_2$ bands of $^{16}O^{12}C^{32}S$ molecule. JQSRT 2002;74:455–70.
[208] Vander Auwera J, Fayt A. Absolute line intensities for carbonyl sulfide from 827 to 2939 cm^{-1}. J Mol Struct 2006;780–781:134–41.
[209] Naïm S, Fayt A, Bredohl H, Blavier JF, Dubois I. Fourier transform spectroscopy of carbonyl sulfide from 3700 to 4800 cm^{-1} and selection of a line-pointing program. J Mol Spectrosc 1998;192:91–101.
[210] Fayt A, Vandenhaute R, Lahaye JG. Global rovibrational analysis of carbonyl sulfide. J Mol Spectrosc 1986;119:233–66.
[211] Lahaye JG, Vandenhaute R, Fayt A. CO_2 laser saturation Stark spectra and global rovibrational analysis of the main isotopic species of carbonyl sulfide ($OC^{34}S$, $O^{13}CS$, and ^{18}OCS). J Mol Spectrosc 1987;123:48–83.
[212] Masukidi LS, Lahaye JG, Fayt A. Intracavity CO and CO_2 laser Stark spectroscopy of the isotopomers of carbonyl sulfide. J Mol Spectrosc 1992;154:137–62.
[213] Strugariu T, Naïm S, Fayt A, Bredohl H, Blavier JF, Dubois I. Fourier transform spectroscopy of ^{18}O-enriched carbonyl sulfide from 1825 to 2700 cm^{-1}. J Mol Spectrosc 1998;189:206–19.
[214] Sung K, Toth RA, Brown LR, Crawford T. Line strength measurements of carbonyl sulfide ($^{16}O^{12}C^{32}S$) in the $2\nu_3$, $\nu_1+2\nu_2+\nu_3$, and $4\nu_2+\nu_3$ bands. JQSRT 2009; submitted for publication.
[215] Toth RA, Sung K, Brown LR, Crawford T. Intensities of 43 bands of five isotopologues of OCS near 4100 cm^{-1}. JQSRT, in preparation.
[216] Bermejo D, Domenech JL, Santos J, Bouanich JP, Blanquet G. Absolute line intensities in the $2\nu_3$ band of $^{16}O^{12}C^{32}S$. J Mol Spectrosc 1997;185:26–30.
[217] Rohart F. Université de Lille, Lille, France, private communication, 2008.
[218] Matton S, Rohart F, Bocquet R, Mouret G, Bigourd D, Cuisset A, et al. Terahertz spectroscopy applied to the measurement of strengths and self-broadening coefficients for high-J lines of OCS. J Mol Spectrosc 2006;239:182–9.
[219] Koshelev MA, Tretyakov MY. Collisional broadening and shifting of OCS rotational spectrum lines. JQSRT 2009;110:118–28.
[220] Domenech JL, Bermejo D, Bouanich JP. Pressure lineshift and broadening coefficients in the $2\nu_3$ band of OCS. J Mol Spectrosc 2000;200:266–76.
[221] Bouanich JP, Campers C, Blanquet G, Walrand J. Diode-laser measurements of Ar- and CO_2-broadened linewidths in the ν_1 band of OCS. JQSRT 1988;39:353–65.
[222] Perrin A, Jacquemart D, Kwabia Tchana F, Lacome N. Absolute line intensities measurements and calculations for the 5.7 and 3.6 μm bands of formaldehyde. JQSRT 2009; this issue, doi:10.1016/j.jqsrt.2008.11.005.
[223] Steck T, Glatthor N, von Clarmann T, Fischer H, Flaud JM, Funke B, et al. Retrieval of global upper tropospheric and stratospheric formaldehyde (H_2CO) distributions from high-resolution MIPAS-Envisat spectra. Atmos Chem Phys 2008;8:463–70.
[224] Dufour G, Szopa S, Barkley MP, Boone CD, Perrin A, Palmer P, et al. Global upper tropospheric formaldehyde seasonal cycles investigated through ACE-FTS space borne observations. Atmos Chem Phys 2009;9:1051–95.
[225] Tchana FK, Perrin A, Lacome N. New analysis of the ν_2 band of formaldehyde ($H_2{}^{12}C^{16}O$): line positions for the ν_2, ν_3, ν_4 and ν_6 interacting bands. J Mol Spectrosc 2007;245:141–4.
[226] Margulés L, Perrin A, Janeckovà R, Bailleux S, Endres CP, Giesen TF, et al. Rotational transitions within the ν_2, ν_3, ν_4 and ν_6 bands of formaldehyde $H_2{}^{12}C^{16}O$. Can J Phys, accepted.
[227] Perrin A, Valentin A, Daumont L. New analysis of the $2\nu_4$, $\nu_4+\nu_6$, $2\nu_6$, $\nu_3+\nu_4$, $\nu_3+\nu_6$, ν_1, ν_5, $\nu_2+\nu_4$, $2\nu_3$, $\nu_2+\nu_6$, and $\nu_2+\nu_3$ bands of formaldehyde H_2CO. J Mol Struct 2006;780–781:28–44.
[228] Sharpe SW, Johnson TJ, Sams RL, Chu PM, Rhoderick GC, Johnson PA. Gas-phase databases for quantitative infrared spectroscopy. Appl Spectrosc 2004;58:1452–61.
[229] Gratien A, Picquet-Varrault B, Orphal J, Perraudin E, Doussin JF, Flaud JM. Laboratory intercomparison of the formaldehyde absorption cross sections in the infrared (1660–1820 cm^{-1}) and ultraviolet (300–360 nm) spectral regions. J Geophys Res 2007;112:D05305.
[230] Gratien A, Nilsson E, Doussin JF, Johnson MS, Nielsen CJ, Stenstrom Y, et al. UV and IR absorption cross-sections of HCHO, HCDO, and DCDO. J Phys Chem A 2007;111:11506–13.
[231] Goldman A, Tipping RH, Ma Q, Boone CD, Bernath PF, Demoulin P, et al. On the line parameters for the $X^1\Sigma_g^+$ (1–0) infrared quadrupolar transitions of $^{14}N_2$. JQSRT 2007;103:168–74.
[232] Li H, Le Roy RJ. Quadrupole moment function and absolute infrared quadrupolar intensities for N_2. J Chem Phys 2007;126:4301.
[233] Yang C, Buldyreva J, Gordon IE, Rohart F, Cuisset A, Mouret G, et al. Oxygen, nitrogen and air broadening of HCN spectral lines at terahertz frequencies. JQSRT 2008;109:2857–68.
[234] Rinsland CP, Malathy Devi V, Smith MAH, Benner DC, Sharpe SW, Sams RL. A multispectrum analysis of the ν_1 band of $H^{12}C^{14}N$: part II. Air- and N_2-broadening, shifts and their temperature dependences. JQSRT 2003;82:343–62.
[235] Devi VM, Benner DC, Smith MAH, Rinsland CP, Predoi-Cross A, Sharpe SW, et al. A multispectrum analysis of the ν_2 band of $H^{12}C^{14}N$: part I. Intensities, broadening, and shift coefficients. J Mol Spectrosc 2005;231:66–84.
[236] Nikitin A, Champion JP, Burger H. Global analysis of $^{12}CH_3{}^{35}Cl$ and $^{12}CH_3{}^{37}Cl$: simultaneous fit of the lower five polyads (0–2600 cm^{-1}). J Mol Spectrosc 2005;230:174–84.
[237] Perrin A, Valentin A, Flaud JM, Camy-Peyret C, Schriver L, Schriver A, et al. The 7.9-μm band of hydrogen peroxide: line positions and intensities. J Mol Spectrosc 1995;171:358–73.
[238] Klee S, Winnewisser M, Perrin A, Flaud JM. Absolute line intensities for the ν_6 band of H_2O_2. J Mol Spectrosc 1999;195:154–61.
[239] Lyulin OM, Perevalov VI, Mandin JY, Dana V, Gueye F, Thomas X, et al. Line intensities of acetylene: measurements in the 2.5-μm spectral region and global modeling in the $\Delta p = 4$ and 6 series. JQSRT 2007;103:496–523.

[240] Jacquemart D, Lacome N, Mandin JY, Dana V, Lyulin OM, Perevalov VI. Multispectrum fitting of line parameters for $^{12}C_2H_2$ in the 3.8-μm spectral region. JQSRT 2007;103:478–95.
[241] Jacquemart D, Lacome N, Mandin JY, Dana V, Tran H, Gueye FK, et al. The IR spectrum of $^{12}C_2H_2$: line intensity measurements in the 1.4 μm region and update of the databases. JQSRT 2009; this issue, doi:10.1016/j.jqsrt.2008.10.002.
[242] Jacquemart D, Lacome N, Mandin JY. Line intensities of $^{12}C_2H_2$ in the 1.3, 1.2, and 1 μm spectral regions. JQSRT 2009; this issue, doi:10.1016/j.jqsrt.2008.11.009.
[243] Matsuura M, Wood PR, Sloan GC, Zijlstra AA, van Loon JT, Groenewegen MAT, et al. Spitzer observations of acetylene bands in carbon-rich asymptotic giant branch stars in the Large Magellanic Cloud. Mon Not R Astron Soc 2006;371:415–20.
[244] Vander Auwera J. Absolute intensities measurements in the (ν_4+ν_5) band of $^{12}C_2H_2$: analysis of Herman–Wallis effects and forbidden transitions. J Mol Spectrosc 2000;201:143–50.
[245] Rothman LS, Gamache RR, Barbe A, Goldman A, Gillis JR, Brown LR, et al. AFGL atmospheric absorption line parameters compilation: 1982 edition. Appl Opt 1983;22:2247–56.
[246] Vander Auwera J, Moazzen-Ahmadi N, Flaud JM. Toward an accurate database for the 12 μm region of the ethane spectrum. Astrophys J 2007;662:750–7.
[247] Cooper JR, Moazzen-Ahmadi N. Global fit analysis including the ν_9+ν_4−ν_4 hot band of ethane: evidence of an interaction with the ν_{12} fundamental. J Mol Spectrosc 2006;239:51–8.
[248] Pine AS, Stone SC. Torsional tunneling and A_1−A_2 splittings and air broadening of the $^rQ_0$ and $^pQ_3$ subbranches of the ν_7 band of ethane. J Mol Spectrosc 1996;175:21–30.
[249] Blass WE, Halsey GW, Jennings DE. Self- and foreign-gas broadening of ethane lines determined from diode laser measurements at 12 μm. JQSRT 1987;38:183–4.
[250] Kurtz J, Reuter DC, Jennings DE, Hillman JJ. Laboratory spectra of ^{13}C ethane. J Geophys Res 1991;96(E2):17489–92.
[251] Weber M, Blass WE, Reuter DC, Jennings DE, Hillman JJ. The ground state of $^{13}C^{12}CH_6$ (ethane) derived from ν_{12} at 12.2 μm. J Mol Spectrosc 1993;159:388–94.
[252] Weber M, Reuter DC, Sirota JM, Blass WE, Hillman JJ. Fourier transform infrared and tunable diode laser spectra of $^{13}C^{12}CH_6$ ν_{12} torsion–vibration–rotation band: frequencies, intensities, and barriers to internal rotation. J Chem Phys 1994;100:8681–8.
[253] Weber M, Reuter DC, Jennings DE, Blass WE, Hillman JJ. A spectral atlas of the ν_{12} fundamental of $^{13}C^{12}CH_6$ in the 12 μm region. NASA technical memorandum 104601, Greenbelt; 1994.
[254] Beer R, Taylor FW. Phosphine absorption in the 5-μm window of Jupiter. Icarus 1979;40:189–92.
[255] Butler RAH, Sagui L, Kleiner I, Brown LR. The absorption spectrum of phosphine (PH_3) between 2.8 and 3.7 μm: line positions, intensities, and assignments. J Mol Spectrosc 2006;238:178–92.
[256] Nikitin AV, Champion JP, Butler RAH, Brown LR, Kleiner I. Global modeling of the lower three polyads of PH_3 preliminary results. J Mol Spectrosc, in press, doi:10.1016/j.jms.2009.01.008.
[257] Boudon V, Pierre G. Rovibrational spectroscopy of sulphur hexafluoride: a review. In: Pandalai SG, editor. Recent research developments in molecular spectroscopy, vol. 1. Trivandrum, India: Transworld Research Network; 2002. p. 25–55.
[258] Boudon V, Pierre G, Bürger H. High resolution spectroscopy and analysis of the ν_4 bending region of SF_6 near 615 cm^{-1}. J Mol Spectrosc 2001;205:304–11.
[259] Kim KC, Person WB, Seitz D, Krohn BJ. Analysis of the ν_4 (615 cm^{-1}) region of the Fourier transform and diode laser spectra of SF_6. J Mol Spectrosc 1979;76:322–40.
[260] Person WB, Krohn BJ. Coriolis intensity perturbations of the ν_4 band of SF_6. J Mol Spectrosc 1983;98:229–57.
[261] Wenger Ch, Boudon V, Champion JP, Pierre G. Highly-spherical top data system (HTDS) software for the spectrum simulation of octahedral XY_6 molecules. JQSRT 2000;66(1):1–16 [see also: 〈http://icb.u-bourgogne.fr/OMR/SMA/SHTDS〉].
[262] Vander Auwera J, Didriche K, Perrin A, Keller F. Absolute line intensities for formic acid and dissociation constant of the dimer. J Chem Phys 2007;126:124311.
[263] Perrin A, Vander Auwera J. An improved database for the 9 μm region of the formic acid spectrum. JQSRT 2007;108:363–70.
[264] Perrin A, Vander Auwera J, Zelinger Z. High-resolution Fourier transform study of the ν_3 fundamental band of trans-formic acid. JQSRT 2009; this issue, doi:10.1016/j.jqsrt.2008.09.006.
[265] Coheur PF, Herbin H, Clerbaux C, Hurtmans D, Wespes C, Carleer M, et al. ACE-FTS observation of a young biomass burning plume: first reported measurements of C_2H_4, C_3H_6O, H_2CO and PAN by infrared occultation from space. Atmos Chem Phys Discuss 2007;7:7907–32.
[266] Herndon SC, Zahniser MS, Nelson DD, Shorter J, McManus JB, Jimenez R, et al. Airborne measurements of HCHO and HCOOH during the New England Air Quality Study 2004 using a pulsed quantum cascade laser spectrometer. J Geophys Res 2007;112:D10S03.
[267] Goldman A, Gillis JR. Line parameters and line calculation for molecules of stratospheric interest. Technical report, Department of Physics, University of Denver, 1984.
[268] Perrin A, Rinsland CP, Goldman A. Spectral parameters for the ν_6 region of HCOOH and its measurement in the infrared tropospheric spectrum. J Geophys Res 1999;104(D15):18661–6.
[269] López-Puertas M, Flaud JM, Peralta-Calvillo J, Funke B, Gil-López S. NO^+ fundamental and first hot ro-vibrational line frequencies from MIPAS/Envisat atmospheric spectra. J Mol Spectrosc 2006;237:218–24.
[270] Bowman WC, Herbst E, de Lucia FC. Millimeter and submillimeter spectrum of NO^+. J Chem Phys 1982;77:4261.
[271] Ho WC, Ozier I, Cramb DT, Gerry MCL. Diode laser spectroscopy of the vibrational fundamental of NO^+. J Mol Spectrosc 1991;149:559–61.
[272] Hilpert G, Linnartz H, Havenith M, ter Meulen JJ, Meerts WL. Tunable infrared and far-infrared direct absorption spectroscopy of molecular ions in a supersonic jet expansion. Chem Phys Lett 1994;219:384–8.
[273] Miescher E. Rotationsanalyse der NO^+-banden. Helv Phys Acta 1956;29:135–44.
[274] LeRoy RJ. DParfit 3.3, A computer program for fitting multi-isotopomer diatomic molecule spectra. University of Waterloo Chemical Physics research report CP-660, 2005. See: 〈http://leroy.uwaterloo.ca/〉.
[275] Lary DJ. Gas phase atmospheric bromine photochemistry. J Geophys Res 1996;101(D1):1505–16.
[276] Lary DJ, Chipperfield MP, Toumi R, Lenton T. Heterogeneous atmospheric bromine chemistry. J Geophys Res 1996;101(D1):1489–504.
[277] Hanson DR, Ravishankara AR, Lovejoy ER. Reaction of $BrONO_2$ with H_2O on submicron sulfuric acid aerosol and the implications for the lower stratosphere. J Geophys Res 1996;101(D4):9063–9.
[278] Pfeilsticker K, Sturges WT, Bösch H, Camy-Peyret C, Chipperfield MP, Engel A, et al. Lower stratospheric organic and inorganic bromine budget for the arctic winter 1998/99. Geophys Res Lett 2000;27:3305–8.
[279] Sander R, Crutzen PJ. Model study indicating halogen activation and ozone destruction in polluted air masses transported to the sea. J Geophys Res 1996;101:9121–38.
[280] Vogt R, Crutzen PJ, Sander R. A mechanism for halogen release from sea-salt aerosol in the remote marine boundary layer. Nature 1996;383:327–30.
[281] Johnson DG, Traub WA, Chance KV, Jucks KW. Detection of HBr and upper limit for HOBr: Bromine partitioning in the stratosphere. Geophys Res Lett 1995;22:1373–6.
[282] Orphal J, Flaud JM, Kou Q, Tchana FK, Pirali O. The far infrared rotational spectrum of HOBr: line positions and intensities. J Mol Struct 2005;742:153–9.
[283] Orphal J, Kou Q, Kwabia Tchana F, Pirali O, Flaud JM. The ν_3 bands of HOBr around 16 μm studied by high-resolution Fourier-transform spectroscopy. J Mol Spectrosc 2003;221:239–43.

[284] Orphal J, Flaud JM, Kwabia Tchana F, Kou Q, Pirali O. High-resolution spectroscopy and analysis of the $2\nu_1$ bands of HOBr in the near-infrared. J Mol Spectrosc 2009, to be submitted.
[285] Rothman LS, Barbe A, Benner DC, Brown LR, Camy-Peyret C, Carleer MR, et al. The HITRAN molecular spectroscopic database: edition of 2000 including updates through 2001. JQSRT 2003;82:5–44.
[286] Rotger M, Boudon V, Vander Auwera J. Line positions and intensities in the ν_{12} band of ethylene near 1450 cm^{-1}: an experimental and theoretical study. JQSRT 2008;109:952–62.
[287] Blanquet G, Bouanich JP, Walrand J, Lepère M. Self-broadening coefficients in the ν_7 band of ethylene at room and low temperatures. J Mol Spectrosc 2003;222:284–90.
[288] Brannon JF, Varanasi P. Tunable diode laser measurements on the 951.7393 cm^{-1} line of $^{12}C_2H_4$ at planetary atmospheric temperatures. JQSRT 1992;47:237–42.
[289] Reuter DC, Sirota JM. Absolute intensities and foreign gas broadening coefficients of the $11_{1,10} \leftarrow 11_{2,10}$ and $18_{0,18} \leftarrow 18_{1,18}$ lines in the ν_7 band of C_2H_4. JQSRT 1993;50:477–82.
[290] Blanquet G, Walrand J, Bouanich JP. Diode-laser measurements of N_2-broadening coefficients in the ν_7 band of C_2H_4. J Mol Spectrosc 2000;201:56–61.
[291] Xu LH. University of New Brunswick, St John, Canada, private communication, 2007.
[292] McElroy MB, Salawitch RJ, Wofsy SC, Logan JA. Reductions of Antarctic ozone due to synergistic interactions of chlorine and bromine. Nature 1986;321:759–62.
[293] Kurylo MJ, Rodriguez JM, Andreae MO, Atlas EL, Blake DR, Butler JH, et al. World Meteorological Organization; 1999.
[294] Kwabia Tchana F, Kleiner I, Orphal J, Lacome N, Bouba O. New analysis of the Coriolis-interacting ν_2 and ν_5 bands of $CH_3^{79}Br$ and $CH_3^{81}Br$. J Mol Spectrosc 2004;228:441–52.
[295] Kwabia Tchana F, Jacquemart D, Lacome N, Kleiner I, Orphal J. Absolute line intensities in methyl bromide: the 7-μm region. J Mol Spectrosc 2006;235:132–43.
[296] Jacquemart D, Kwabia Tchana F, Lacome N, Kleiner I. A complete set of line parameters for CH_3Br in the 10-μm spectral region. JQSRT 2007;105:264–302.
[297] Benedict WS, Kaplan LD. Calculation of line widths in H_2O–H_2O and H_2O–O_2 collisions. JQSRT 1964;4:453–69.
[298] Toth RA, Brown LR. Oxygen broadening parameters of water vapour: 1212–2136 cm^{-1}. J Mol Spectrosc 2003;218:135–50.
[299] Rothman LS, Gamache RR, Goldman A, Brown LR, Toth RA, Pickett HM, et al. The HITRAN database: 1986 edition. Appl Opt 1987;26:4058–97.
[300] Bouanich JP, Blanquet G, Walrand J. Theoretical O_2- and N_2-broadening coefficients of CH_3Cl spectral lines. J Mol Spectrosc 1993;161:416–26.
[301] Colmont JM, Rohart F, Wlodarczak G, Bouanich JP. *K*-dependence and temperature dependence of N_2- and O_2-broadening coefficients for the $J = 14$–13 transition of methyl chloride $CH_3\ ^{35}Cl$. J Mol Struct 2006;780–781:268–76.
[302] Gamache RR, Davies RW. Theoretical N_2-, O_2-, and air-broadened halfwidths of $^{16}O_3$ calculated by Quantum Fourier Transform Theory with realistic collision dynamics. J Mol Spectrosc 1985;109:283–99.
[303] Jacquemart D, Tran H. Temperature dependence of self- and N_2-broadening coefficients for CH_3Br in the 10-μm spectral region. JQSRT 2008;109:569–79.
[304] Tran H, Jacquemart D, Mandin JY, Lacome N. Line-mixing calculation in the ν_6 *Q* branches of methyl bromide broadened by nitrogen: experiment and modelling. JQSRT 2008;109:119–31.
[305] Gomez L, Tran H, Jacquemart D. Line-mixing calculation in the ν_6 Q branches of ν_2-broadened CH_3Br at low temperatures. J Mol Spectrosc 2009, in press.
[306] Rinsland CP, Malathy Devi V, Chris Benner D, Blake TA, Sams RL, Brown LR, et al. Multispectrum analysis of the ν_4 band of CH_3CN: positions, intensities, self- and N_2-broadening, and pressure-induced shifts. JQSRT 2008;109:974–94.
[307] Fabian M, Morino I, Yamada KMT. Analysis of the line profiles of CH_3CN for the $J = 5 \rightarrow 4$ and $6 \rightarrow 5$ rotational transitions. J Mol Spectrosc 1998;190:232–9.
[308] Colmont JM, Rohart F, Wlodarczak G, Bouanich JP. K-Dependence and temperature dependence of N_2-, H_2- and He-broadening coefficients for the $J = 12$–11 transition of acetonitrile $CH_3C^{14}N$ located near 220.7 GHz. J Mol Spectrosc 2006;238:98–107.
[309] Worton DR, Sturges WT, Gohar LK, Shine KP, Martinerie P, Oram DE, et al. Atmospheric trends and radiative forcings of CF_4 and C_2F_6 inferred from firn air. Environ Sci Technol 2007;41:2184–9.
[310] Cicerone RJ. Atmospheric carbon tetrafluoride: a nearly inert gas. Science 1979;206:59–61.
[311] Zander R, Solomon S, Mahieu E, Goldman A, Rinsland CP, Gunson MR, et al. Increase of stratospheric carbon tetrafluoride (CF_4) based on ATMOS observations from space. Geophys Res Lett 1996;23:2353–6.
[312] Rinsland CP, Mahieu E, Zander R, Nassar R, Bernath P, Boone C, et al. Long-term stratospheric carbon tetrafluoride (CF_4) increase inferred from 1985–2004 infrared space-based solar occultation measurements. Geophys Res Lett 2006;33:02808.
[313] Goldman A, Murcray DG, Murcray FJ, Cook GR, van Allen JW, Bonomo FS, et al. Identification of the ν_3 vibration–rotation band of CF_4 in infrared balloon-borne solar spectra. Geophys Res Lett 1979;6:609–12.
[314] Brown LR, Farmer CB, Rinsland CP, Toth RA. Molecular line parameters for the atmospheric trace molecule spectroscopy (ATMOS) experiment. Appl Opt 1987;26:5154–82.
[315] Gabard T, Pierre G, Takami M. Study of the ν_3 and $2\nu_4$ interacting states of $^{12}CF_4$. Mol Phys 1995;85:735–44.
[316] Wenger C, Boudon V, Rotger M, Sanzharov M, Champion JP. XTDS and SPVIEW: graphical tools for the analysis and simulation of high-resolution molecular spectra. J Mol Spectrosc 2008;251:102–13.
[317] Papoušek D, Papouskova Z, Chong DP. Density functional computations of the dipole moment derivatives for halogenated methanes. J Phys Chem 1995;99:15387–95.
[318] Boudon V, Domanskaya A, Maul C, Georges R, Mitchell J, Harter WG. High-resolution spectroscopy and analysis of the $2\nu_4/\nu_3$ dyad of CF_4. In preparation.
[319] Höjer S, May RD. Air-broadening coefficients for the ν_3 band of CF_4. J Mol Spectrosc 1996;178:139–42.
[320] Massie ST, Goldman A. The infrared absorption cross-section and refractive-index data in HITRAN. JQSRT 2003;82:413–28.
[321] Di Lonardo G, Masciarelli G. Infrared absorption cross-sections and integrated absorption intensities of HFC-125 and HFC-143a. JQSRT 2000;66:129–42.
[322] Smith K, Newnham D, Page M, Ballard J, Duxbury G. Infrared absorption cross-sections and integrated absorption intensities of HFC-134 and HFC-143a vapour. JQSRT 1998;59:437–51.
[323] Clerbaux C, Colin R, Simon PC, Granier C. Infrared cross sections and global warming potentials of 10 alternative hydrohalocarbons. J Geophys Res 1993;98(D6):10491–7.
[324] Rinsland CP, Sharpe SW, Sams RL. Temperature-dependent infrared absorption cross sections of methyl cyanide (acetonitrile). JQSRT 2005;96:271–80.
[325] Allen G, Remedios JJ, Smith KM. Low temperature mid-infrared cross-sections for peroxyacetyl nitrate (PAN) vapour. Atmos Chem Phys 2005;5:3153–8.
[326] Allen G, Remedios JJ, Newnham DA, Smith KM, Monks PS. Improved mid-infrared cross-sections for peroxyacetyl nitrate (PAN) vapour. Atmos Chem Phys 2005;5:47–56.
[327] Remedios JJ, Allen G, Waterfall AM, Oelhaf H, Kleinert A, Moore DP. Detection of organic compound signatures in infra-red, limb emission spectra observed by the MIPAS-B2 balloon instrument. Atmos Chem Phys 2007;7:1599–613.

[328] Rinsland CP, Devi VM, Blake TA, Sams RL, Sharpe S, Chiou L. Quantitative measurement of integrated band intensities of benzene vapor in the mid-infrared at 278, 298, and 323 K. JQSRT 2008;109:2511–22.
[329] Mérienne MF, Jenouvrier A, Coquart B, Carleer M, Fally S, Colin R, et al. Improved data set for the Herzberg band systems of $^{16}O_2$. J Mol Spectrosc 2001;207:120.
[330] Chance K. Ultraviolet and visible spectroscopy and spaceborne remote sensing of the Earth's atmosphere. C R Phys 2005;6:836–47.
[331] Bass AM, Paur RJ. UV absorption cross-sections for ozone: the temperature dependence. J Photochem 1981;17:41;
Bass AM, Paur RJ. The ultraviolet cross-sections of ozone: I—the measurements. In: Zerefos CS, Ghazi A, editors. Atmospheric ozone. Dordrecht: Reidel D; 1985. p. 606–10;
Bass AM, Paur RJ. The ultraviolet cross-sections of ozone: II—results and temperature dependence. In: Zerefos CS, Ghazi A, editors. Atmospheric ozone. Dordrecht: Reidel D; 1985. p. 611–6.
[332] Liu X, Chance K, Sioris CE, Kurosu TP. Impact of using different ozone cross sections on ozone profile retrievals from Global Ozone Monitoring Experiment (GOME) ultraviolet measurements. Atmos Chem Phys 2007;7:3571–8.
[333] Daumont D, Brion J, Charbonnier J, Malicet J. Ozone UV spectroscopy I: absorption cross-sections at room temperature. J Atmos Chem 1992;15:145–55;
Brion J, Chakir A, Daumont D, Malicet J. High-resolution laboratory absorption cross section of O_3. Temperature effect. Chem Phys Lett 1993;213:610–2;
Malicet C, Daumont D, Charbonnier J, Parisse C, Chakir A, Brion J. Ozone UV spectroscopy, II. Absorption cross sections and temperature dependence. J Atmos Chem 1995;21:263–73;
Brion J, Chakir A, Charbonnier J, Daumont D, Parisse C, Malicet J. Absorption spectra measurements for the ozone molecule in the 350–830 nm region. J Atmos Chem 1998;30:291–9.
[334] Fleischmann OC, Hartmann M, Burrows JP, Orphal J. New ultraviolet absorption cross-sections of BrO at atmospheric temperatures measured by time-windowing Fourier transform spectroscopy. J Photochem Photobiol A 2004;168:117–32.
[335] Wilmouth DM, Hanisco TF, Donahue NM, Anderson JG. Fourier transform ultraviolet spectroscopy of the $A\,^2\Pi_{3/2} \leftarrow X\,^2\Pi_{1/2}$ transition of BrO. J Phys Chem A 1999;103:8935–45.
[336] Meller R, Moortgat GK. Temperature dependence of the absorption cross sections of formaldehyde between 223 and 323 K in the wavelength range 225–375 nm. J Geophys Res 2000;105(D6):7089–101.
[337] Cantrell CA, Davidson JA, McDaniel AH, Shetter RE, Calvert JG. Temperature-dependent formaldehyde cross sections in the near-ultraviolet spectral region. J Phys Chem 1990;94:3902–8.
[338] Carlos Gómez Martín J, Spietz P, Burrows JP. Spectroscopic studies of the I_2/O_3 photochemistry: part 1: determination of the absolute absorption cross sections of iodine oxides of atmospheric relevance. J Photochem Photobiol A 2005;176:15–38.
[339] Saiz-Lopez A, Chance K, Liu X, Kurosu TP, Sander SP. First observations of iodine oxide from space. Geophys Res Lett 2007;34:12812.
[340] Warneck P, Marmo FF, Sullivan JO. Ultraviolet absorption of SO_2: dissociation energies of SO_2 and SO. J Chem Phys 1964;40:1132–6.
[341] Vandaele AC, Simon PC, Guilmot JM, Carleer M, Colin R. SO_2 absorption cross-section measurement in the UV using a Fourier transform spectrometer. J Geophys Res 1994;99:25599–605.
[342] Woods PT, Jolliffe BW, Marx BR. High-resolution spectroscopy of SO_2 using a frequency-doubled pulsed dye laser, with application to the remote sensing of atmospheric pollutants. Opt Commun 1980;33:281–91.
[343] Vattulainen J, Wallenius L, Stenberg J, Hernberg R, Linna V. Experimental determination of SO_2, C_2H_2, and O_2 UV absorption cross sections at elevated temperatures and pressures. Appl Spectrosc 1997;51:1311–5.
[344] Wu CF, Yang BW, Chen F, Judge D, Caldwell JJ, Trafton LM. Measurements of high-, room-, and low-temperature photoabsorption cross sections of SO_2 in the 2080- to 2950-A region, with application to Io. Icarus 2000;145:289–96.
[345] Wu CF, Judge D. SO_2 and CS_2 cross section data in the ultraviolet region. Geophys Res Lett 1981;8:769–71.
[346] Thompson Jr. RT, Hoell Jr. JM, Wade WR. Measurements of SO_2 absorption coefficients using a tunable dye laser. J Appl Phys 1975;46:3040–3.
[347] Rufus J, Stark G, Smith PL, Pickering JC, Thorne AP. High-resolution photoabsorption cross section measurements of SO_2, 2: 220 to 325 nm at 295 K. J Geophys Res 2003:108.
[348] Manatt SL, Lane AL. A compilation of the absorption cross-sections of SO_2 from 106 to 403 nm. JQSRT 1993;50:267–76.
[349] McGee TJ, Burris Jr. J. SO_2 absorption cross sections in the near UV. JQSRT 1987;37:165–82.
[350] Leroy B, Rigaud P, Jourdain JL, Le Bras G. Spectres d'absorption dans le proche ultraviolet de CS_2 et SO_2 entre 200 et 300 K. Moon Planets 1983;29:177–83.
[351] Hearn CH, Joens JA. The near uv absorption spectrum of CS_2 and SO_2 at 300 K. JQSRT 1991;45:69–75.
[352] Brassington DJ. Sulfur dioxide absorption cross-section measurements from 290 to 317 nm. Appl Opt 1981;20:3774–9.
[353] Bogumil K, Orphal J, Homann T, Voigt S, Spietz P, Fleischmann OC, et al. Measurements of molecular absorption spectra with the SCIAMACHY pre-flight model: instrument characterization and reference data for atmospheric remote-sensing in the 230–2380 nm region. J Photochem Photobiol A 2003;157:167–84.
[354] Ahmed SM, Kumar V. Quantitative photoabsorption and fluorescence spectroscopy of SO_2 at 188–231 and 278.7–320 nm. JQSRT 1992;47:359–73.
[355] Danielache SO, Eskebjerg C, Johnson M, Ueno Y, Yoshida N. High-precision spectroscopy of ^{32}S, ^{33}S, and ^{34}S sulfur dioxide: ultraviolet absorption cross sections and isotope effects. J Geophys Res 2008:113.
[356] Sidebottom HW, Badcock CC, Jackson GE, Calvert JG, Reinhardt GW, Damon EK. Photooxidation of sulfur dioxide. Environmental Science & Technology 1972;6:72–9.
[357] Clements JH. On the absorption spectrum of sulphur dioxide. Phys Rev 1933;47:224–32.
[358] Sprague KE, Joens JA. SO_2 absorption cross-section measurements from 320 to 405 nm. JQSRT 1995;53:349–52.
[359] Vandaele AC, Hermans C, Fally S. Fourier transform measurements of SO_2 absorption cross sections: II. Temperature dependence in the 29 000–44 500 cm^{-1} (225–345 nm) region. JQSRT 2009; submitted for publication.
[360] Hermans C, Vandaele AC, Fally S. Fourier transform measurements of SO_2 absorption cross sections: I. Temperature dependence in the 23 500–29 000 cm^{-1} (345–425 nm) region. JQSRT 2009; this issue, doi:10.1016/j.jqsrt.2009.01.031.
[361] WHO air quality guidelines for Europe, 2nd ed. WHO Regional Publications, European Series no. 91, Copenhagen, Denmark, ISBN 92-890-1358-3, ISSN 0378-2255, 2000.
[362] Finlayson-Pitts BJ, Pitts JNJ. Chemistry of the upper and lower atmosphere. New York: Academic Press; 2000.
[363] Volkamer R, Etzkorn T, Geyer A, Platt U. Correction of the oxygen interference with UV spectroscopic (DOAS) measurements of monocyclic aromatic hydrocarbons in the atmosphere. Atmos Environ 1998;32:3731–47.
[364] Kim SJ, Caldwell J, Rivolo AR, Wagener R, Orton GS. Infrared polar brightening on Jupiter: III. Spectrometry from the Voyager 1 IRIS experiment. Icarus 1985;64:233–48.
[365] Bézard B, Drossart P, Encrenaz T, Feuchtgruber H. Benzene on the giant planets. Icarus 2001;154:492–500.
[366] Coustenis A, Salama A, Schulz B, Ott S, Lellouch E, Encrenaz Th, et al. Titan's atmosphere from ISO mid-infrared spectroscopy. Icarus 2003;161:383–403.
[367] Bruston P, Khlifi M, Bénilan Y, Raulin F. Laboratory studies of organic chemistry in planetary atmospheres: from simulation experiments to spectroscopic determinations. J Geophys Res 1994;99(E9):19047–62.
[368] Shindo F, Benilan Y, Guillemin JC, Chaquin P, Jolly A, Raulin F. Spectroscopy of two organic compounds involved in Titan's atmosphere chemistry: tetracetylene (C_8H_2) and vinylacetylene (CH_2CHCCH). Bull Am Astron Soc 2001:1109.
[369] Wu R, Chen F, Judge D. Cross section measurements of gaseous and liquid H_2O, D_2O, and C_6H_6. Bull Am Astron Soc 2000:1646.

[370] Okruss M, Müller R, Hese A. High resolution UV laser spectroscopy of jet-cooled benzene molecules: complete rotational analysis of the $S_1 \leftarrow S_0$ $6^1 0$ ($l = \pm 1$) band. J Mol Spectrosc 1999;193:293–305.
[371] Fally S, Carleer M, Vandaele AC. UV Fourier transform absorption cross sections of benzene, toluene, meta-, ortho-, and para-xylene. JQSRT 2009; this issue, doi:10.1016/j.jqsrt.2008.11.014.
[372] Etzkorn T, Klotz B, Sorensen S, Patroescu IV, Barnes I, Becker KH, et al. Gas-phase absorption cross sections of 24 monocyclic aromatic hydrocarbons in the UV and IR spectral ranges. Atmos Environ 1999;33:525–40.
[373] Suto M, Wang X, Shan J, Lee LC. Quantitative photoabsorption and fluorescence spectroscopy of benzene, naphthalene, and some derivatives at 106–295 nm. JQSRT 1992;48:79–89.
[374] Trost B, Stutz J, Platt U. UV-absorption cross sections of a series of monocyclic aromatic compounds. Atmos Environ 1997;31:3999–4008.
[375] Wagner R, Benz S, Mohler O, Saathoff H, Schnaiter M, Schurath U. Mid-infrared extinction spectra and optical constants of supercooled water droplets. J Phys Chem A 2005;109:7099–112.
[376] Downing HD, Williams D. Optical constants of water in the infrared. J Geophys Res 1975;80:1656–61.
[377] Warren SG, Brandt RE. Optical constants of ice from the ultraviolet to the microwave: a revised compilation. J Geophys Res 2008:113.
[378] Warren SG. Optical constants of ice from the ultraviolet to the microwave. Appl Opt 1984;23:1206–25.
[379] Clapp ML, Miller RE, Worsnop DR. Frequency-dependent optical constants of water ice obtained directly from aerosol extinction spectra. J Phys Chem 1995;99:6317–26.
[380] Matzler C. Microwave dielectric properties of ice. In: Matzler C, et al., editors. Thermal microwave radiation—applications for remote sensing, electromagnetization, waves series, vol. 52. Stevenage, UK: Inst Eng Technology; 2006. p. 455–62 [chapter 5].
[381] Lund Myhre CE, Christensen DH, Nicolaisen FM, Nielsen CJ. Spectroscopic study of aqueous H_2SO_4 at different temperatures and compositions: variations in dissociation and optical properties. J Phys Chem A 2003;107:1979–91.
[382] Lund Myhre CE, Grothe H, Gola AA, Nielsen CJ. Optical constants of HNO_3/H_2O and $H_2SO_4/HNO_3/H_2O$ at low temperatures in the infrared region. J Phys Chem A 2005;109:7166–71.
[383] Norman ML, Miller RE, Worsnop DR. Ternary $H_2O/HNO_3/H_2O$ Optical constants: new measurements from aerosol spectroscopy under stratospheric conditions. J Phys Chem A 2002;106:6075–83.
[384] Biermann UM, Luo BP, Peter T. Absorption spectra and optical constants of binary and ternary solutions of H_2SO_4, HNO_3, and H_2O in the mid infrared at atmospheric temperatures. J Phys Chem A 2000;104:783–93.
[385] Tennyson J, Bernath PF, Brown LR, Campargue A, Carleer MR, Csaszar AG, et al. IUPAC critical evaluation of the rotational–vibrational spectra of water vapor. Part I: energy Levels and transition wavenumbers for $H_2{}^{17}O$ and $H_2{}^{18}O$. JQSRT 2009; this issue, doi:10.1016/j.jqsrt.2009.02.014.
[386] Bernath PF. Spectra of atoms and molecules. 2nd ed. New York: Oxford University Press; 2005.
[387] Šimečková M, Jacquemart D, Rothman LS, Gamache RR, Goldman A. Einstein *A*-coefficients and statistical weights for molecular absorption transitions in the *HITRAN* database. JQSRT 2006;98:130–55.
[388] Rothman LS, Rinsland CP, Goldman A, Massie ST, Edwards DP, Flaud JM, et al. The HITRAN molecular spectroscopic database and HAWKS (HITRAN Atmospheric Workstation): 1996 edition. JQSRT 1998;60:665–710.
[389] De Bièvre P, Gallet M, Holden NE, Barnes IL. Isotopic abundances and atomic weights of the elements. J Phys Chem Ref Data 1984;13:809–91.